2015-01-01

A Methodology for Physically-based Contact and Meniscus Properties in Rigid-Body Computational Knee Modeling

Stephen Wilson
University of Texas at El Paso, readingword@gmail.com

A METHODOLOGY FOR PHYSICALLY–BASED CONTACT

AND MENISCUS PROPERTIES IN RIGID-BODY

COMPUTATIONAL KNEE MODELING

by

STEPHEN P. WILSON

Department of Mechanical Engineering

APPROVED:

Roger V. Gonzalez, Ph.D., Chair

Jerome Hausselle, Ph.D.

Trent M. Guess, Ph.D.

Charles H. Ambler, Ph.D.

Dean of the Graduate School

A METHODOLOGY FOR PHYSICALLY–BASED CONTACT AND MENISCUS PROPERTIES IN RIGID-BODY COMPUTATIONAL KNEE MODELING

by

STEPHEN P. WILSON, B.S.

Thesis

Presented to the Faculty of the Graduate School of

The University of Texas at El Paso

in Partial Fulfillment

of the Requirements

for the Degree of

MASTER OF SCIENCE

Department of Mechancial Engineering

THE UNIVERSITY OF TEXAS AT EL PASO

May 2015

Abstract

Determining natural inner knee mechanics is a longstanding goal for researchers with applications to prevention and treatment of knee trauma and osteoarthritis. Physical testing has only provided limited information of knee mechanics due to technical challenges and cost. Modeling has been used for decades to obtain some of this otherwise inaccessible information, and recently finite element analysis (FEA) has become a popular means to this end. However, FEA requires time intensive mesh-creation and has large computational requirements. Ideally, model creation should be easy and simulations should be fast to allow for sensitivity analysis. Although allowing easier model creation and offering over an order of magnitude more computational efficiency than FEA, current rigid body modeling of the knee is limited by imprecise methodologies for defining material properties. Cartilage and meniscus are particular points of weakness.

The following thesis develops an improved methodology for cartilage contact which is user-friendly and allows for precise definition of contact via user-supplied material properties while accounting for changes in stiffness due to discretization. Additionally, meniscus modeling is improved by developing and implementing equations which directly define stress-strain relationships to match values reported in literature or those selected by the user. Results from two implemented knee models are compared to experimental results in literature and sensitivity to material properties and driving kinematics is investigated.

Table of Contents

List of Tables

List of Figures

1 Introduction

1.1 Motivation for computational modeling of the knee joint

1.1.1 As an alternative to *in vivo* testing

Few persons argue against the importance of science in promoting an economically healthy country. Science related to health has received special attention: since 2007 the National Institutes of Health (NIH) has received ~$30 Billion annually to support medical research (NIH, 2012). For comparison, the National Science Foundation (NSF) supports non-medical research and education and receives ~$7 Billion annually (NSF, 2013). Models are often used to study the complex nature of the knee joint, investigating mechanics and internal joint loads during daily activities. This knowledge is very difficult to obtain otherwise since *in vivo* human experimentation is generally unethical with current technologies. For example, to obtain pressures endured by cartilage during walking, a pressure film/pad would have to be implanted and anchored. But this is impossible, for practical purposes, without damaging an abundance of connective tissues around the joint. This may change as arthroscopic surgery matures and more flexible films and anchoring methods are developed, but currently only limited information about the knee can be ethically gathered from live human experimentation: such as, for example, the measure of anterior cruciate ligament (ACL) strain using medical imaging (Fleming et al., 2001). Thus, modeling is a popular method to approach traditionally unattainable data.

Dynamic cadaveric experimentation is an alternate approach that bypasses most of the ethical difficulties of live experimentation. However, current experimentation is limited by the high cost associated with developing, constructing, and maintaining stable and accurate actuation systems, the difficulty of obtaining and preparing cadaver specimens, and the destructive nature of testing (partially due to degredation of cadaveric specimens and partially due to non-physiological testing conditions). Computer models on the other hand are comparitively inexpensive, require very little lab space, have few regulations, are reusable, and are easily adjustable. Thus, while cadaveric experiments are the primary source for validated data in knee biomechanics, computer models are frequently used when low capital investment, repeatability, and controlled variance of specific factors are desired. These factors make computer models useful for preliminary hypothesis testing. Computer models also hold potention for patient-specific clinical application, since models can be constructed from medical images from live patients.

1.1.2 To understand and prevent disease and injury

Knee Osteoarthritis (OA) is a disease that affects a large percentage of the population and is highly correlated with age (Figure 1.1). It is characterized by pain and degeneration of cartilage in the knee joint and, depending on severity, can impair a patient's mobility. However, the progression of the disease is highly non-uniform among individuals and the cause of this is unknown.

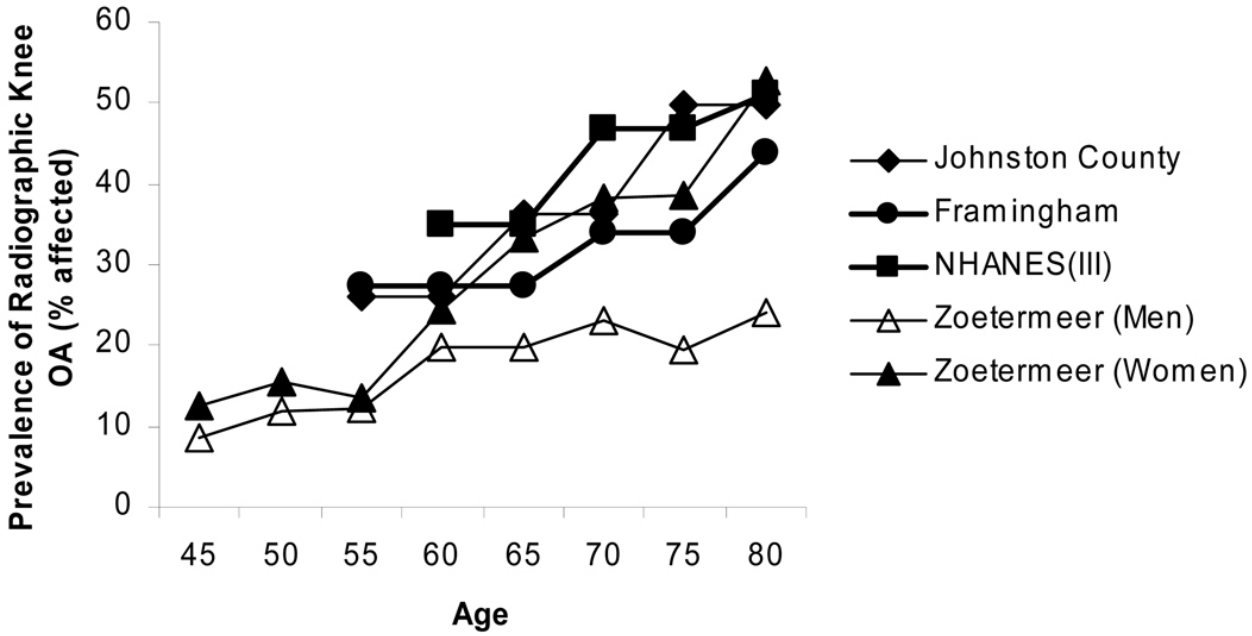

Figure 1.1: Incidence of radiographic knee OA versus age. Figure taken from Anderson and Loeser (2010), who utilized data from Felson et al. (1987); Van Saase et al. (1989); Dillon et al. (2006); Jordan et al. (2007)

Understanding what causes degenerative changes to the knee joint is an essential step in prevention. The development of a robust computational knee model would enable investigation into which motions and environments cause increased knee wear[1] and subsequently enable recommendations for OA prevention. The importance of prevention will only increase as medicine advances the average lifespan.

Knee injuries are very common. A national study of knee injuries in New Zealand (Gianotti et al., 2009) reports the information in Table 1.1.

[1] Andriacchi et al. (2006) used an FE model to investigate wear due to changes in gait caused by ACL injury. Fregly et al. (2005) investigated wear in a total knee replacement using a multibody model.

Table 1.1: Data regarding knee injuries in New Zealand compiled from Gianotti et al. (2009)

Type of knee surgery required	Incidence /100,000	Treatment visits	Cost/case	Injury at place of recreation	Injury at home
No surgery	1147.1	6.6	$885	32.5%	26.1%
Ligament surgery involving ACL	36.9	27.1	$11,157	65.1%	11.1%
Ligament surgery not involving ACL	9.1	31.3	$15,663	26.8%	29.7%

The high percentage of injuries at home might indicate that the general population is engaging in high-risk behavior without realizing it. Coupled with an array of common knee behaviors at home, a sufficiently accurate knee model could identify behaviors that put knee structures (especially ligaments) at risk. Once high-risk behavior is identified, the number of knee injuries that occur should decrease with increasing awareness of those detrimental behaviors.

1.1.3 To simulate surgical outcomes

Computer models can also assist physicians in discerning the best surgery techniques. For example, placement techniques for cruciate ligament reconstruction are still being investigated. Instead of utilizing cadavers (Zantop et al., 2008) or post-operative imaging (Abebe et al., 2011) to determine the efficacy of these techniques, physicians could investigate before performing surgery if a robust and convenient computer model were available. While imaging of volunteer cohorts is better for comparison of established techniques, a computational model could investigate experimental techniques without risking poor outcomes for volunteer patients. Similarly, as meniscus implants are developed, the biomechanical effect of a variety of attachment strategies can be investigated before starting clinical trials.

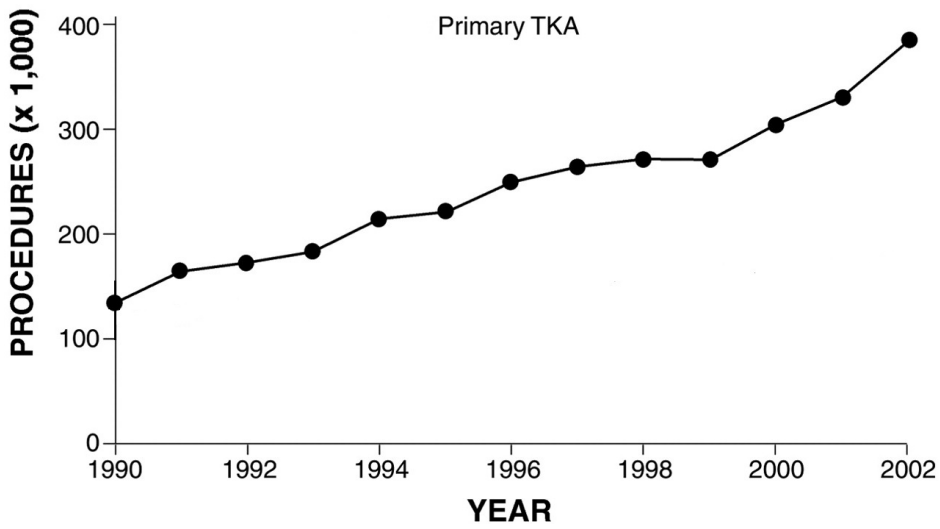

Figure 1.2: Prevalence of Total Knee Arthroplasty in the USA. Figure adapted from Kurtz et al. (2005).

1.1.4 To design novel prostheses

Development of an accurate working model of the physiological knee has substantial implications for the development of prostheses. Sensitivity analyses of computational models may determine which knee structures are most important to natural knee function—prosthesis design should then focus on mimicking the function of those most important structures. This is termed "design by analogy". At this time, transfemoral prostheses for amputees are not generally designed by analogy for reasons of complexity. However, prothesis design for the increasingly prevalent (see Figure 1.2) total knee arthroplasty is dominated by analogy and would greatly benefit from the increased clarity a multi-body computational knee model could provide. For example, by modeling different tibial tray shapes and inclines made from novel biomaterials and comparing to results to those from a normal knee.

1.2 Background

1.2.1 Knee structures and their function

The knee is a complex joint. It has many ligaments that passively stabilize as well as muscles that actively stabilize. Figure 1.3a shows the Patella and how it redirects the quadriceps tendon so that it wraps around the joint to become the patellar ligament. Notice also the Medial Collateral Ligament (MCL). It stabilizes the knee against valgus motion. On the opposite side of the knee (see Figure 1.3c), the Lateral Collateral Ligament (LCL) protects against excessive varus motion. In Figure 1.3b the patella is removed to expose

the femoral cartilage, cruciate ligaments, and the menisci. The ACL protects the knee against anterior tibial translation (Fleming et al., 2001) while the posterior cruciate ligament (PCL) (see Figure 1.3b) protects against posterior tibial translation (Race and Amis, 1996). The cartilage of the knee provides lubrication—by surface structure (Kumar et al., 2001) and distribution of pressure—due to its deformable nature (Kempson et al., 1971).

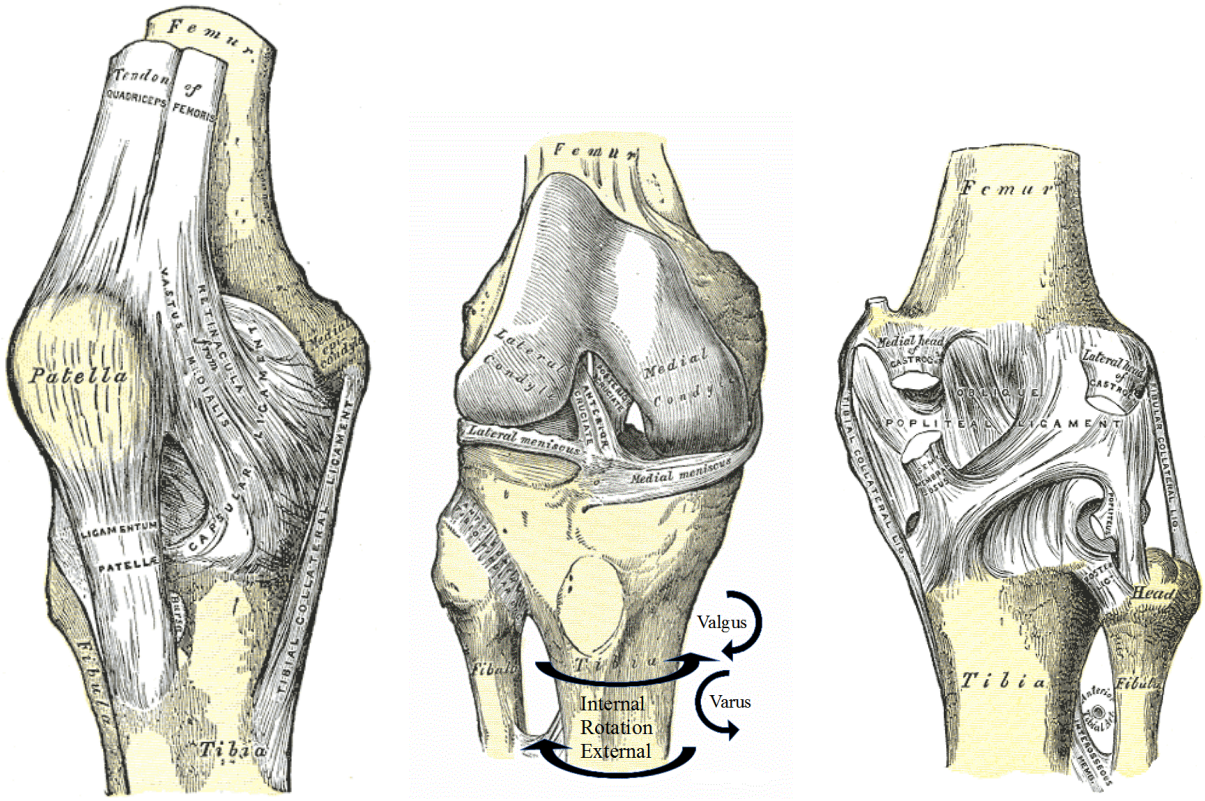

(a) (b) (c)

Figure 1.3: Knee anatomy. (a) Anterior view of the knee/patella. (b) Anterior view of right knee/ACL. (c) Posterior view of right knee/popliteal ligament. Figures adapted from Gray (1918).

Besides cartilage, the menisci's (Figure 1.4a) role is to lubricate and increase joint congruency (McCann et al., 2009). The menisci are important structures that distribute about 50% of the load between the femoral and tibial cartilage over a larger surface area (Shrive et al., 1978). This results in reduced peak pressure on the cartilage. In cadaveric experiments, lateral meniscectomy was found to increase peak local contact pressure by 60% for a load of 310N (Chen et al., 1996) and 235-335% for a load of 1800N (Paletta et al., 1997). This corresponds to the increased congruity of the joint for higher loads (>1000N) described by Kurosawa et al. (1980). Thus, as Fairbank (1948) proposed, the menisci are very significant in cartilage

protection. How much so is demonstrated by the approximately 5-fold increase in OA radiographic changes for individuals who had a meniscectomy compared to age and sex matched controls (Roos et al., 1998).

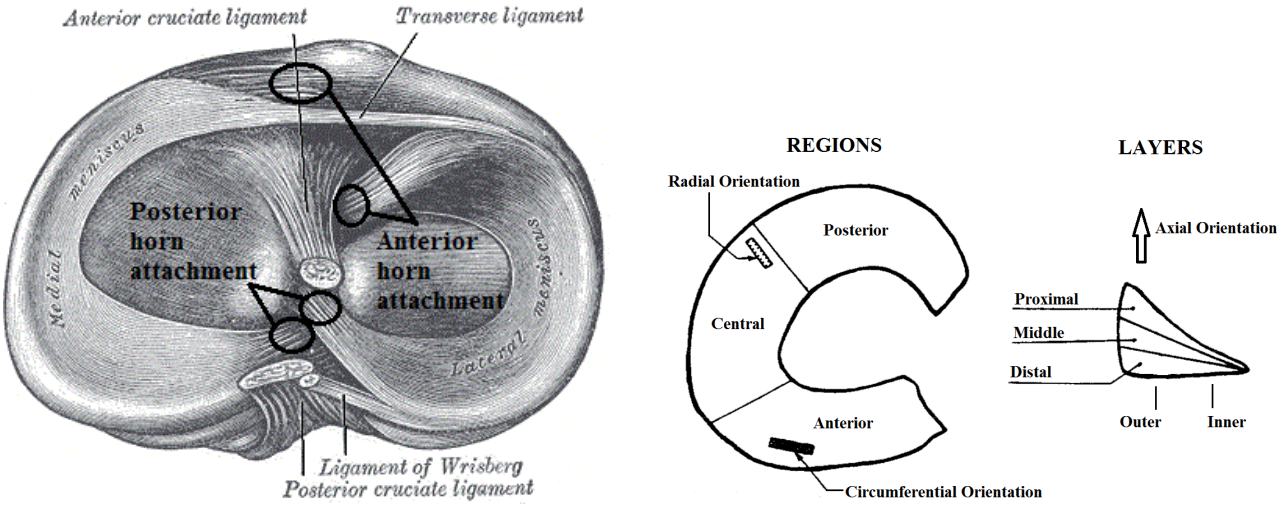

(a) (b)

Figure 1.4: (a) Superior view of the knee/menisci. Figure adapted from Gray (1918). (b) Meniscus diagram adapted from Tissakht and Ahmed (1995).

The correlation between aging and OA may result in part from increased meniscal damage (Gupte et al., 2002; Englund et al., 2008) that appears to accompany aging. The meniscus has different material properties depending on region, layer, (see Figure 1.4b) and stress state (tension, compression, shear).

Unfortunately, the stress states of the meniscus are not accurately known. Brown (1990) presumed that the meniscus experiences compression for axial and radial deformation and tension for circumferential. The meniscal horn attachments have been shown to be extremely important for appropriate functioning of the menisci. If the horn attachments are released, the load-distributing properties of the meniscus are essentially nullified (Chen et al., 1996; Paletta et al., 1997). This could explain the high correlation between OA incidence and increased subluxation of the menisci (Gale et al., 1999).

1.2.2 Knee kinematics

Rather than being a simple hinge joint, the knee has three main types of motion in the sagittal plane: slipping, rolling, and sliding. Slipping is purely rotational and corresponds to the motion of a hinge. Rolling is a result of rotational motion acting in tandem with friction to produce translation as well and corresponds to the motion of a tire of a traveling car. Sliding is purely translational and is the type of motion experienced in ice-skating.

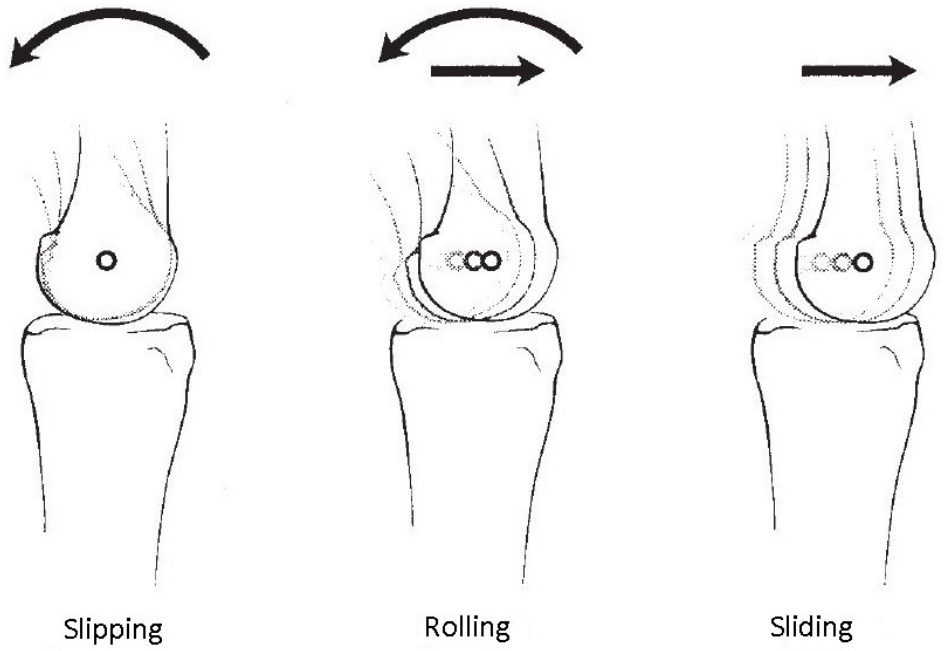

Figure 1.5: Three main types of knee motion in the sagittal plane. Figure adapted from Yamaguchi (2001).

1.2.3 Knee modeling

Modeling is a difficult task with multiple stages of development that may be termed generations. Zhang et al. (1998) describes these generations as follows: "The first generation of the modeling is linear analysis established under linear assumptions . . . . The second generation can be called nonlinear analysis, taking into consideration the nonlinear effects . . . . The third generation of the analyses should be dynamic." Any of these generations may be 2D or 3D, since 2D can be an important first step when proposing a new methodology. Modeling of the knee in 2D has decreased with the increased use of multi-body software packages.

Within 3D models/simulations, it is important to distinguish different types: quasi-static, static analysis via dynamic simulation, and fully dynamic simulations. Quasi-static is defined as neglect of inertia for models with "slow" changes in position and therefore small inertial effects. Thus quasi-static models are useful for physiological motions such as a slow squat or slow gait but are inaccurate for motions with high accelerations such as normal gait, cutting, and jumping.

Static analysis via dynamic simulation is almost identical to quasi-static except that inertia is not neglected. It is used mainly for settling simulations where the response at a particular point in time or position is desired.

A fully dynamic model/simulation is one in which a dynamic motion can be/is replicated. These models are the most useful since they can produce results at any point in time for stationary, slow, and fast motions. However, they are more difficult to build because constraints and boundary conditions must be valid for more scenarios and thus cannot be simplified as much. This greater complexity also necessitates greater computational power for solving.

1.2.3.1 3D rigid body modeling vs. finite element modeling There are two popular types of computer models in biomechanics: Rigid Body (RB) and Finite Element (FE). FE modeling has inherent capability to model deformable bodies while rigid body modeling does not. For this reason, FE models of the knee have been more popular since the knee has deformable components such as cartilage and meniscus. It has been claimed that RB modeling "cannot provide details of the loads and stresses in the hard and soft tissues, like FE models can" (Ali and Rouhi, 2010). While this is true to a certain extent and should be noted as a limitation, techniques exist which alleviate this problem (I specifically address techniques for ADAMS, MSC Software Corporation, CA, USA).

Loads (forces) in more rigid tissues can be measured by separating bodies into multiple components and then "locking" them together. Strains are easily measured in the soft tissues by including measures in the model which calculate the distance between the origin and insertion points. Stresses are more difficult to measure since MSC Adams does not measure surface area. However, stress can still be calculated by separating a body, such as the lateral tibial cartilage, into discrete components of known area and then "locking" them together. Thus, while RB modeling has more difficulty measuring loads and stresses, it should not be assumed that measuring such in RB models is impossible or impractical. However it must be admitted that by dividing bodies into discrete components some computational efficiency is sacrificed.

Since a RB model is based on rigid body mechanics, it is significantly more computationally efficient than finite element analysis[2]. This increased usability does come with the cost of the assumptions inherent to rigid body mechanics, but it enables probabalistic and optimization[3] studies to be conducted within a reasonable time frame. Therefore, it may be good practice to develop a rigid body model as a first estimate and then develop an FE model if more accuracy is necessary.

1.2.3.2 Recent improvements in rigid body modeling The current number of non-trivial (DOF $>$ 1) 3D rigid body (RB) models of the knee which utilize commercial software is small compared to the number of finite elements reported in literature. Furthermore, of those RB knee studies, almost all focus on

[2]For example, Guess et al. (2013), utilizing the same geometries and boundary conditions in a 5sec gait simulation, found 127sec. and 10hr. simulation times for Adams (RB) and ABAQUS (FE) respectively.

[3]For example, it is popular to study muscle activation using optimization in the OpenSim rigid body dynamics software.

total knee arthroplasty (TKA) and thus use artificial instead of natural knee geometry. Thus, current RB modeling of the natural knee joint is less developed and needs improvement.

To the author's knowledge, the work at the University of Missouri - Kansas City (UMKC) headed by Trent Guess was the only rigid-body work studying plateau pressures using a natural knee since Bei and Fregly (2004). Guess' group used the ADAMS software line (MSC Software Corporation, Santa Ana, CA, USA). Use of industry software allows fully dynamic simulations that are not based on gross simplifications (such as single point contact) or one specific knee position or loading while remaining highly reliable. Of particular interest in studying natural knee mechanics are solutions such as tibial cartilage division (Figure 1.6a) to allow for better contact force control, force mapping, and pressure calculation (Liu et al., 2009; Guess et al., 2013), wrapping of the patellar tendon/ligament on the tibia by the inclusion of ellipsoid bodies (Guess et al., 2010; Kia, 2011), and inclusion of deformable menisci (Figure 1.6b) via segmentation and associated spring attachments (Guess et al., 2010; Kia, 2011).

However, significant limitations remain. Usually when defining contact the default Adams contact formula (the so-called "Impact" function) has been used. This default contact formula is

$$d < d_{damp} \{F = k * d^e - d/d_{damp} * c * v\} \tag{1.1}$$

$$d \geq d_{damp} \{F = k * d^e - c * v\} \tag{1.2}$$

where "d" is the depth of maximum interpenetration of the contacting geometries, "k" is a stiffness coefficient, "e" is user-chosen exponent, "c" is a damping coefficient, "d_damp" is the chosen depth of interpenetration at which full damping is operating, and "v" is the velocity of interpenetration. The most obvious problem with using this formulation is that it doesn't include the area of contact when solving for the resulting force. This problem can be alieveated by assuming that whenever a discretized cartilage piece experiences a force it experiences it on its entire surface (for example, 9mm^2 for cartilage discretized into 3x3mm pieces) (Guess et al., 2013). However, this means contact force is overestimated when approaching the periphery of contact unless the contacting surfaces have a similar radius of curvature. This is especially a problem when considering meniscus-to-cartilage contact (at least for estimation of contact area). Overall, the traditional method allows precision in neither the contact definition nor in the resulting pressure.

Rigid Body modeling inherently uses non-deformable bodies—yet the deformability of the meniscus is clearly essential to its function as a distributor of pressure (Walker and Erkman, 1975; Paletta et al., 1997). Kia and Guess partially solved this problem by dividing the meniscus into segments and then attaching springs (or rather, by defining forces) which hold the segments together (Figure 1.6b). Unfortunately, the

spring parameters are the same for every meniscus segment, regardless of geometry, and based on a finite element solution (Kia, 2011) rather than defined directly from a stress-strain relationship.

These issues with contact and meniscus material properties are addressed in the current work.

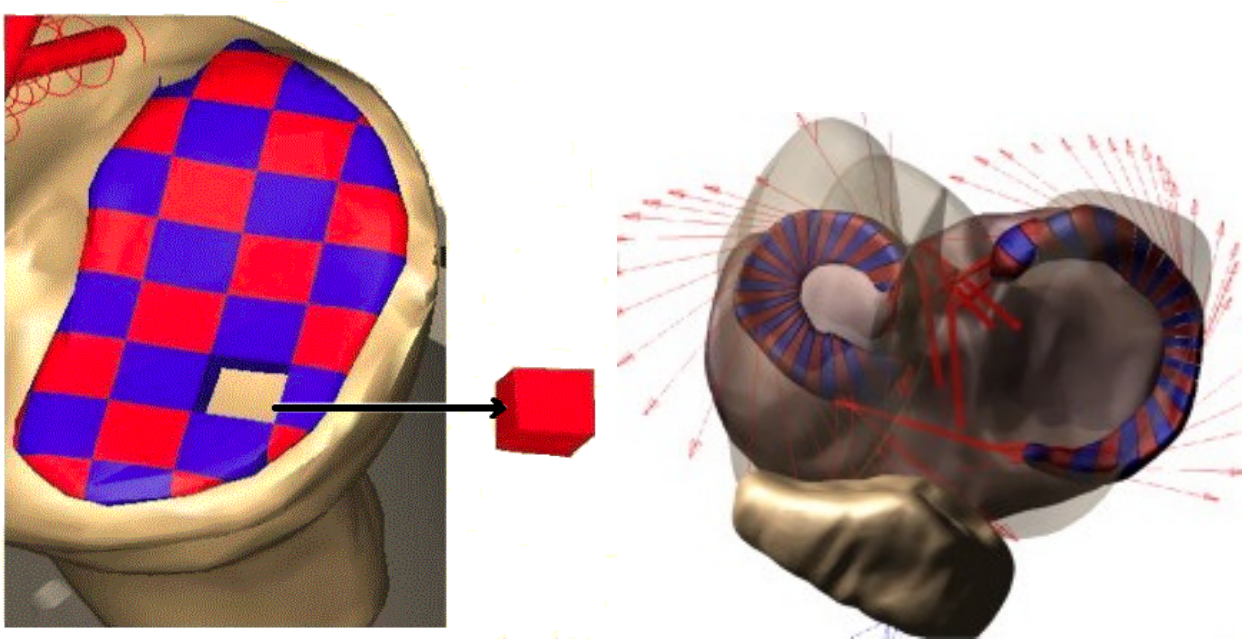

(a) (b)

Figure 1.6: (a) Discretized medial tibial cartilage. Figure from Liu et al. (2009). (b) Discretized menisci allowing for deformation. Figure from Guess et al. (2010).

2 Methods

2.1 Meniscus

2.1.1 Meniscus material parameters

Material parameters for menisci are drawn from Moran (2001) via Fraser (2011)[4] or Erdemir and Sibole (2010) and do not include viscoelastic terms. Although meniscus material properties vary according to region and layer (Tissakht and Ahmed, 1995), this was not implemented. Radial shear and compression/tension is not included in the model and the consequences of this are unknown. Material parameters used are circumferential tension-compression, axial compression, circumferential shear (shear in the plane perpendicular to the circumferential axis), and circumferential torsion stiffness (see Figure 2.1a). Density of the meniscus was estimated as 2.74E-006 kg/mm^3 but this was multiplied by 4 in simulations to reduce high frequency oscillations.

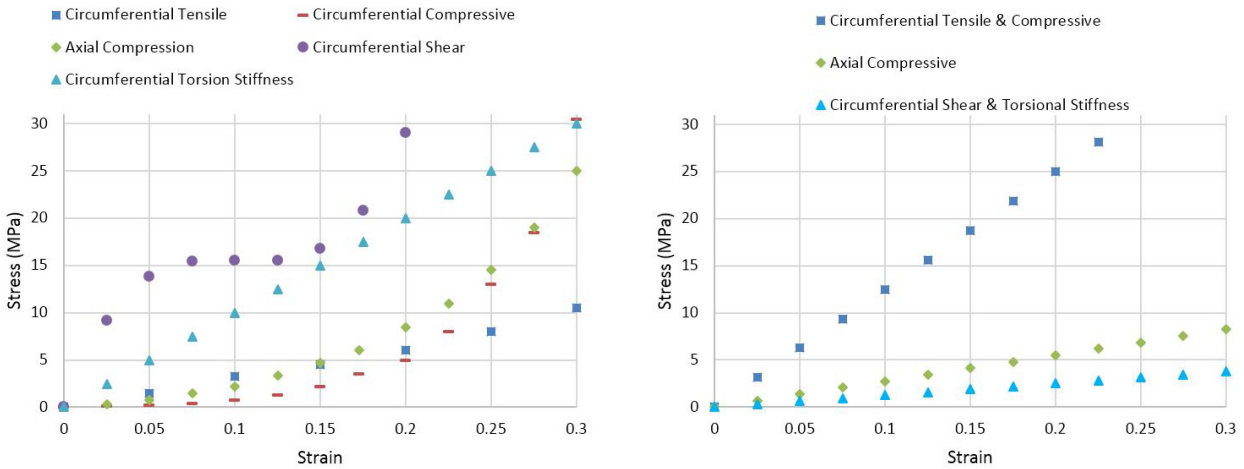

(a) (b)

Figure 2.1: Meniscus material property polynomial approximations from data from (a) Moran (2001) via Fraser (2011) (b) Erdemir and Sibole (2010).

2.1.2 Meniscus attachements

Meniscus attachment at the anterior and posterior horns was modeled by creating a 180 N/mm spring attaching the horn to the tibia (Hauch et al., 2010). Coronary ligaments (LaPrade et al., 2000; Bezerra

[4]Moran was referenced via Fraser because of the difficulty in obtaining Moran's thesis directly. Fraser and Moran both published as students of the University of Edinburgh under professor J.A. McGeough.

et al., 2007), also known as meniscotibial ligaments, were added for numerical stability and approximated by attaching 2N/mm springs to each meniscus segment (one spring for the anterior-posterior axis and one for the medial-lateral axis). Other attachments, such as the transverse and meniscofemoral ligaments, were not included. It should be noted that transection of the meniscofemoral ligaments increased peak contact pressure by ~10% and mean pressure by ~4 to 10% in a cadaver study by Amadi et al. (2008). Thus contact pressures for simulations with the mensicus are probably overestimated in the current study. Haut Donahue et al. (2003), in a FEA DOE analysis, concluded that the transverse ligament and deep MCL are important to knee function, though inclusion of each only decreased the RMSNE (root mean squared normalized error) of their contact results by ~3%.

2.1.3 Segmenting of menisci

A custom-made macro (figure 2.3c) was used to segment the mensici radially using a 15deg increment (Guess, 2012) in order to allow deformation and resulting hoop stresses (see Figure 2.2).

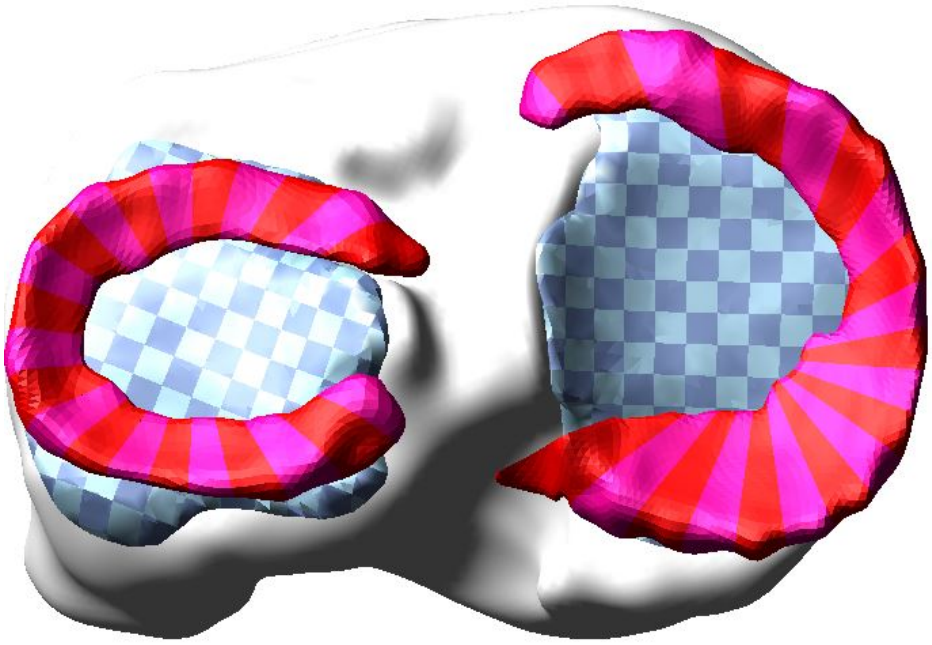

Figure 2.2: Top view showing segmented menisci

2.1.4 Implementation of matertial properties

Once segmentation is complete, another custom-made macro (figure 2.3e) is used to define the material properties through the creation of force and torque equations between adjacent segments. The user inputs the coefficients of polynomials approximating the stress-strain relationships. Damping terms are chosen during creation but may be adjusted later. The material property macro uses force reference markers to orient the forces and torques applied. Figure 2.3d shows a typical force reference marker. The Z-axis is preserved and the Y-axis (circumferential) is oriented perpendicular to the common surface of the two segments of interest (see Figure 2.3d).

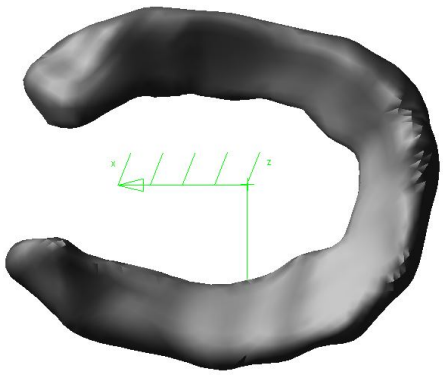

(a)

(b)

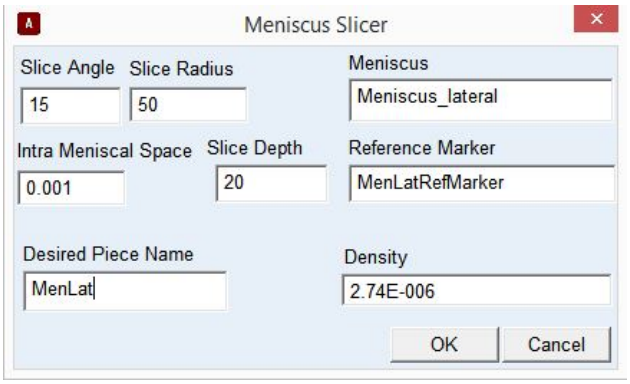

(c)

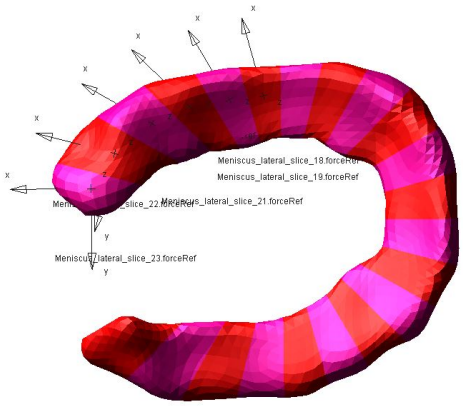

(d)

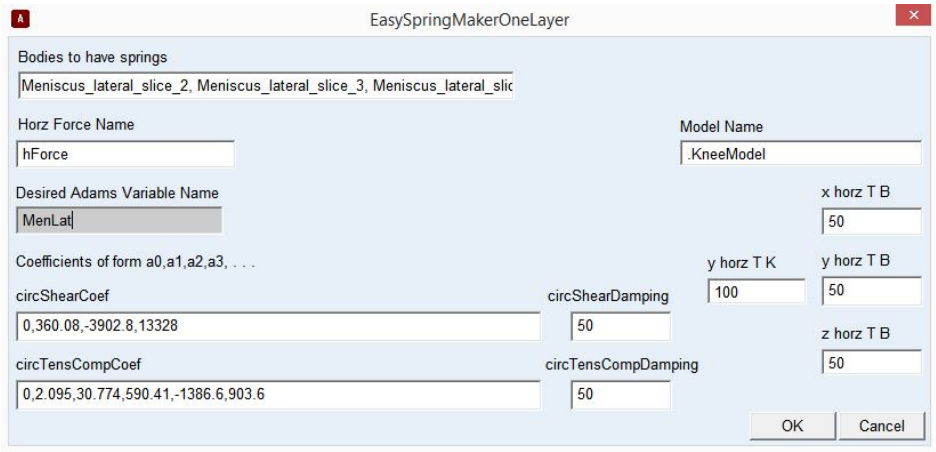

(e)

Figure 2.3: (a) Original meniscus geometry with reference marker. (b) Discretized lateral meniscus (c) Meniscus slicing program. (d) Example of force reference marker orientation. (e) Material property defining program.

Force and torque equations were defined as follows:

Force = Area*Stress(Strain)

Bending torque = Area*Stress(Strain)*Moment_arm

Twisting torque = θ*J*G/L

Where θ is the torsion angle, G is the shear modulus, L is the length of the segment along the axis of torsion, and J is the torsion constant defined by Roark's equation (Young and Budynas, 2002).

$$J \approx a*b^3*\left(\frac{1}{3} - 0.21 * \frac{b}{a} * \left(1 - \frac{b^4}{12 * a^4}\right)\right) \tag{2.1}$$

Where "a" is the length of the long side of the rectangular surface and "b" is the length of the short side.

This approximation of twisting torque seems very reasonable since Paiva (2011) did not find that varying torsional stiffness of the circumferential axis had a significant effect on results.

The value used for area in the equations was found for each segment by using the program-reported inertias to solve for segment dimensions using the formula for inertia of rectangular cuboid $\left(I_i = \frac{1}{12} * m * (I_{i+1}^2 + I_{i+2}^2)\right)$. For a general dimension $dim_i = \sqrt{\frac{6}{mass} * (I_{i+2} + I_{i+1} - I_i)}$. The next section discusses further how the dimensions of the meniscus segments (estimated as if they were cuboids) are used to define meniscus stiffness on a per-segment-pair basis, since forces are defined between adjacent segments. Originally, only circumferential tension was planned to be segment-specific and a cylindrical estimation was selected due to the simplicity of calculating cross-sectional area. However, it was later noted that bending stiffness could also be calculated on a segment-specific basis if the other dimensions of the segment were known since strain could then be calculated. Rather than using a cylindrical estimation which does not account for one dimension being longer (which greatly changes bending stiffness for a given axis), a cuboid estimation was chosen because segment dimensions can still be extracted from inertial data but it can account for varying dimensions of the segments. Use of a wedge shape approximation would have been more accurate but would have complicated calculation of bending strains and torques. Note also that the use of cuboid approximation only pertains to the internal forces of a meniscus and does not affect calculation of contact forces which depend on the actual geometry and a user-supplied thickness parameter.

2.1.5 Derivation of bending strain and torque equations

Note: The following section is original work. However, it is possible that similar work has been done previously since a thorough search of literature was not conducted.

If mensicus segments are represented by rectangular cuboids such as the blue and orange ones shown in Figure 2.4.

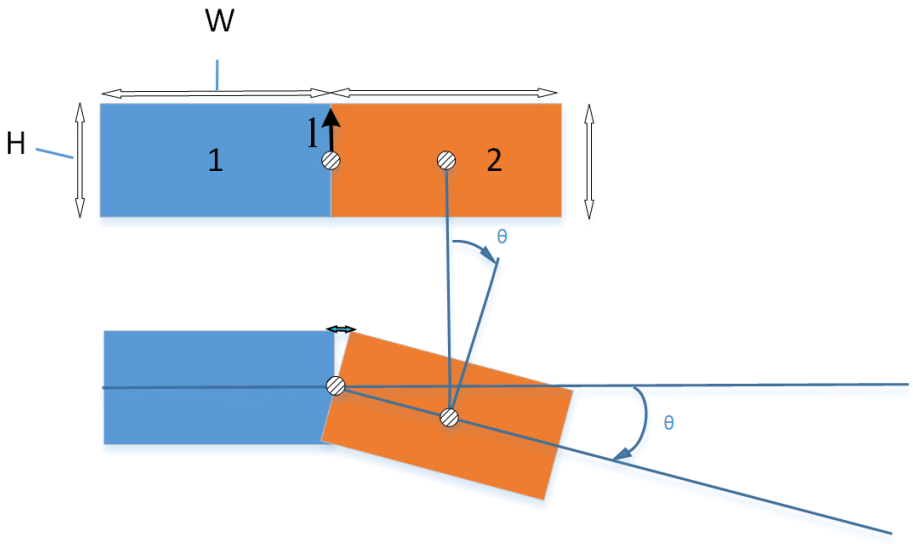

Figure 2.4: Bending Strain Diagram

A change in angle of θ produces a gap between the two cuboids and induces a gap at one end and an overlap at the other. The magnitude of the gap/overlap may be estimated as $w_g = 2 * sin(\theta/2) * l$. Where l is the length from the point which experiences no translation due to the rotation to the location of interest along the midline of the gap/overlap. Thus the strain is $\varepsilon = w_g/(w_1 + w_2)$, where w_1 and w_2 are the widths of the two rectangular cuboids (see Figure 2.4) and the differential force produced is $dF = \sigma(\varepsilon) * dA$. Where $\sigma(\varepsilon)$ is stress as a function of strain and $dA = D * dl$, where D is the average depth of the cuboids. So then the negative of differential torque is

$$-dT = l * dF = l * \sigma(\varepsilon) * dA = l * \sigma(\varepsilon) * D * dl \tag{2.2}$$

$$-\int dT = \int l * \sigma(\varepsilon) * D * dl \tag{2.3}$$

$$-T = \int l * \sigma(\varepsilon) * D * dl = D * \int l * \sigma(\varepsilon) * dl \tag{2.4}$$

Where T is torque, and l ranges from 0 to the half the average height of the two cuboids.

$$-T = D * \int_0^{H_{ave}/2} \sigma(\varepsilon) * l * dl \tag{2.5}$$

$$-T = D * \int_0^{-\frac{H_{ave}}{2}} -\sigma_c(\varepsilon) * l * dl + D * \int_0^{\frac{H_{ave}}{2}} \sigma_t(\varepsilon) * l * dl \tag{2.6}$$

Where $\sigma_c(\varepsilon)$ and $\sigma_t(\varepsilon)$ are the compressive and tensile stress-strain functions defined by user-input polynomials with order k and coefficients a and b, respectively.

$$\sigma_c(\varepsilon) = \sum_{n=0}^{k} a_n * \varepsilon^n \tag{2.7}$$

$$\sigma_t(\varepsilon) = \sum_{n=0}^{k} b_n * \varepsilon^n \tag{2.8}$$

The torque equation is simplified as follows.

$$\varepsilon = \frac{2 * sin(\theta/2)}{w_1 + w_2} * l \tag{2.9}$$

$$l = \varepsilon * \frac{w_1 + w_2}{2 * sin(\theta/2)} \tag{2.10}$$

$$-T = D * \int_0^{-\frac{H_{ave}}{2}} -\sigma_c(\varepsilon) * \varepsilon * \frac{w_1 + w_2}{2 * sin(\theta/2)} * dl + D * \int_0^{\frac{H_{ave}}{2}} \sigma_t(\varepsilon) * \varepsilon * \frac{w_1 + w_2}{2 * sin(\theta/2)} * dl \tag{2.11}$$

$$\frac{d\varepsilon}{dl} = \frac{2 * sin(\theta/2)}{w_1 + w_2} \tag{2.12}$$

$$dl = \frac{(w_1 + w_2) * d\varepsilon}{2 * sin(\theta/2)} \tag{2.13}$$

$$\varepsilon_1 = \frac{2 * sin(\theta/2)}{w_1 + w_2} * \frac{H_{ave}}{2} = \frac{H_{ave} * sin(\theta/2)}{w_1 + w_2} \tag{2.14}$$

$$-T = D * \left(\frac{(w_1 + w_2)}{2 * sin(\theta/2)}\right)^2 * \left(\int_0^{-\varepsilon_1} -\sigma_c(\varepsilon) * \varepsilon * d\varepsilon + \int_0^{\varepsilon_1} \sigma_t(\varepsilon) * \varepsilon * d\varepsilon\right) \tag{2.15}$$

$$-T = D * \left(\frac{(w_1 + w_2)}{2 * sin(\theta/2)}\right)^2 * \left(\int_0^{-\varepsilon_1} -(\sum_{n=0}^{k} a_n * \varepsilon^n) * \varepsilon * d\varepsilon + \int_0^{\varepsilon_1} (\sum_{n=0}^{k} b_n * \varepsilon^n) * \varepsilon * d\varepsilon\right) \tag{2.16}$$

$$-T = D * \left(\frac{(w_1 + w_2)}{2 * sin(\theta/2)}\right)^2 * \left(\left[\sum_{n=0}^{k} -\frac{a_n}{n+2} * (-\varepsilon_1)^{n+2} + 0\right] + \left[\sum_{n=0}^{k} \frac{b_n}{n+2} * (\varepsilon_1)^{n+2} - 0\right]\right) \tag{2.17}$$

$$-T = D * \left(\frac{(w_1 + w_2)}{2 * sin(\theta/2)}\right)^2 * (-\varepsilon_1)^2 * \left(\left[\sum_{n=0}^{k} -\frac{a_n}{n+2} * (-\varepsilon_1)^{n}\right] + \left[\sum_{n=0}^{k} \frac{b_n}{n+2} * (\varepsilon_1)^{n}\right]\right) \tag{2.18}$$

Then, using equation 2.14

$$-T = D * \frac{H_{ave}^2}{4} * \left(\left[\sum_{n=0}^{k} -\frac{a_n}{n+2} * (-\varepsilon_1)^{n}\right] + \left[\sum_{n=0}^{k} \frac{b_n}{n+2} * (\varepsilon_1)^{n}\right]\right) \tag{2.19}$$

If the user specifies the same polynomial coefficients (c_n) for compression and tension, the equation simplifies further:

$$-T = D * \frac{H_{ave}^2}{2} * \left(\sum_{n=1,3,\ldots}^{k} \frac{c_n}{n+2} * \varepsilon_1^n\right) \tag{2.20}$$

2.1.6 Verification and validation of implementation

All equations used in the defining the forces inside the meniscus were validated by testing each individual degree of freedom with either a 100N force or 100N*mm torque. The resulting simulation strain/angle was used to backsolve for the applied force/torque. The predicted force/torque matched the applied force to within a tenth of one percent for all cases.

In order to show that the present ADAMS meniscus implementation is valid on a larger scale and produces results similar to those obtained using FE methods, the lateral meniscus was isolated and its horn positions locked. A tension-producing velocity of 2mm/sec oriented at 0.1597 radians anterior to the medial-lateral axis was then applied to a middle element and forces at the horns recorded (see Figure). An FEBio model[5] using the same base geometry was then implemented with a cubic mesh of size 2.045 ± 0.345 mm (mean ± SD) and both results are shown in Figure 2.6. The FEBio meniscus was defined as a homogeneous linear elastic transversely-isotropic materials with material parameters from Erdemir and Sibole (2010)(see Table 2.1). The Adams meniscus was defined using a circumferential modulus of 125MPa and a circumferential shear[6] modulus of 12.5MPa[7]. Using the FEBio results as baseline, the mean percent error and standard

[5] **FE work was graciously done by Dr. Jerome Hausselle.**

[6] Shear which happens perpendicular to the circumferential axis.

[7] There is a discrepency between the value of the shear modulus reported in Erdemir and Sibole (2010) and the value calculated (10.34) using the equation provided. Yao et al. (2006), who Erdemir et al. references as the material properties source, only provides the equation.

deviation of the resultant x-force in the anterior and posterior horns, of the Adams meniscus, is +18.9 ± 11.7% and -6.2 ± 6.7%. respectively. Figure 2.6 shows results of the drawer test for FEBio and Adams.

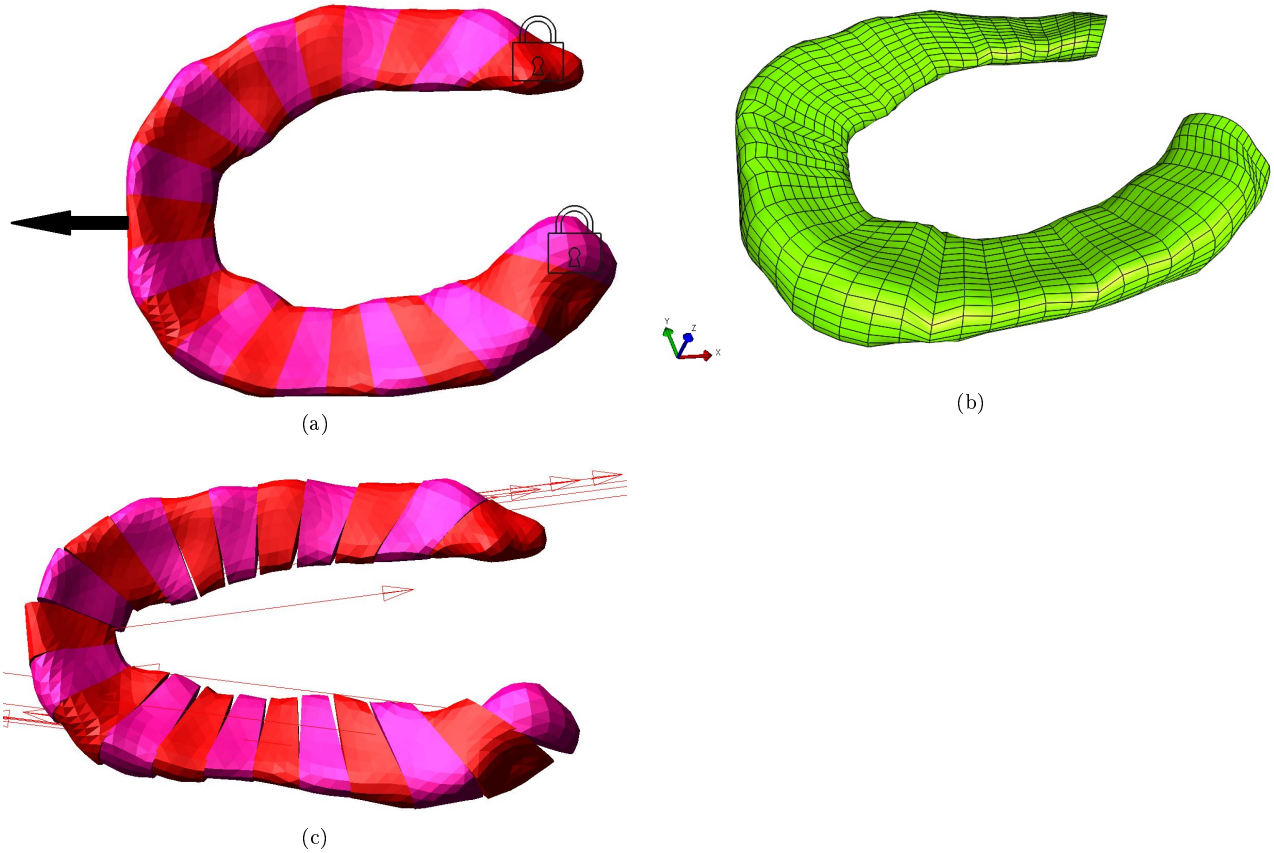

(a) (b) (c)

Figure 2.5: (a) Drawer test configuration of the Adams meniscus. (b) Picture of FEBio meniscus. (c) Adam meniscus at 5mm extension.

Table 2.1: Material properties used for FEBio meniscus from Erdemir and Sibole (2010).

Density	E_1	E_2	E_3	v_12	v_23	v_31	G_12	G_23	G_31
1.5e-9	125.0	27.5	27.5	0.1	0.33	0.1	2.0	12.5	2.0

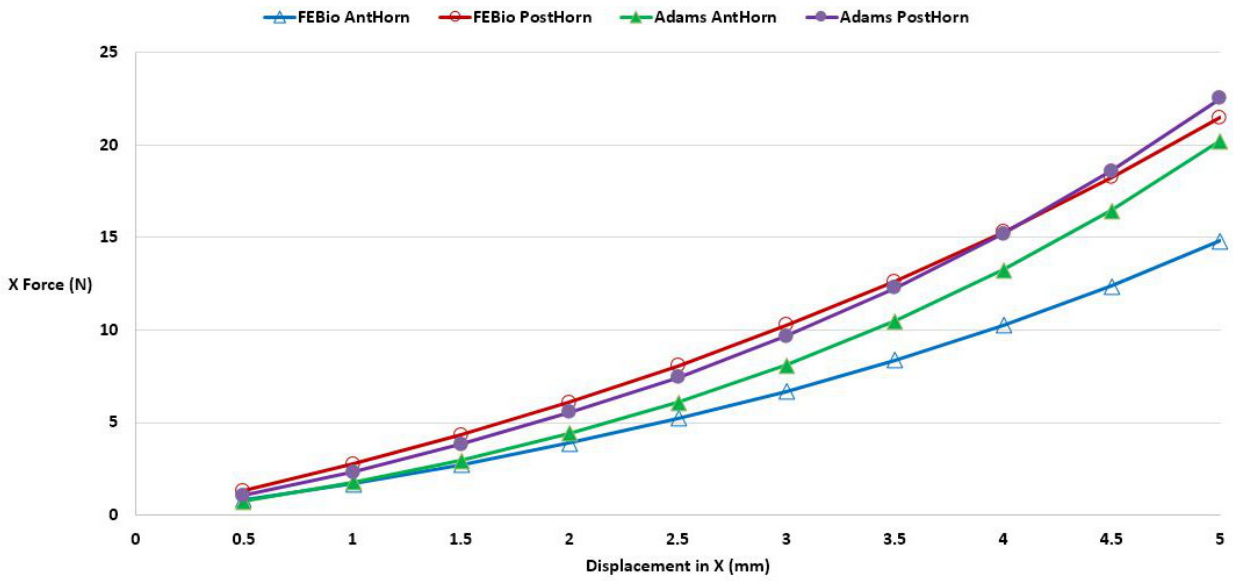

Figure 2.6: Lateral meniscus horn force in Adams vs. FEBio

2.2 Contact modeling

Rather than using the default Adams contact formulation, which neglects the area of contact, a custom subroutine was created. This subroutine utilizes the area of contact and user-supplied thickness of the contacting bodies to produce a stress-strain relationship based on user-supplied third-order polynomials describing the stress-strain characterstics of the two geometries of interest. The subroutine takes the two stress-strain polynomials and solves for the "strain" experienced by one body given the penetration depth. This is possible since the contact area and resultant force is equal for both bodies. The solved strain is then input into one of the stress-strain equations and multiplied by the contact area to produce the contact force reported to Adams. The technique is summarized in Figure 2.7.

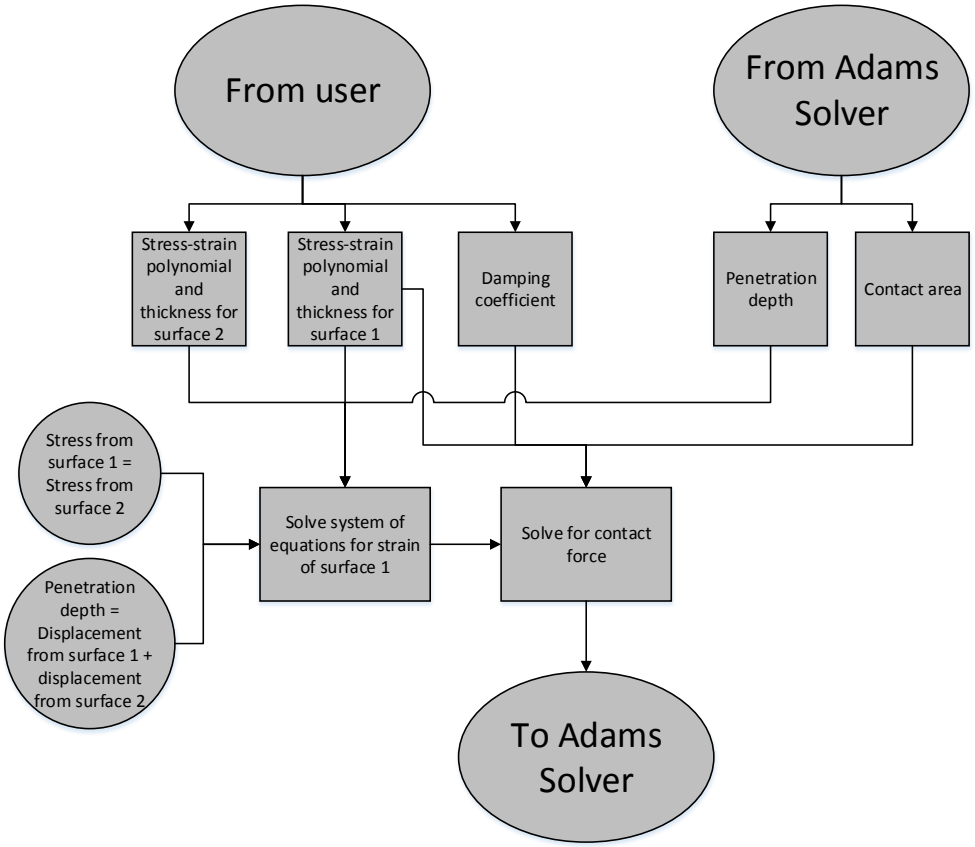

Figure 2.7: Contact subroutine technique

An advantage of using cubic polynomials is that a large variety of curves may be approximated. Thus it becomes simple to change between experimental results from different studies even when the user only has access to fitted equations. The cubic polynomials chosen for Tibial and Femoral cartilage were designed to match the transversely isotropic eight-chain network of freely jointed chains (TI) model equations of Femoral and Tibial stress-strain which best matched experimental results in Deneweth (2013). Implementation of regional variance is very similar to the recommendation of Deneweth (2013): the difference being that cartilage-to-cartilage contact is always assumed to have cartilage properties of the central region in the current study. This seems reasonable since the periphery with different region properties is covered by the menisci. The cubic polynomial chosen for meniscus was designed to match stress-strain results from Moran (2001) via Fraser (2011). The base equation is Equation 2.21 and theparameters for each contact surface are listed in Table 2.2. McCann et. al. report a frictional coefficient of ~0.02 with meniscus and ~0.05 without

for bovine samples at a load of 250N (McCann et al., 2009). A dynamic friction coefficient of 0.02 was chosen and a static friction coefficient of 0.04 for purposes of stability. For simulations which utilize regional variance in cartilage properties, the average of thicknesses reported by Shepherd and Seedhom (1999) was used. Meniscus thickness was graphically estimated for regional simulations. However, note that in actual implementation, the thickness reported in Table 2.2 was halved since the meniscus experiences deformable contact from both the femoral and tibial cartilage.

$$Stress = CR * (C1 * strain + C2 * strain^2 + C3 * strain^3) \tag{2.21}$$

Table 2.2: Contact parameters

		CR	C1	C2	C3	Height (mm)
Moran Meniscus	Med. Side and Post.	1	24.732	129.94	1071.6	3.5
	Med. Ant.	1	24.732	129.94	1071.6	3.0
	Lat. Side and Post	1	24.732	129.94	1071.6	3.0
	Lat. Ant.	1	24.732	129.94	1071.6	2.5
Erdemir Meniscus	Med. Side and Post.	1	27.5	0.002	0.003	3.5
	Med. Ant.	1	27.5	0.002	0.003	3.0
	Lat. Side and Post	1	27.5	0.002	0.003	3.0
	Lat. Ant.	1	27.5	0.002	0.003	2.5
Tibial Cart	Med. Direct	0.10551	37.893	360.76	3904.9	2.59
	Med. Covered Side and Post.	0.36264	37.893	360.76	3904.9	1.981
	Med. Covered Ant.	0.18595	37.893	360.76	3904.9	1.981
	Lat. Direct	0.10675	37.893	360.76	3904.9	2.59
	Lat. Covered Side and Post.	0.28575	37.893	360.76	3904.9	1.981
	Lat. Covered Ant.	0.12613	37.893	360.76	3904.9	1.981
Femoral Cart	Med.	0.540	26.418	144.77	2067.2	2.143
	Lat.	0.637	26.418	144.77	2067.2	2.143

2.3 Modeling of ligaments, soft tissues, and bones

2.3.1 Ligaments, muscles, and other soft tissues

Traditional ligaments are not included in this model becuase anterior-posterior, flexion-extension, and internal-external rotation displacements are directly defined from published values. Although rarely modeled, many other soft tissues besides the four traditional ligaments (PCL, LCL, ACL, MCL), are involved in knee biomechanics (the often ignored popliteofibular ligament is important for passive knee stability (Shahane et al., 1999)). Medial-lateral and proximal-distal tibial translations are the only implicitly determined

degrees of freedom of the model. Inclusion of traditional ligaments might impact these two DOF, but inclusion of ligaments while excluding muscles *assumes passive motion*. Thus, addition of traditional ligaments would complicate the model while providing very limited improvment in clinically relevant kinematics and pressure imformation. Inclusion of major muscles is a complex task since, like ligaments, muscles interact with each other and with bony geometry; but also because individual muscle forces are not well established: static optimiztion (Adouni and Shirazi-Adl, 2014) and EMG-driven models (Winby et al., 2013) being common methods to estimate muscle forces in light of this problem. Although the computational efficiency of rigid-body modeling lends itself to optimization problems and the present model may well be updated in the future for this purpose, addition of major ligaments and muscles is beyond the scope of the current study.

2.3.2 Bones and cartilage

Bones and cartilage are modeled as rigid. Bone rigidity seems a benign assumption since bone stiffness is orders of magnitude higher than cartilage and meniscus. Furthermore, driving kinematics are experimental measurements of bone movements close to the joint. The assumption of rigid cartilage is mostly irrelevant since overlap between cartilage geometries is allowed during contact. Though this means the model cannot accurately account for shear stresses within cartilage and distribution of load due to surface tension. This means that forces are not distributed as evenly as occurs physiologically and contacts with small area ought to be stiffer, than is actually implemented, due to surrounding tissue.

2.4 Simulations

Specimen information for the M1 and M2 models may be found in Table 2.3. Image aquisition data for the M1 model is recorded in Table 2.4. For the M1 model, the total potential contact area on the medial side was estimated as 1194mm^2 and the lateral side as 1045mm^2. The M2 model was constructed using geometries supplied by the Open Knee Project via SimTK.org. Additional details of image aquisition for the M2 model geometries may be found inErdemir and Sibole (2010). For the M2 model, the total potential contact area on the medial side was estimated as 1078mm^2 and the lateral side as 1037mm^2.

Table 2.3: Specimen information

Model	M1	M2
Side	Left	Right
Age	43	70
Weight		77.1kg
Height		1.68m
Gender	Male	Female
Cause of Death	Respiratory failure	Pneumonia/Cancer

Table 2.4: Image aquisition data for model geometries

Model	M1	M2
Tesla	3	1.0
TR	5	30
TE	14.1	6.7
FOV	150*150	150*150
Slice Thickness	0.6mm	1.5mm

2.4.1 Computational settings

Simulations were run on a Dell OptiPlex 990 with Windows 7 Enterprise SP1, a 3.4GHz Intel Core i7-2600 CPU, and 16.0 GB of RAM. The graphics card was a ATI Radeon HD 4670 with 1GB memory. The version of Adams was 2013.0.1 and the units used were mm, kg, N, ms, deg, and Hertz. The Adams solver was set to run with 6 threads using the default contact library with a faceting tolerance of 1000. The integrator used was HHT, formulation I3, with a tolerance of 1.0E-005 and interpolation off. The graphics display option was turned off to improve simulation time. An output step size of 1ms was selected.

2.4.2 Stand simulations

For stand simulations, all degrees of freedom were constrained except vertical displacment. Freeing varus-valgus was considered to account for possible misalignment, but preliminary simulations with varus-valgus free did not show contact area and average pressure results grealty different from constrained simulations. Vertical loads (see Figure 2.8) were applied to the tibia using the Adams "STEP" function which was used to smooth the transition from zero load to final load in the first 10 milliseconds. Each simulation was allowed to run for 50 milliseconds to ensure convergence to a steady state solution.

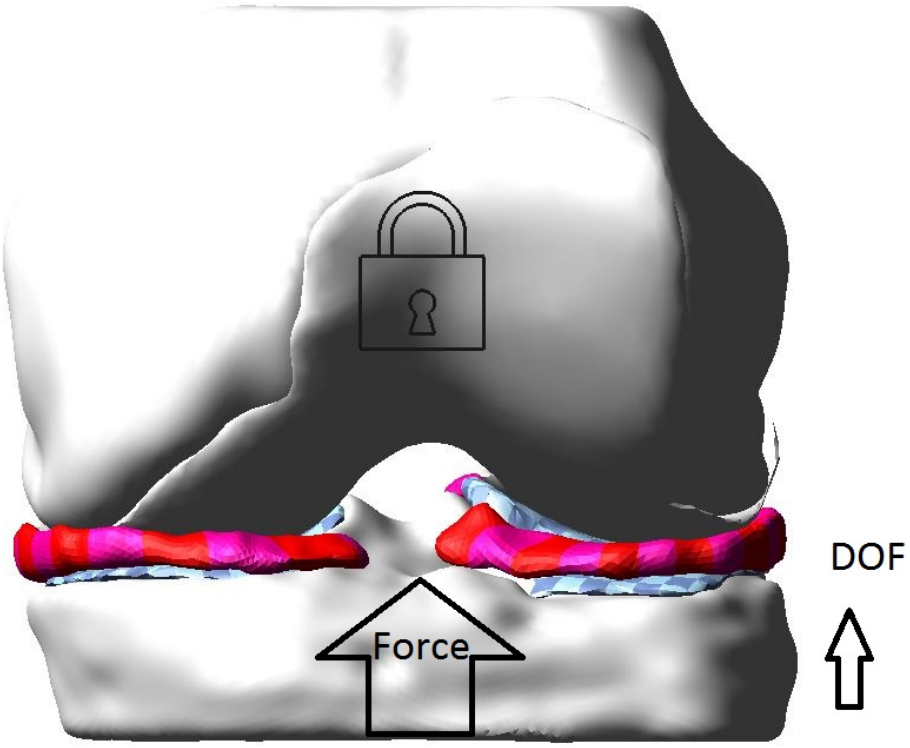

Figure 2.8: Setup of Stand Simulations

2.4.2.1 Contact formulation comparison To allow for comparison to traditional methods, three different contact formulations were used and all used a cartilage grid piece size of 3x3mm.

A) Linear Impact (Impact120): Uses the standard Adams impact function to produce 120N per mm of penetration for each grid piece experiencing contact.

B) Nonlinear Impact (Impact50): Uses the standard Adams impact function (see Equations 1.1 and 1.2) with k = 50 and e = 1.8.

C) Deneweth (Cubic): Uses a custom subroutine to produce regionally-varying material properties similar to those defined in Deneweth (2013) with cubic extrapolation past 15% strain.

2.4.2.2 Meniscus property comparison FE programs commonly use linear material properties for the meniscus. This simulation set compares nonlinear experimental results (Moran) to a common linear FE implementation (Erdemir).

A) Meniscus material properties from Moran (2001).

B) Meniscus material properties from Erdemir and Sibole (2010).

2.4.3 Gait simulations

For Gilbert gait simulations, vertical loading as defined in Gilbert et al. (2014) (see Figure 2.11) was applied at the geometric centroid of the truncated bony tibia (see location of Reference Marker in Figure 2.9). The orientation of the anterior-posterior and medial-lateral axes (shown in Figure 2.9), and thus the tibial rotation axis, was designated by rotating the long axis of the Magnetic Resonance Imaging (MRI) coordinate system until the medial-lateral axis was parallel to a line connecting the geometric centers of the medial and lateral femoral condyles (see figure 2.10). Rotation of the tibia was applied at the midpoint of the medial and lateral tibial eminences. Anterior-posterior translation and internal-external rotation were constrained to match motion results from Gilbert et al. (2014). Anterior-posterior translation in Gilbert et al. (2014) is measured from the midpoint of the femoral collateral attachments to the midpoint of the tibial collateral attachments. Medial-lateral translation and varus-valgus rotation were free in order to match the experimental setup of Gilbert et al. (2014). Flexion-extension as defined in Gilbert et al. (2014) was applied to the femur with the axis of rotation being defined by a line connecting the attachments of the collateral ligaments. For Benoit motions, the MRI position was used as the initial position at 0% stance phase. For Gilbert motions, the MRI position was used as the zero reference. For gait simulations, the model was enhanced by reducing the stiffness of the posterior horns from 180N/mm to 100N/mm (Hauch et al., 2010) and the stiffness of the coronal ligament of the mensicus segment closest to the medial collateral attachment was increased to 10N/mm.

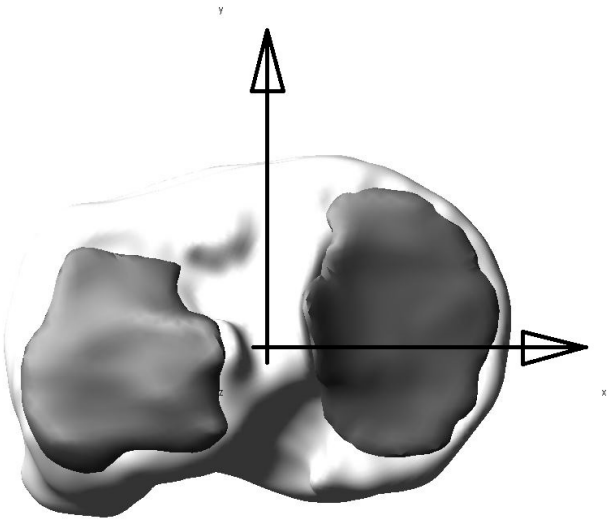

Figure 2.9: Reference frame for motions.

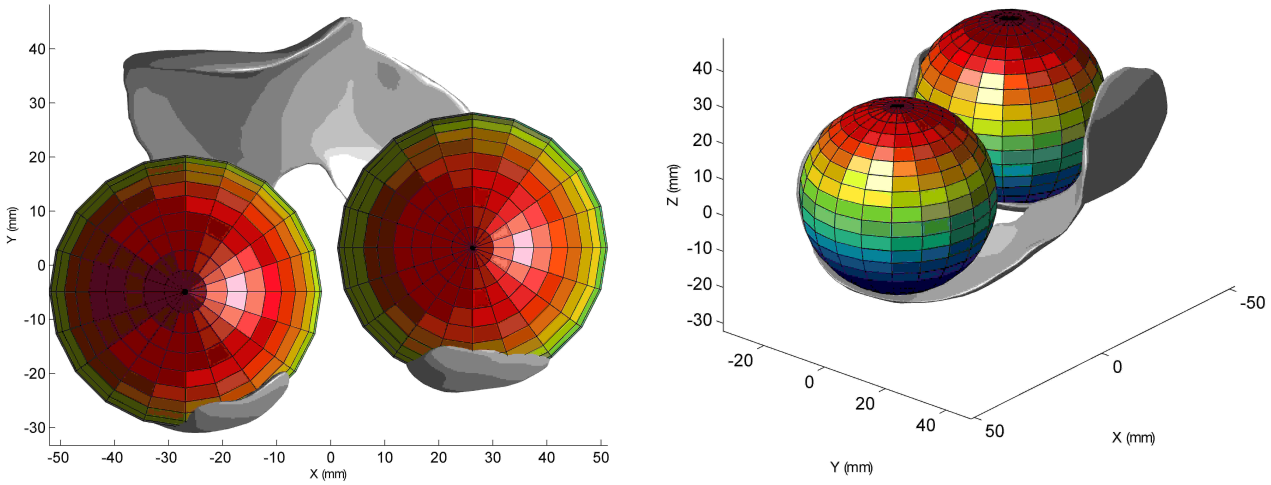

(a) (b)

Figure 2.10: (a) Top view of femoral condyle geometric centers. (b) Isometric view of femoral condyle geometric centers.

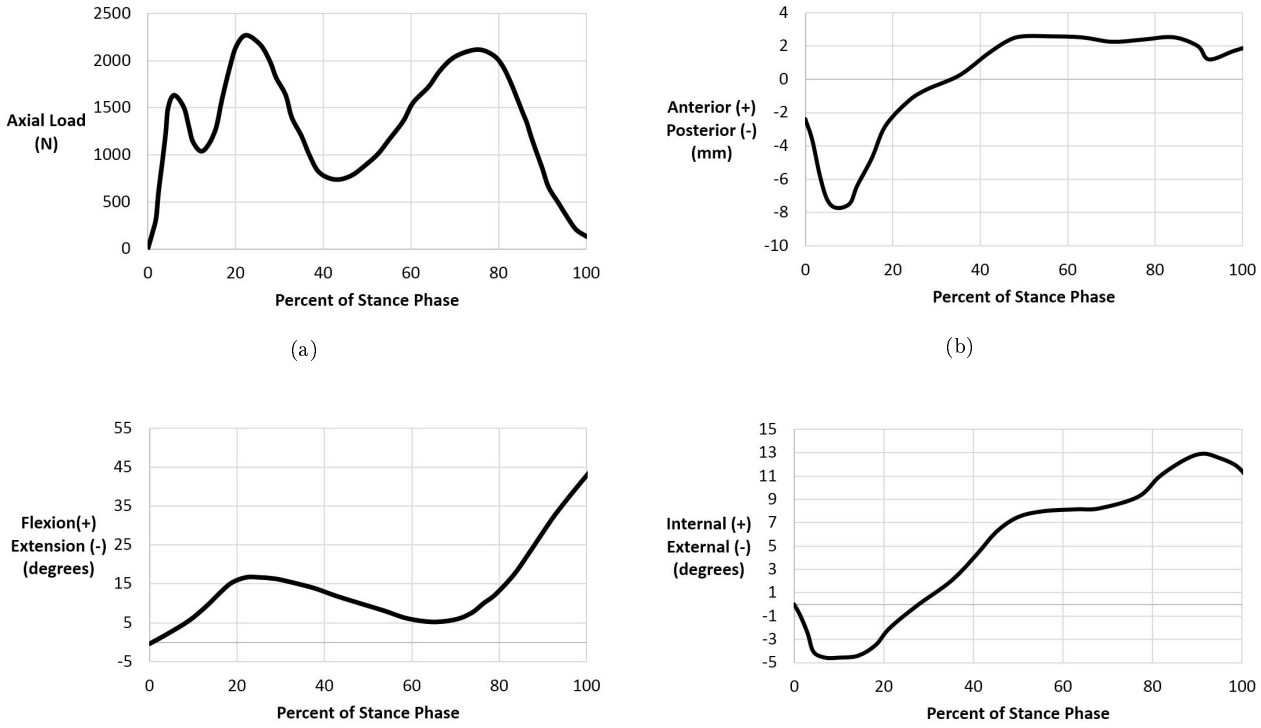

Figure 2.11: (a) Axial loading (b) Anterior-posterior tibial translation (c) Flexion-Extension (d) Internal-external tibial rotation as defined in Gilbert et al. (2014).

2.4.4 Clinical application

As a preliminary investigation of contributing factors to osteoarthritis, cartilage properties of five seperate cadaver knees as reported in Deneweth (2013) were implemented in gait simulation and the peak pressure throughout gait compared. The knees used were numbers 1,3,5,6, and 7. Knee 2 and knee 4 were excluded from this study because at least one CR value for the central cartilage region is not reported. For knee 6 and knee 7, the CR of cartilage in the anterior region on the medial plateau was not reported and therefore values from the lateral plateau were used. For those planning to use knee-specific femoral cartilage properties as reported in Table 7.3 of Deneweth (2013), be aware that the condyle lateral weight bearing (L WB) and condyle medial low weight bearing (M LWB) columns are switched. This was confirmed in personal correspondence with Jessica Deneweth. For the purpose of clarity, table 2.5 shows the correct CR values for M WB and L WB which were also used in this study.

Table 2.5: Femoral material property CR values of knees K1-K7 adapted/corrected from Deneweth (2013).

	CONDYLES			
Knee	M WB	M LWB	L WB	L LWB
1	0.228	0.335	0.270	0.707
2	0.504	0.614	0.617	1.465
3	1.620	2.163	1.658	1.862
4	0.215	0.375	0.208	0.543
5	0.598	0.535	0.439	0.634
6	0.358	0.595	0.657	1.008
7	0.256	0.483	0.607	0.332

3 Stand Simulations Results & Discussion

NOTE: It was observed at a late date that the M2 model may not be in a neutral position but rather somewhere around 18deg of flexion. However, adjusting flexion to test this possibililty caused load to be applied soley on the lateral side. Without ligaments it was impractical to attempt to reach true "stand" initial conditions and therefore there was no reference simulation for interrpreting current results in light of a potential 18deg of flexion. However, experiments by Lee et al. (2006) at 30deg flexion show around a 15% decrease in contact area and 30% decrease in peak and average pressure compared to 0deg of flexion for the medial compartment with intact meniscus. Without meniscus, contact area at 30deg flexion decreased by around 30% and peak and average pressure decreased by around 15%.

Pressure maps shown have been interpolated on a 1mm grid for clarity; for non-interpolated pressure maps, see Appendix 6.1.2.2. Simulation times ranged from about 2sec to 5min, with ~100X increase caused by addition of the menisci and a small increase observed from applying higher load. Defining meniscus contact between non-discretized cartilage while retaining discretized cartilage for tibio-femoral contact increased simulation speed by 4X.

3.1 Contact method comparison: Linear Impact, Nonlinear Impact, Cubic

3.1.1 Intramodel comparison

Cubic (Deneweth) simulations showed medial-lateral force distribution within 2% of the total applied load compared to the nonlinear Impact formulation (see Figure 3.1a). Linear impact formulation medial-lateral distribution differed from Deneweth simulations with 14% redistribution of the total applied load at 500N and 6% at 1000N. The linear formulation shows very different distribution of load compared to nonlinear formulations and the physiological response of cartilage for low strains is linear (Figure 6.8 in Deneweth 2013). However, the linear distribution may be less reliable for 500N load since linearity is reasonable for strains less than 8%, which corresponds to around 0.5MPa and excess of 2.5MPa peak pressure was found. However, since both nonlinear formulations are fitted equations, they may underestimate relatively low stress at low strains. Thus a true distribution may be somewhere in between linear and nonlinear results for a load of 500N.

Peak pressures had average standard deviation of 0.67MPa, ranging from 47 to 18% of the mean peak pressure, for the medial plateau and 0.89MPa, ranging from 40 to 20% of the mean peak pressure, for the lateral plateau, between methods, with linear Impact formulation (120N/mm) giving the highest pressures and non-linear Impact giving the lowest (see Figure 3.1d).

Medial contact areas show a logarithmic progression for all simulation types but lateral contact areas show

parabolic, linear, and logarithmic progression (see Figure 3.1b). Average pressure on the medial plateau was very similar for all simulations, with 500N and 1000N simulations showing a 0.05MPa maximum difference and 1500N simulations showing 0.1MPa; both differences being smaller than 10% of the lowest pressure value. However, the average pressure range on the lateral plateau was 0.31MPa (500N), 0.38MPa (1000N), and 0.66MPa (1500N); these ranges being 41%, 30%, and 38% of the lowest pressure value (see Figure 3.1c). The increased variance on the lateral side compared to the medial is postulated to be from either the geometry of the medial side, in general or for this specific specimen, or from the intial position/orientation of the tibia relative to the femur since only motion in the axial degree of freedom was allowed, or a combination thereof.

Table 6.1 in Appendix 6.1.1 gives further numerical results.

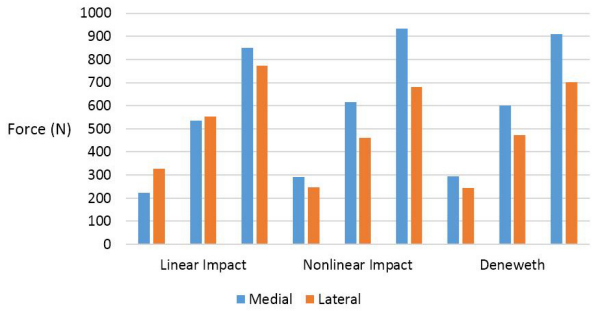

(a) Contact force in simulations without menisci

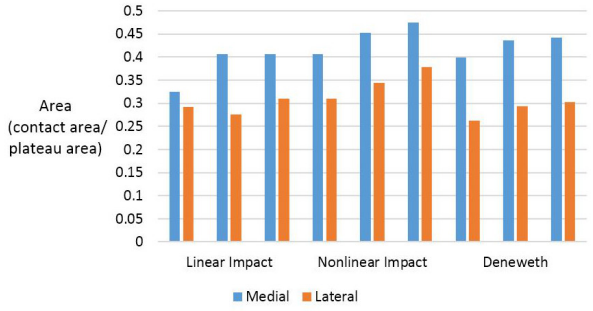

(b) Contact area in simulations without menisci

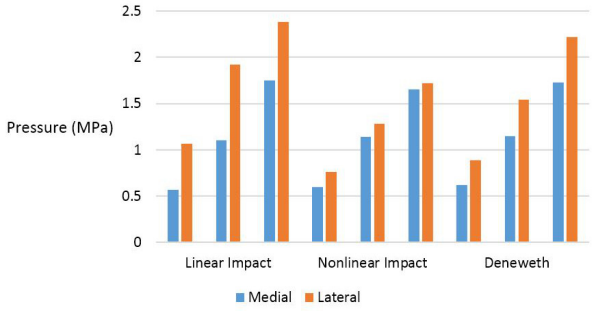

(c) Average pressure in simulations without menisci

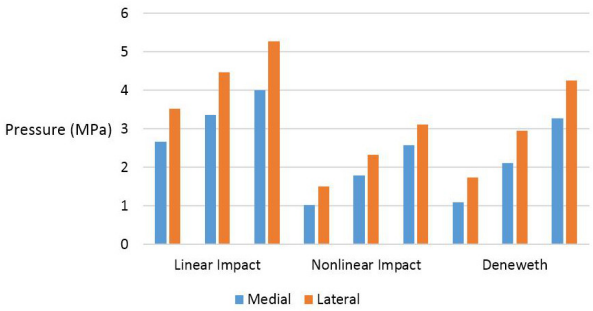

(d) Peak pressure in simulations without menisci

Figure 3.1: Comparison of contact formulation without menisci for loads of 500, 1000, and 1500N for (a) Contact force (b) Contact area (c) Average pressure (d) Peak pressure.

3.1.2 Comparison to experimental studies in literature

Fukubayashi and Kurosawa (1980) and Kurosawa et al. (1980) did not retain ligaments and fully constrained

each knee. Cartilage properties reported by Deneweth (2013) are all derived from experimental testing of cadaver knees of female individuals who died from cancer. Results by Fukubayashi and Kurosawa (1980) and Kurosawa et al. (1980) are derived from experimental testing of knees amputated because of cancer or vascular insufficiency in the limb, gender was not reported.

The linear impact formulation gives results closest to experimental reports and nonlinear impact giving the furthest (see Figure 3.2). However, all formulations show indications of being too soft. This is especially evident for contact area at 500N load. Despite this, average pressure for all contact formulations was within 1.5 standard deviations of experimental results. The author is not aware of a particular reason why the Cubic contact formulation constructed from stress-strain data from Deneweth (2013) is more stiff than the nonlinear formulation found by FEA optimization by Guess et al. (2013). Nor is the author aware of a particular reason why the linear formulation, which is based on combined tibial-femoral cartilage depth of 8mm (Guess et al., 2013), is more stiff than the cubic formulation.

Regarding the cubic formulation, contact area in the M1 model without menisci was 81% and 51% higher on the medial side and 54% and 22% higher on the lateral side under respective loads of 500N and 1000N compared to Fukubayashi and Kurosawa. This was coupled with corresponding decreases in average stress of 46%, 34%, and 28% for loads of 500N, 1000N, and 1500N. Peak pressure was reduced by 43% for a load of 1500N compared to Kurosawa et al. (1980).

For further numerical results, see Table 6.2 in Appendix 6.1.1.

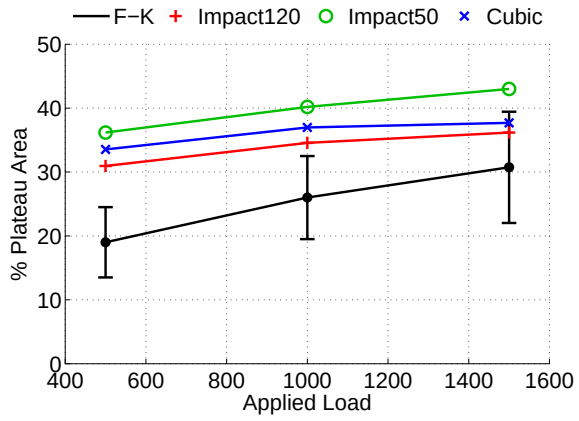

(a)

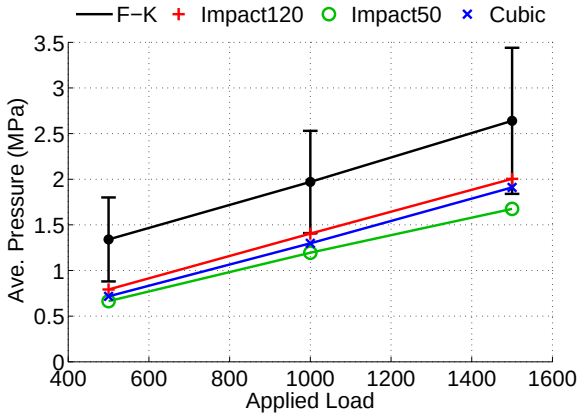

(b)

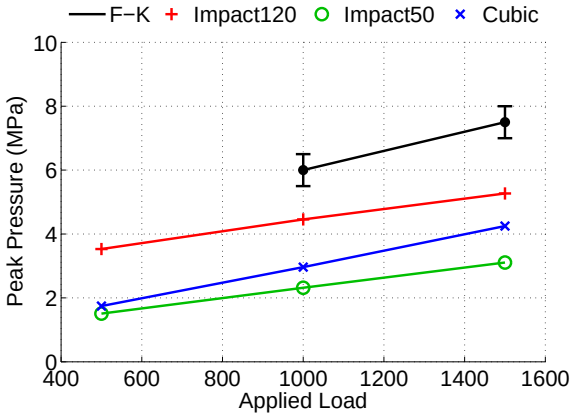

(c)

Figure 3.2: Comparison of M1 results to experimental (Fukubayashi–Kurosawa), without menisci, using cubic formulation for (a) % plateau area (b) Average pressure (c) Peak pressure.

3.1.3 Conclusion

While formulations show difference among themselves (linear formulation showing the greatest difference in peak pressure) the general trend compared to experimental results is the material parameters being too soft. Since the linear formulation is the stiffest, it shows the best agreement with experimental results for peak pressure, being 25% stiffer at 1000N and 13% stiffer at 1500N than the cubic formulation relative to experimental results. The difference between the linear and cubic formulations relative to experimental results for contact area is less than 5% on the medial side and less than 31% on the lateral. The average pressure difference between cubic and linear formulations is 5% or less relative to experimental values. Since

the response of cartilage is known to be nonlinear, especially at high strains (Deneweth, 2013; Brown et al., 2007), and the cubic method is developed in this work, the cubic method was selected for the work described in the following sections.

3.2 Menisci material property comparison: Moran, Erdemir, No Menisci

3.2.1 Intramodel comparison

With Moran meniscus properties, peak pressures were reduced by about 27% for loads of 500N and 20% for loads higher than 500N, compared to simulations without menisci (see Figure 3.3). Simulations with Erdemir meniscus properties showed peak pressure reduction of 35% for loads of 500N and 27% for higher loads. Both Moran and Erdemir menisci tended to reduce average pressures around 40%, with more effect as load increased (see Figure 3.3c).

Medial and lateral differences due to mensicus addition were more pronounced, with contact area being increased approximately 54% medially and 82% laterally. Overall, the effect of the meniscus in increasing contact area increased with increasing load; this effect being approximately twice as prominent on the lateral side compared to the medial. For both Moran and Erdemir stand simulations, distribution of force with respect to medial and lateral was within 6% of results for the simulation without menisci, always accompanied by a shift of force from the medial to the lateral side due to menisci addition. Table 6.3 in Appendix 6.1.1 gives further numerical results.

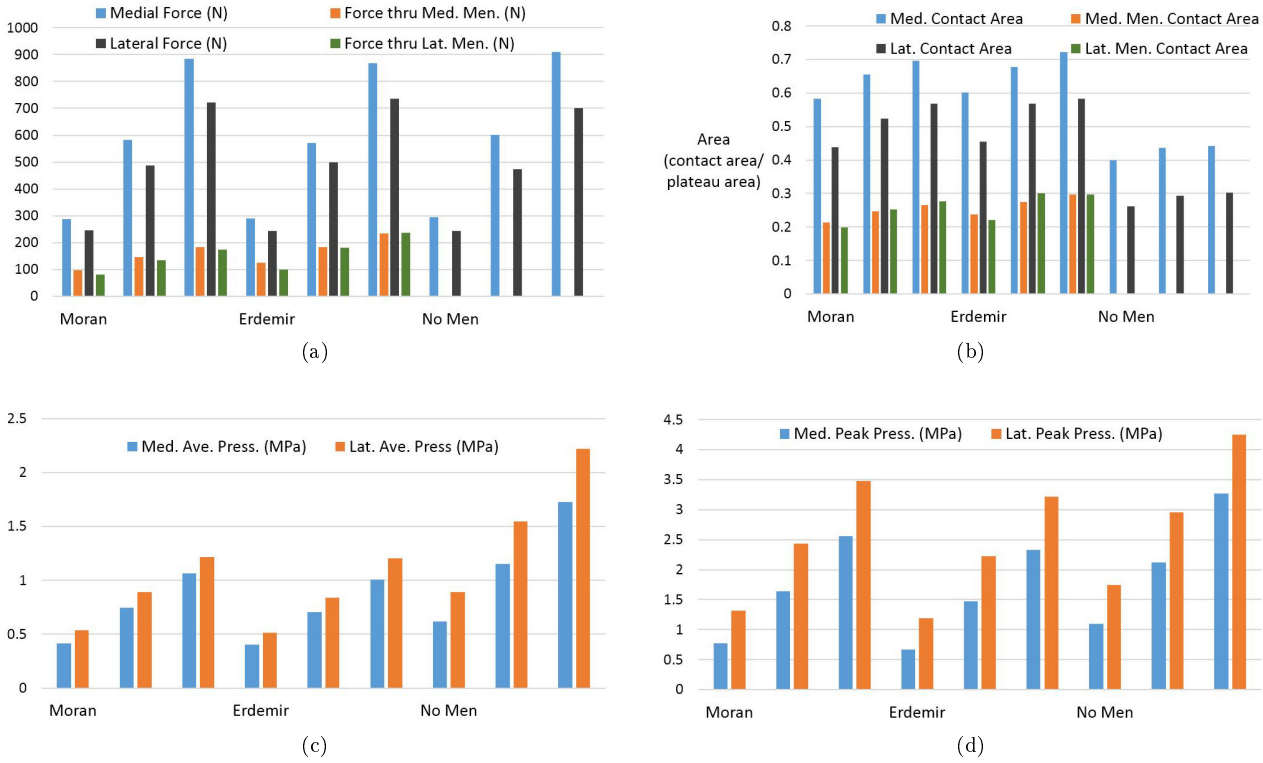

Figure 3.3: Comparison of the effects of menisci material property sets for loads of 500, 1000, and 1500N for (a) Contact force (b) Contact area (c) Average pressure (d) Peak pressure.

Interpolated pressure maps of stand simulations with a load of 1000N are shown in Figure 3.4. Pressure maps for simulations with loads of 500 and 1500N are shown in Figures 6.1 and 6.2 in Appendix 6.1.1.

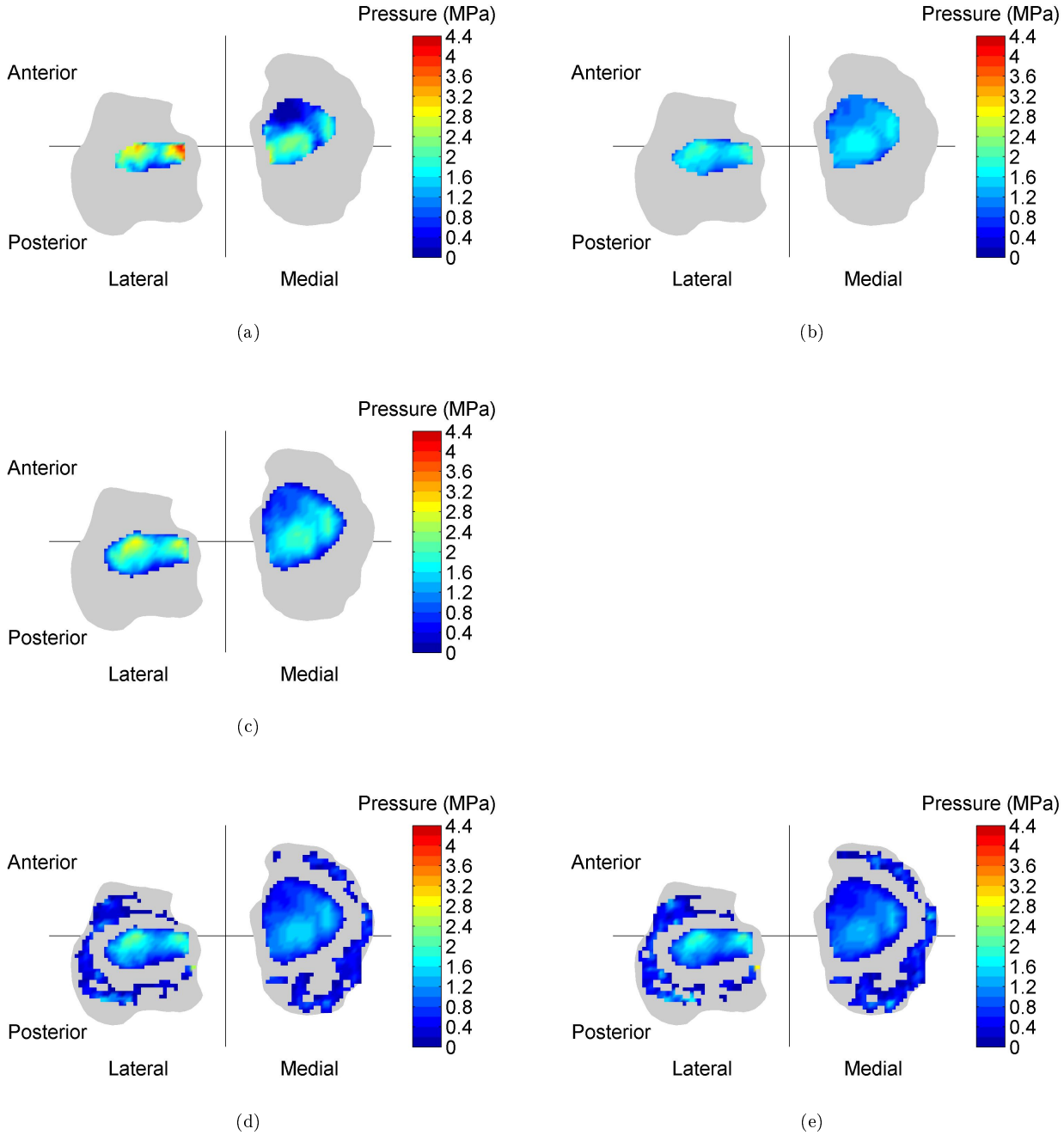

Figure 3.4: Interpolated results for 1000N applied load. (a) Impact120 without Menisci. (b) Impact50 without Menisci. (c) Cubic (Deneweth) without Menisci. (d) Cubic with Moran menisci. (e) Cubic with Erdemir menisci.

3.2.2 Comparison to experimental studies in literature

Total contact area in simulations with menisci is usually within 10% of values reported by Fukubayashi and Kurosawa. However, in the current model meniscal contact accounted for about 45% of the total contact area, while in Fukubayashi and Kurosawa menisci accounted for about 70% of the total contact area. With menisci included, average contact stress was, at most, 5% different between the current model and experiments by Fukubayashi and Kurosawa. Peak pressures for simulations with menisci were well within the reported experimental range (see Figure 3.5).

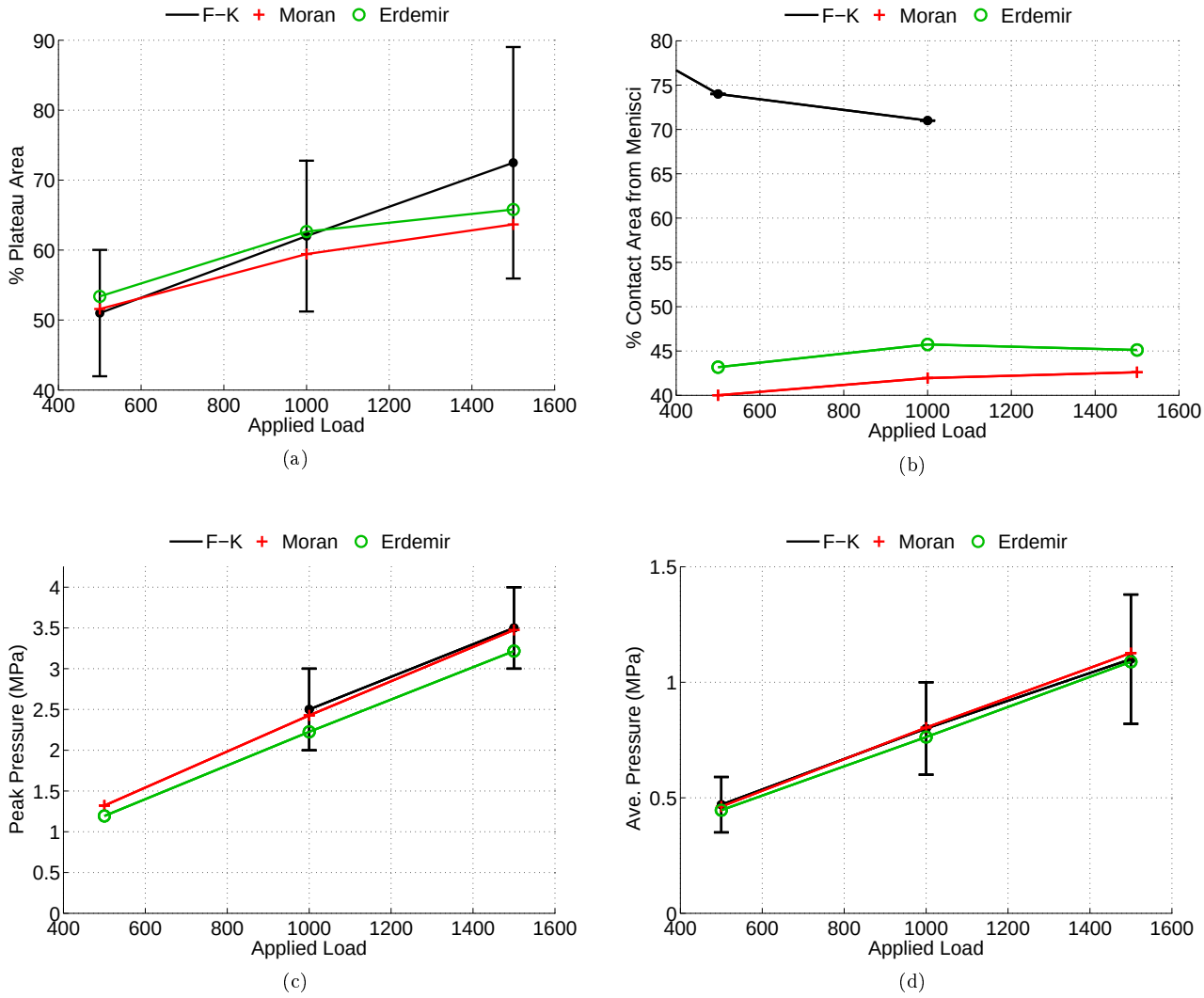

Figure 3.5: Comparison of M1 results to experimental (Fukubayashi–Kurosawa), with menisci, using cubic formulation for (a) % plateau area (b) % plateau area from menisci (c) Peak pressure (d) Average pressure.

3.2.3 Conclusion

Both menisci material property sets give similar results which, apart from menicus contact area, are within the standard deviation of experimental results. Erdemir properties give more meniscal contact area but this is only a 5% difference. The difference in peak pressure between material property sets is less than 10% of the lowest value. Moran material properties are from experimental results and therefore were given preference in the following sections. The large difference between simulated and experimental meniscus contact area is expected to be from the lack of central taper of the menisci geometries used in the model. This taper was removed during the smoothing process after geometries were extracted from the MRI. Special care should be taken in future work to preserve this taper. The reason contact area and average and peak pressure is still within the experimental standard deviation is most likely due to the softness of cartilage-cartilage contact as shown in 3.1.2.

3.3 Comparison of cubic formulation to experimental studies in literature

3.3.1 Fukubayashi and Kurosawa

Comparison of results from Fukubayashi and Kurosawa for M1 (middle aged male) has already been made in previous sections. This section is meant to compliment the coverage of the previous sections by the inclusion of M2 (older female) results, investigation of variance due to material properties, and comparison to experimental results from different groups.

M2 shows good agreement, regardless of which material property set (KRec, K1, K3, etc.) is used from Deneweth (2013), with experimental results for peak and average pressure and for medial contact area (see Figure 3.6). However, lateral contact area is about two SD higher than expected for 200N and 500N load and but within 1SD for 1000N load. Lateral contact area is remarkably consistent between M1 and M2 for all material property sets. However, medial contact area shows more variability due to geometry and position/orientation (i.e. M1 vs. M2) than material property set. M1 results are outside 1SD while M2 results are within 1SD. Peak and average pressure likewise show closer agreement of M2 results rather than M1 results, regardless of material property set, to experimental results. Given the apparent softness of the cubic formulation in M1 results, M2 results without menisci are surprisingly close to experimental results, indicating that resuls were highly dependent on geometry and/or initial position.

Similar to results from the M1 model, percentage area from menisci is still lower than predicted experimentally. However, percentage area from menisci is 10% higher than M1 which makes it 21% lower than the experimental mean instead of 41%. These results are expected if excising the tapered portions of the menisci less than ~0.5mm (since meshing this thin region is difficult) removes less material in M2 than the

smoothing removes in M1.

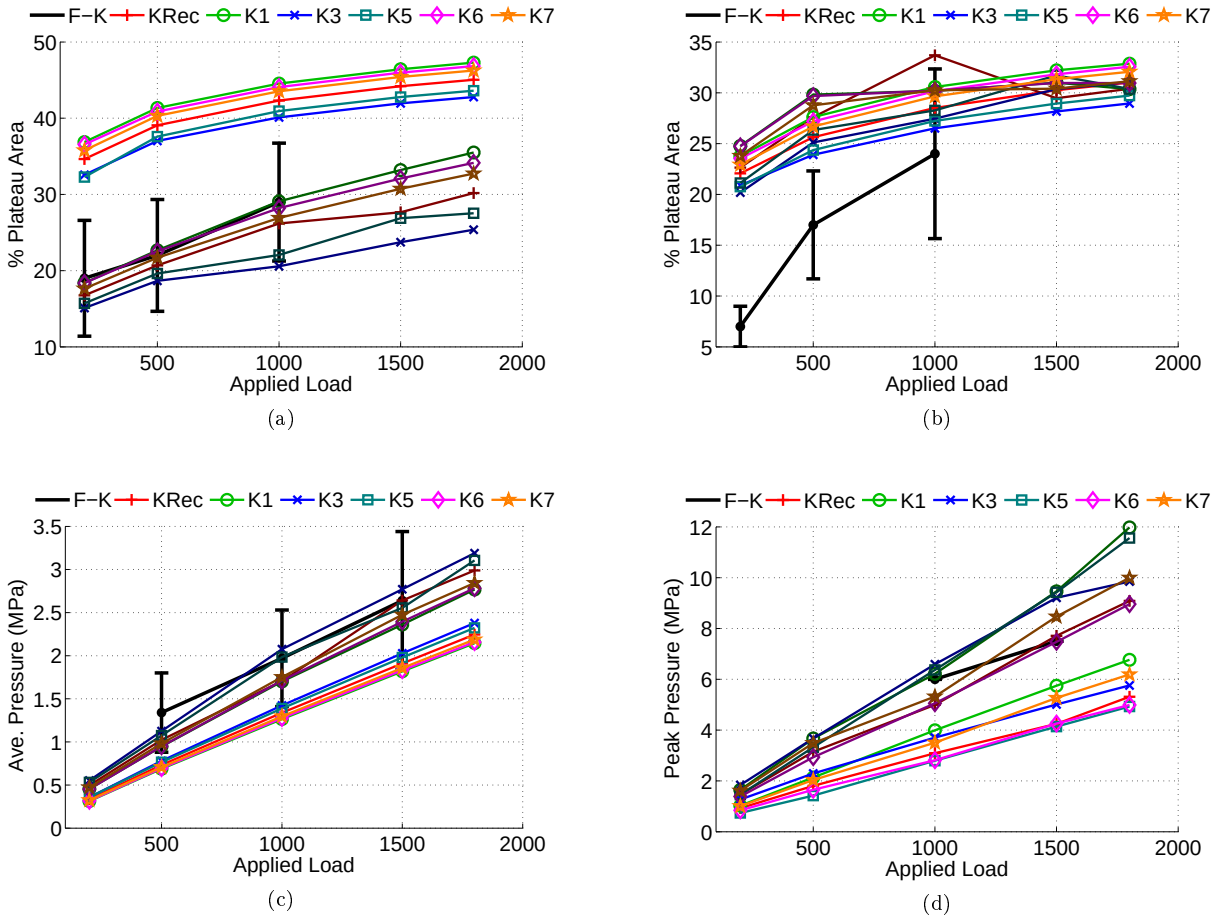

Figure 3.6: Cubic formulation stand results for M1 (bright) and M2 (dark) vs. results from Fukubayashi and Kurosawa (F-K) without menisci. (a) Medial contact area (b) Lateral contact area (c) Ave. pressure (d) Peak pressure.

Table 3.1: Comparison to Fukubayashi and Kurosawa, 500N load

500N Load without Menisci, 1DOF (Axial)	Fukubayashi & Kurosawa	M1		M2
% Contact Area Med	22 ± 7	40		23
% Contact Area Lat	17 ± 5	26		30
Average Pressures (MPa)	1.34 ± 0.46	0.72		0.94

500N Load with Menisci, 1DOF (Axial)	Fukubayashi & Kurosawa	M1, Moran	M1, Erdemir	M2, Moran
% Contact Area Med	54 ± 15	58	60	45
% Contact Area Lat	48 ± 7	44	46	45
Average Pressures (MPa)	0.47 ± 0.12	0.46	0.45	0.55

Table 3.2: Comparison to Fukubayashi and Kurosawa, 1000N load

1000N Load without Menisci, 1DOF (Axial)	Fukubayashi & Kurosawa	M1		M2
% Contact Area Med	29 ± 8	44		26
% Contact Area Lat	24 ± 8	29		32
Peak Pressure (MPa)	6	2.96		4.97
Average Pressure (MPa)	1.97 ± 0.56	1.30		1.72

1000N Load with Menisci, 1DOF (Axial)	Fukubayashi & Kurosawa	M1, Moran	M1, Erdemir	M2, Moran
% Contact Area Med	64 ± 18	66	68	56
% Contact Area Lat	58 ± 8	52	57	60
% Men. / Contact Area	71	42	46	56
Peak Pressure (MPa)	2-3	2.43	2.2	2.93
Average Pressure (MPa)	0.80 ± 0.20	0.80	0.76	0.86

Table 3.3: Comparison to Fukubayashi and Kurosawa, 1500N load

1500N Load without Menisci, 1DOF (Axial)	Fukubayashi & Kurosawa	M1		M2
Peak Pressure (MPa)	7-8	4.3		7.5
Average Pressure (MPa)	2.64 ± 0.80	1.91		2.51

1500N Load with Menisci	Fukubayashi & Kurosawa	M1, Moran	M1, Erdemir	M2, Moran
Peak Pressure (MPa)	3-4	3.5	3.2	4.01
Average Pressure (MPa)	1.10 ± 0.28	1.13	1.09	1.27

3.3.2 Baratz

Baratz et al. (1986) retained ligaments in their specimens. Ligaments were not implemented in the current model. Simulations with only axial, medial-lateral, and varus-valgus DOF should not be greatly affected by lack of ligaments since the response of ligaments is viscoelastic and the stand simulations are meant to imitate a quasistatic situation for ligaments. It was assumed that Baratz et al. only allowed the axial degree of freedom. Without the medial menisci in Model 1, a 20% difference was found between the calculated mean peak pressure of Baratz and simulation results and this difference is within the calculated standard deviation of the experimental mean. Model 2, however, shows peak pressure 37% increased compared to experimental results, although this is within 2 standard deviations. With menisci, peak pressure in simulations was about 115% (M1) and 300% (M2) greater than the calculated mean of experimental peak pressures–well outside the calculated standard deviation. Baratz results show about double the reduction of contact area due to meniscectomy as compared to simulation results. It should be noted that the results of Baratz et al. (1986) are consistent with those of Paletta et al. (1997) but contradict those of Fukubayashi and Kurosawa (1980) as Baratz et al. report peak pressures about 50% lower even though applying greater load. This may be due in

part to the smallness of the area of peak pressure in Fukubayashi and Kurosawa (1980). Or likely, as Baratz et al. (1986) observe, due to retaining most of the joint capsule and all ligaments. The large increase in peak pressure due to meniscectomy (assuming "neutral" position/orientation did not change) reported by Baratz et al. seems to indicate the soft tissue surrounding and attached to the menisci is responsible for a large portion of the menisci effect in an intact knee. Given that the current models are effectively disarticulated, simulation results from M1 may still be soft and those of M2 normal.

Table 3.4: Comparison to Baratz, 1800N load

1800N Load without Medial Meniscus, 1DOF (Axial)	Baratz	M1	M2
Medial Peak Pressure (MPa)	4.36 ± 1.03	3.49	5.98
% Reduction in medial contact area due to meniscectomy	75 ± 7	38	51

1800N Load with Menisci, 1DOF (Axial)	Baratz	M1	M2
Medial Peak Pressure (MPa)	1.38 ± 0.19	3.11	4.13

3.3.3 Marzo

Marzo and Gurske-DePerio (2009) retained ligaments in their specimens but removed the rest of joint capsule (specifically mentioning meniscofemoral and meniscotibial (coronal) ligaments). They also allowed varus-valgus rotation. Ligaments were not implemented in the current model, but varus-valgus rotation was allowed in the relevant simulations of the current model. Instead of using Prescale by Fuji Film (Baratz et al., 1986; Fukubayashi and Kurosawa, 1980), Marzo et al. used a Tekscan 410-N pressure sensor. With normal menisci, M1 simulation medial peak pressure is 35% lower than experimental but lateral peak pressure is within 7%. With avulsion on the posterior medial meniscus horn, M1 simulation medial peak pressure is about 45% lower than experimental, more than two standard deviations, but on the lateral side is within 7% compared to the experimental average (well within one standard deviation, See Figure 3.7). M1 results on the medial side show peak pressure below one standard deviation–consistent with the cartilage softness combined with lack of meniscus effect observed in previous sections. However, the lateral side is well within the standard deviation. This effect could be from an increase in lateral load due to allowing varus-valgus. The lateral contact force before medial posterior horn avulsion is 1034N compared to 860N in a identical simulation with varus-valgus constrained where peak lateral pressure was 4.08MPa and peak medial pressure 3.11MPa. Therefore due to the lateral geometry or initial position/orientation, redistribution of 174N to the lateral side produced a 1.22MPa increase in that side while only reducing medial peak pressure by 0.34MPa.

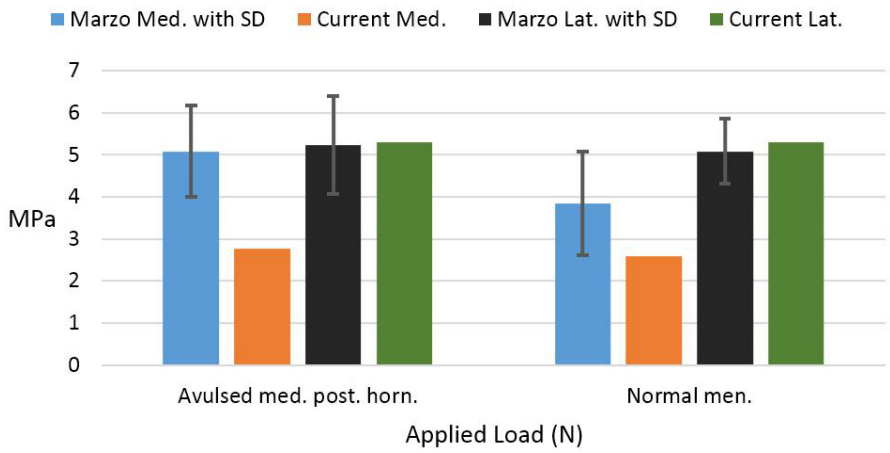

Figure 3.7: Peak pressure comparison, 1800N applied load, Marzo vs. Current (M1) model with Moran meniscus properties.

Table 3.5: Comparison to Marzo

1800N Load with avulsed posterior horn of the medial meniscus, 2DOF (Axial, VV)	Marzo	M1, Moran	M1, Erdemir
Medial Peak Pressure (MPa)	5.08 ± 1.09	2.77	2.72
Lateral Peak Pressure (MPa)	5.23 ± 1.16	5.30	4.76
% Reduction in medial contact area due to posterior horn avulsion	20.2	8.2	11.8

1800N Load with normal menisci, 2DOF (Axial, VV)	Marzo	M1, Moran	M1, Erdemir
Medial Peak Pressure (MPa)	3.84 ± 1.24	2.59	2.42
Lateral Peak Pressure (MPa)	5.08 ± 0.77	5.30	4.76

3.3.4 Other relevant studies

Although Paletta et al. (1997), Huang et al. (2003), Lee et al. (2006), and Amadi et al. (2008) are relevant studies, they did not cut the retaining ligaments and designated certain translations and rotations to be constrained only by these tissues. Simulations corresponding to these studies were not conducted with the current model since the current model does not include ligaments.

3.3.5 Conclusion

Results from the M1 model tend to indicate that material properties are defined too soft, whereas results from M2 do not indicate material properties are too soft; despite both using the same material property

sets. This indicates that geometry and/or initial position was an important factor. Conversely, changing the material property set did not greatly affect results.

There are a number of limitations when comparing current results with the above studies. The initial position and orientation conditions in the experiments discussed may not be the same as those imposed on the models. Given reliable initial position and orientation data, output from the models may be closer to experimental results.Usually experiments use cadaver sets which are regionally localized (specimens come from the same geographical or racial areas) and often more consisent within the sampled population. This means that the true (population) standard deviation is likely to be larger than reported.It is possible that some of the contact area and stress was not recorded in the experiments mentioned above because cartilage near the tibial eminence is not covered by film or tekscan. It is also possible that the pressure film or tekscan did not cover the entire meniscus because the meniscus expands when force is applied to the knee. Therefore, if this increase in area was not accounted for beforehand, the meniscus could go over the sensing device. Some coronal ligaments were excised when the sensing device is placed under the menisci and this could decrease hoops stress, thus increase the spreading of the menisci resulting in higher contact area, and lower force through the menisci creating higher pressure on the cartilage (see Section 3.3.2). Results from Baratz et al. and Fukubayashi et al. indicate this contribution, in addition to other soft tissues such as the meniscofemoral ligaments, may play a large role in decreasing pressure in the intact knee. Future work would do well to include a sensitivity analysis of the inclusion of meniscotibial (coronal) ligaments and the effect of the material properties used for them. Current coronal strength of 2N/mm may not be sufficient to produce physiological results.

Current analysis indicates that, given the sensitivity to geometry and/or intial position and limitations such as the lack of central taper of the menisci, contact and menisci implementations lead to reasonable results.

4 Gait Simulations Results & Discussion

Average gait simulation time for the M1 model ranged from 5 to 10min.

4.1 Simulating the Gilbert experiment

Contact area trends are similar and close in magnitude, but two slight peaks in data from Gilbert et al. are very pronounced features in simulation results (see Figure 4.1b). From about 10-40% of the stance phase for both plateaus and from about 80% onward for the medial plateau, the cartilage-to-meniscus average stress ratio of simulations deviates sharply from the results of Gilbert et al. In simulations, contact area was mainly on the cartilage for both medial and lateral plateaus and this differs from results by Gilbert et al. (2014), in which the mensicus on the lateral side contributed about double the contact area of the cartilage and the meniscus on the medial side contributed about the same area as the cartilage (see Figure 6.6b). This is consistent with stand simulation results and the reasons for these results have therefore already been discussed in that section. Additional numerical results may be found in Table 6.4 of Appendix 6.2.2.

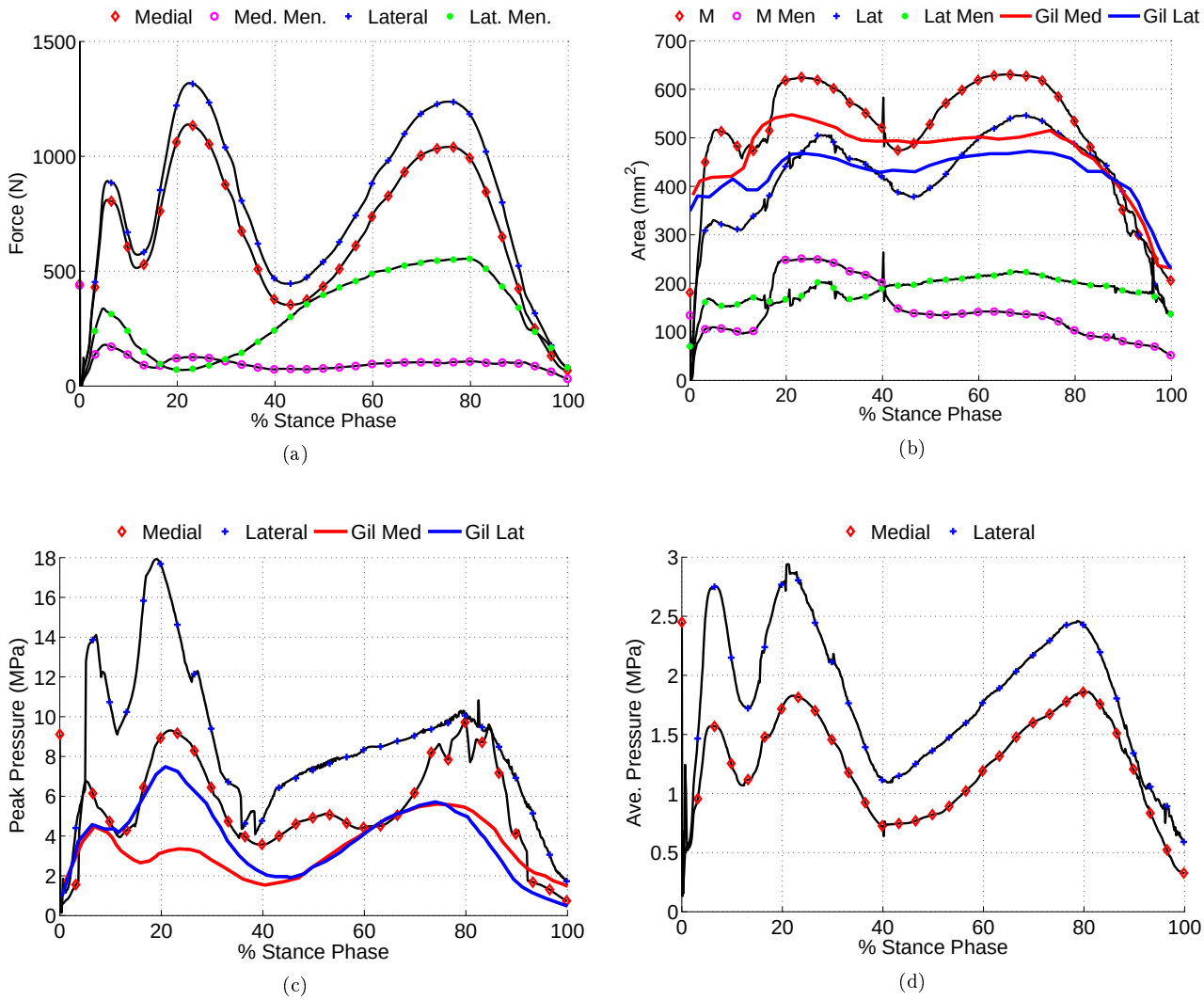

Figure 4.1: Results of M1 with Gilbert kinematics for (a) Force (b) Contact Area (c) Peak pressure (d) Average pressure.

Gait simulations show similar trends but about double the magnitude of peak pressures throughout stance phase compared to Gilbert et al. (2014) (see Figure 4.1c). This may partly be because Gilbert retained the joint capsule whereas the model does not. Large changes in peak pressure due to this difference have been reported(Baratz et al., 1986). In addition, in previous results (see Section 3.3.3) the lateral plateau showed peak pressure sensitivity to higher force on lateral plateau and this is exactly what occurs during the gait cycle (see Figure 6.6). Throughout stance phase in simulations, the lateral plateau was found to transmit about 20% more force than the medial plateau (see Figure 6.6a and Table 6.4). However, since stand simulations showed a tendency of the M1 model toward being too soft in cartilage material properties. The

high peak pressures must still be explained by another factor.

For pressure maps at 10% intervals of stance phase, see Figure 6.7 in Appendix 6.2.2. For the location of the weighted center of pressure at 10% intervals of stance phase, see Figure 6.8 in Appendix 6.2.2. Simulation pressure patterns at 23 and 75% of stance phase are similar to those shown in Gilbert et al. (2014) (see Figure 4.2)[8]. This probably, though not necessarily, indicates generally similar geometries and initial position since simulation kinematics are driven and may point to the use of literature-based cartilage thickness as a weakness in the current model. The tibial cartilage of the M1 model in the central region (near the tibial eminence) is ~4mm whereas the average value reported in literature is 2.59 (Shepherd and Seedhom, 1999). Since contact force is based on the stress-strain relationship, the medial-lateral and varus-valgus degrees of freedom will shift differently based on the percieved strain, regardless of the actual thickness of the geometry in the model. Furthermore, for any given geometry different contact area will occur at different penetration depths regardless of the force required to reach that penetration. If the strain stays the same but the penetration depth changes because of a change in cartilage thickness, then the contact area will change as well. Thus for many reasons, changing the thickness parameter of contact has potential to greatly alter the med/lat force ratio and pressure as well as additional results. Discrepency between M1 results and those of Gilbert et al. (2014) may thus be partly the result of using non-subject specific thickness parameter in the contact formulation as preliminary results using M1-specific estimates of cartilage thickness show highly changed peak pressure values (see Appendix 6.6). Future work should investigate the sensitivity of results to the thickness parameter and, depending on results, develop a methodology for determining region-specific cartilage thickness parameters given the geometry.

[8]Note that although Gilbert et al. crop the pressure values at 5MPa, they report the peak pressure on the lateral side at 23% stance phase is around 7MPa.

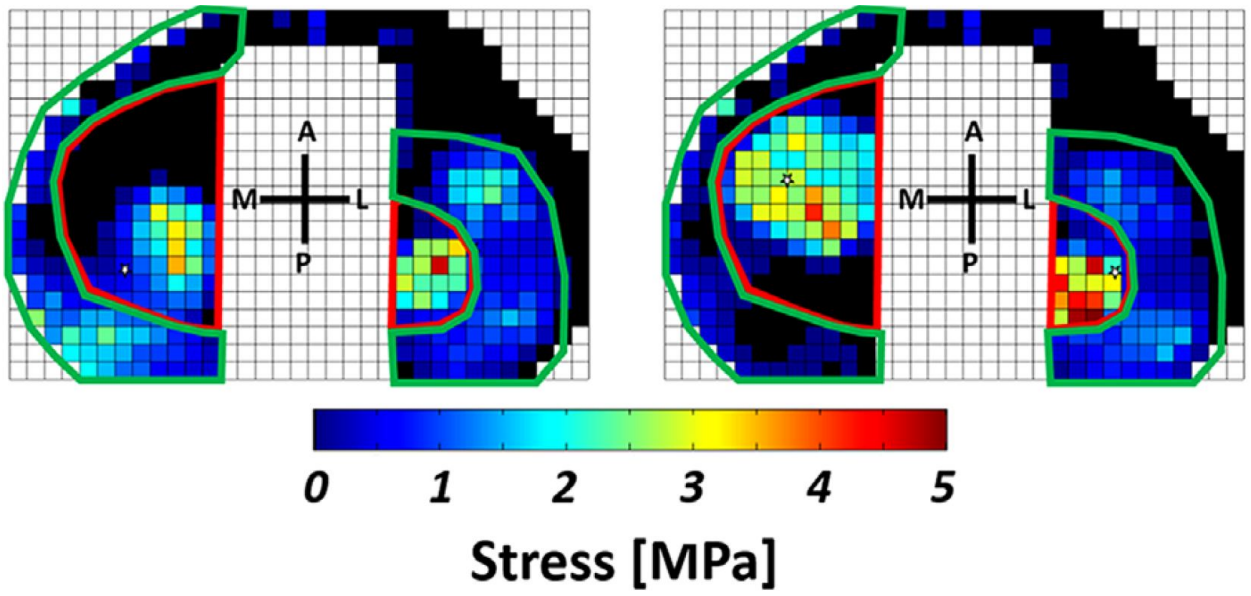

(a)

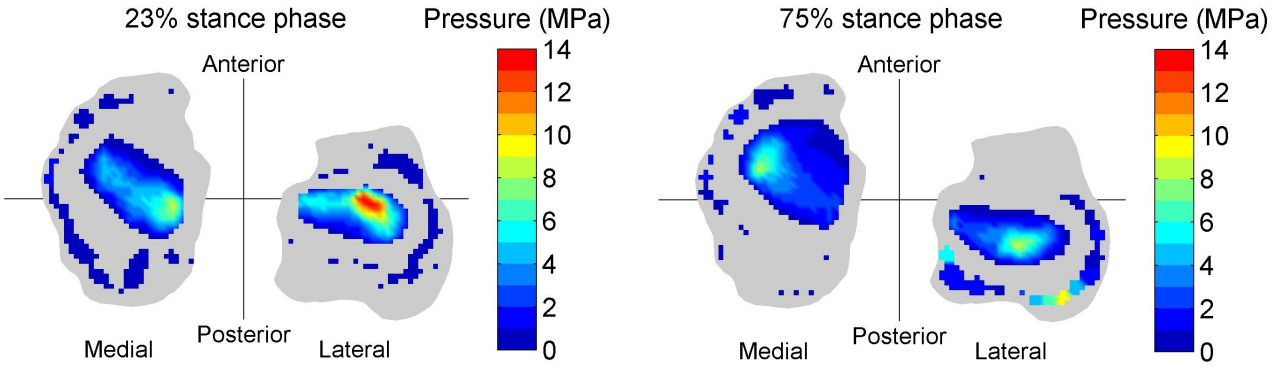

(b)

Figure 4.2: Pressure maps for 23 and 75% stance phase from (a) Gilbert et al. (b) M1 simulation.

4.1.1 Conclusion

M1 results from simulations utilizing the Gilbert kinematic set show results consistent with those already presented in stand simulations. However, simulations shows pressure which are very high even considering highly reduced menisci function. Since simulations give pressure patterns similar to experimental results, this may indicate that use of subject-specific contact parameters may be necessary for realistic pressures.

4.2 Material property sensitivity

In order to determine whether individual variance in material property values play a large role in determining results, a sensitivity analyisis using five seperate experimentally determined knee cartilage material property sets (K1,K3,K5,K6,K7) reported by Deneweth (2013) was conducted. This sensitivity analysis used gait kinematics from Gilbert et al. (2014). However, axial loading was defined from Hsiung et al. (2013) instead of Gilbert et al. (2014), increasing peak axial loading by about 300N.

Results from all five simulations are remarkably similar and therefore an easy way to intpret results was needed. The CR factor is a loose approximation of the stiffness of the femoral-to-tibial cartilage contact, calculated by treating the CR value of the central tibial cartilage and the femoral weight-bearing cartilage as hookean springs in series (see Figure 4.3) and taking the normalized difference relative to the values recommended by Deneweth (2013). By treating the CR values of the femoral cartilage and tibial cartilage as stiffnessess of springs in series, the softness and hardness of both surfaces is taken into account. Normalizing by the recommended values allows deviation due to differing CR values to be more easily understood. For example, the medial CR factor for K1 is about half the mean stiffness and is calculated as shown in equation 4.1.

$$CR_{factor} = \frac{1/(\frac{1}{0.228} + \frac{1}{0.05255}) - 1/(\frac{1}{0.540} + \frac{1}{0.10551})}{1/(\frac{1}{0.540} + \frac{1}{0.10551})} = -0.5161 \tag{4.1}$$

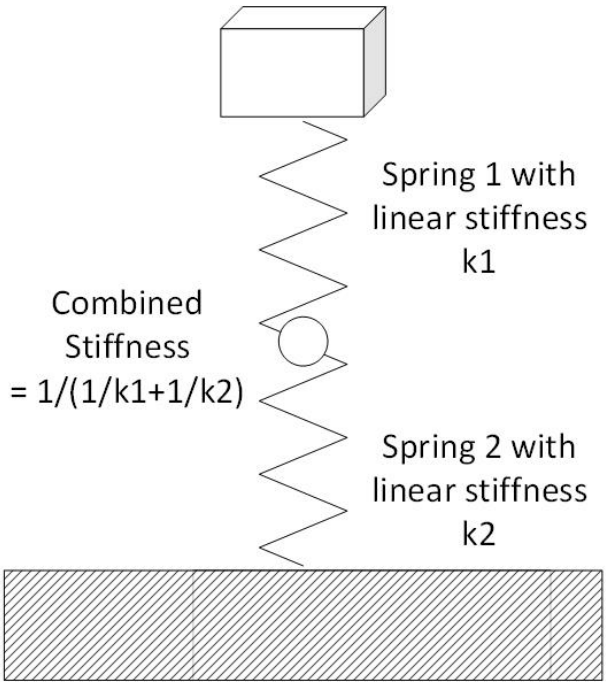

Figure 4.3: Two hookean springs in series.

While there was generally a strong correlation between CR factor and contact area and pressure, there were no relative changes greater than 30% and most changes were within 15% (see Figure 4.4). The lateral side shows very high standard deviation in peak pressure. Simulations gave less than 15% difference in average pressure and less than 20% difference for mean peak pressure and contact area despite increasing or decreasing the CR factor by 50%.This indicates that subject-specific sensitivity of the CR factor is not an important factor in determining gait results. This also may mean that changes in material properties over time may not be relevant to the development of osteoarthritis. Given the weak correlation between material properties and osteoarthritis reported by Brown et al. (2007), this hypothesis seems reasonable.

This means that the primary cause of variance between in the M1 and experimental results from Gilbert et al. (2014) is may be reasonably narrowed to the cartilage thickness parameter, the cubic contact formulation, or misalignment of the model in regard to driving kinematics. It remains possible that M1 contains unusual geometry. However, M1 gait simulations using driving kinematics from Benoit et al. (2006) show pressure values far more similar to the expected range (see Appendix 6.5) and this indicates the importance of driving kinematics and preliminary analysis shows initial position to also be an important factor in gait (see Appendix 6.4).

For additional graphs and a table of results for this sensitivity study, see Appendix 6.3.

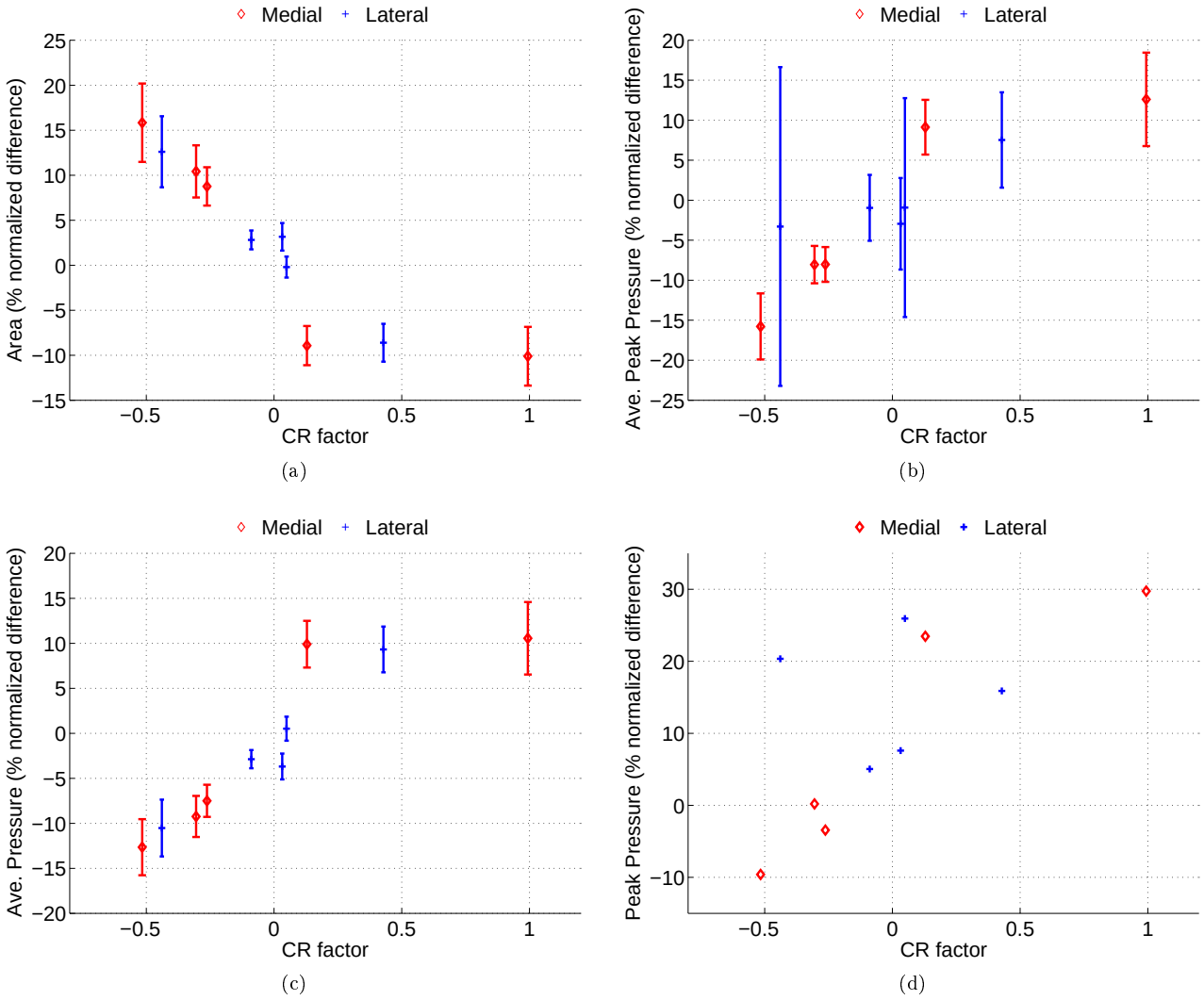

Figure 4.4: Difference in (a) Contact area (b) Mean Peak pressure (c) Ave. Pressure (d) Maximum peak pressure versus CR factor for 5 simulations with respective cartilage properties of Deneweth (2013) K1, K3, K5, K6 and K7.

5 Conclusion

If individuals change muscle activation patters this could cause large changes in peak pressure without changing the material properties. Given the weak correlation between material properties reported by Brown et al. (2007) and the CR study in this thesis, this hypothesis seems reasonable.

5.1 Stand results

Implementation of physically-based material properties reported by Deneweth (2013) show mixed results, with M1 commonly exceeding one SD in giving lower pressure values and higher contact areas relative to experimental literature and M2 usually giving results within one SD. It is possible that the cartilage material properties from Deneweth are too soft for the M1 knee geometry or that the M1 knee geometry is more congruous due to mild[9] arthritis (Fukubayashi and Kurosawa, 1980). Meniscus implementation has been reasonably verified given the lack of taper in menisci geometry and imprecise definition of the soft tissue attachments which may be key to force bearing.

5.2 Gait results

Gait results show contact area in good agreement with reported values but maximum peak pressures are generally over twice those reported experimentally (Gilbert et al., 2014; Bedi et al., 2010; Lee et al., 2006; Huang et al., 2003; Paletta et al., 1997). Simulation pressure levels are similar to those reported in an FE analysis of a knee joint replacement (Godest et al., 2002) but further analysis is needed to determine the cause of the high pressure. Strong consistency of simulation results using different material property sets of individual knees as reported by Deneweth (2013) was observed, indicating this is a lesser factor. Sensitivity of gait results to both initial position and different kinematic sets is shown in appendices, with differences in average pressure, peak pressure, and contact area commonly exceeding 30%. Preliminary analysis has also shown the cartilage thickness parameter changes results considerably and may need to be adjusted per model instead of using a literature average.

5.3 Limitations and Future work

Cartilage material properties from Deneweth (2013) are only validated for strain up to 16%, since cartilage was only tested to this strain. For a 500N applied load without menisci, cartilage strain is around 15%. For a 1800N applied load without menisci, strain is around 25%. To give perspective, this means that pressures

[9] No degredation of the tibial cartilage surface was noted on visual inspection. Severe patellofemoral osteoarthritis was clearly present.

above about 1.2MPa are calculated from a cubic extrapolation. This lack of experimental data exists despite reports of higher presures (cited throughout this work) and that the knee commonly experiences strains in the range of 20-30% (Bingham et al., 2008). Future work should use experimental stress-strain data for >15% strain as soon as it becomes available to avoid dependece on extrapolation.

The cartilage thicknesses for each model were defined from averages reported by Shepherd and Seedhom (1999). Ideally, actual thickness of cartilage in the model should be used; however M1 has very thick central cartilage (~4mm) and this made contact more compliant than expected from literature. Therefore it was decided that since stiffness factors (CR) are taken from experimental averages, the average experimental thicknesses may reasonably be used in conjunction. Analysis has shown that cartilage thickness may be a much more significant factor than previously thought and future work should examine this further.

Much of the natural tapering of the menisci in the central portion of the plateaus was eliminated due to smoothing (M1) or meshing (M2). This is believed to be the primary cause of the low contact area and force transmission in the current models as compared to experimental studies. Additionally sensitivity analysis of meniscal attachements such as the coronal ligaments should be conducted since they may be key to reducing pressures inside the intact knee.

The M2 model menisci geometeries are incomplete in the insertion regions due to low MRI contrast(Erdemir and Sibole, 2010), this may be the reason M2 gait simulations excessively loaded the meniscal horns during gait such that the data was deemed unviable.

Inaccuracy in examination of the MRI for the locations of the collateral attachments and therefore the epicondylar axis is possible and Bedi et al. (2010) assert the alignment of the epicondylar axis is crucial for ensuring physiological motion.

A further limitation of the current data sets (not the models themselves) is use of non-subject specific kinematic data. This can be alievated in future work by modeling using geometry from a subject/specimen from whom/which kinematics have also been recorded.

5.4 Conclusion

Physically-based contact and meniscus properties were implemented with good computational efficiency and showed reasonable results compared to experiments in literature. However, simulations show sensitivity to many factors. These sensitivites are key to being able to reproduce experimental results and better understand internal knee mechanics.

5.5 Acknowlegments

The Author would like to especially thank Dr. Jerome Hausselle for the one-on-one weekly meetings and his help and encouragement throughout this work and particularly for writing the code for interpolated pressure mapping. The Author is also grateful to Dr. Roger Gonzalez for providing the opportunity to engage in this work and the instruction received in and out of the classroom. Gratitude is extended to Dr. Trent Guess for providing direction for this work and serving on the committee. Special appreciation is given to the Author's parents since they inspired and supported this work. Not least, acknowledgement is given to the king of heaven; who has given authority, ability, and mercy to mankind to tend creation.

5.6 Funding

This work was funded in part by the NSF (RUI 1258555) and by the UTEP 2014 COURI-Provost Summer Student Research Assistant Program.

6 Appendices

6.1 Appendix A: Supplemental stand simulation data

6.1.1 Appendix A-1: Tables of numerical stand results

Table 6.1: Numerical results of contact formulations without menisci

	Impact: 120N/mm			Impact: Stiffness 50, Exp 1.8			Cubic (Deneweth)		
Applied Force (N)	500	1000	1500	500	1000	1500	500	1000	1500
Med. Contact Force (N)	222	534	851	291	614	934	294	601	910
Lat. Contact Force (N)	327	553	772.5	247	462	680	244	474	702
Med. Contact Area (mm^2)	387	486	486	486	540	567	476	521	528
Lat. Contact Area (mm^2)	306	288	324	324	360	396	274	307	316
Med. % Plateau Area	32.4	40.7	40.7	40.7	45.2	47.5	39.9	43.6	44.2
Lat. % Plateau Area	29.3	27.5	31.0	31.0	34.4	37.9	26.2	29.4	30.2
Med. Ave. Press. (MPa)	0.57	1.10	1.75	0.60	1.14	1.65	0.62	1.15	1.73
Lat. Ave. Press. (MPa)	1.07	1.92	2.38	0.76	1.28	1.72	0.89	1.54	2.22
Med. Peak Press. (MPa)	2.66	3.37	4.01	1.03	1.79	2.58	1.1	2.12	3.27
Lat. Peak Press. (MPa)	3.53	4.46	5.27	1.51	2.32	3.11	1.74	2.96	4.25

Table 6.2: Comparison of simulated and experimental results for different contact formulations.

500N Load without Menisci, 1DOF (Axial)	Fukubayashi & Kurosawa	Cubic	Impact: Stiffness 50, Exp 1.8	Impact: 120N/mm
% Contact Area Med	22 ± 7	40	41	32
% Contact Area Lat	17 ± 5	26	31	29
Average Stress (MPa)	1.34 ± 0.46	0.72	0.66	0.79

1000N Load without Menisci, 1DOF (Axial)	Fukubayashi & Kurosawa	Cubic	Impact: Stiffness 50, Exp 1.8	Impact: 120N/mm
% Contact Area Med	29 ± 8	44	45	41
% Contact Area Lat	24 ± 8	29	34	28
Peak Pressure (MPa)	6 ± 0.5?	2.96	2.32	4.46
Average Stress (MPa)	1.97 ± 0.56	1.30	1.20	1.40

1500N Load without Menisci, 1DOF (Axial)	Fukubayashi & Kurosawa	Cubic	Impact: Stiffness 50, Exp 1.8	Impact: 120N/mm
Peak Pressure (MPa)	7.5 ± 0.5?	4.3	3.11	5.27
Average Stress (MPa)	2.64 ± 0.80	1.91	1.68	2.00

Table 6.3: Numerical comparison of the effects of menisci material property sets using the cubic formulation.

	Erdemir			Moran			No Meniscus		
Applied Force (N)	500	1000	1500	500	1000	1500	500	1000	1500
Med. Contact Force (N)	289.9	572.2	868.2	287.6	582.3	884.2	294	601	910
Force thru Med. Men. (N)	124.8	183.3	235.1	96.7	145.4	183.8			
Lat. Contact Force (N)	243.6	498.2	736.1	246.4	487.6	722.3	244	474	702
Force thru Lat. Men. (N)	99.7	181.9	237.4	82.2	135.2	173.7			
Med. Contact Area (mm^2)	719.3	809.0	863.2	696.8	782.5	831.5	476	521	528
Area of Med. Men. Contact (mm^2)	284.7	327.3	355.0	254.3	294.4	318.1			
Lat. Contact Area (mm^2)	476.1	593.9	610.3	458.1	548.3	594.2	274	307	316
Area of Lat. Men. Contact (mm^2)	231.4	314.4	309.7	207.8	263.9	289.3			
Med. Contact Area ratio (area/potential area)	0.603	0.678	0.723	0.584	0.656	0.697	0.399	0.436	0.442
Lat. Contact Area ratio (area/potential area)	0.455	0.568	0.584	0.438	0.524	0.568	0.262	0.294	0.302
Med. Ave. Press. (MPa)	0.40	0.71	1.01	0.41	0.74	1.06	0.62	1.15	1.72
Lat. Ave. Press (MPa)	0.51	0.84	1.21	0.54	0.89	1.22	0.89	1.54	2.22
Med. Peak Press. (MPa)	0.67	1.47	2.32	0.77	1.64	2.56	1.1	2.12	3.27
Lat. Peak Press. (MPa)	1.19	2.23	3.22	1.32	2.43	3.48	1.74	2.96	4.25

6.1.2 Appendix A-2: Stand simulation pressure maps

6.1.2.1 Interpolated pressure maps by applied force

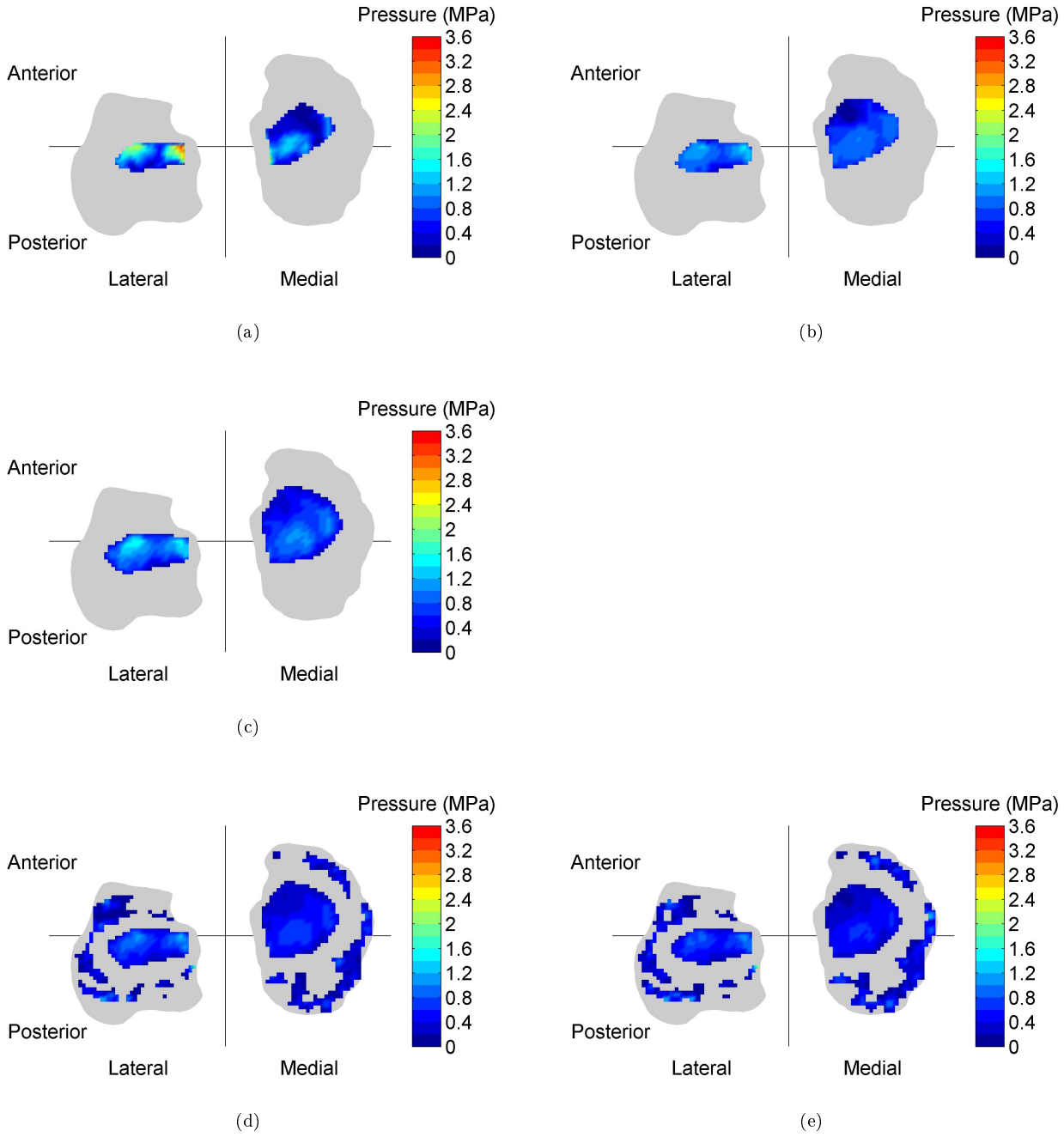

Figure 6.1: Interpolated results for 500N applied load. (a) Impact120 without Menisci. (b) Impact50 without Menisci. (c) Cubic (Deneweth) without Menisci. (d) Cubic with Moran menisci. (e) Cubic with Erdemir menisci.

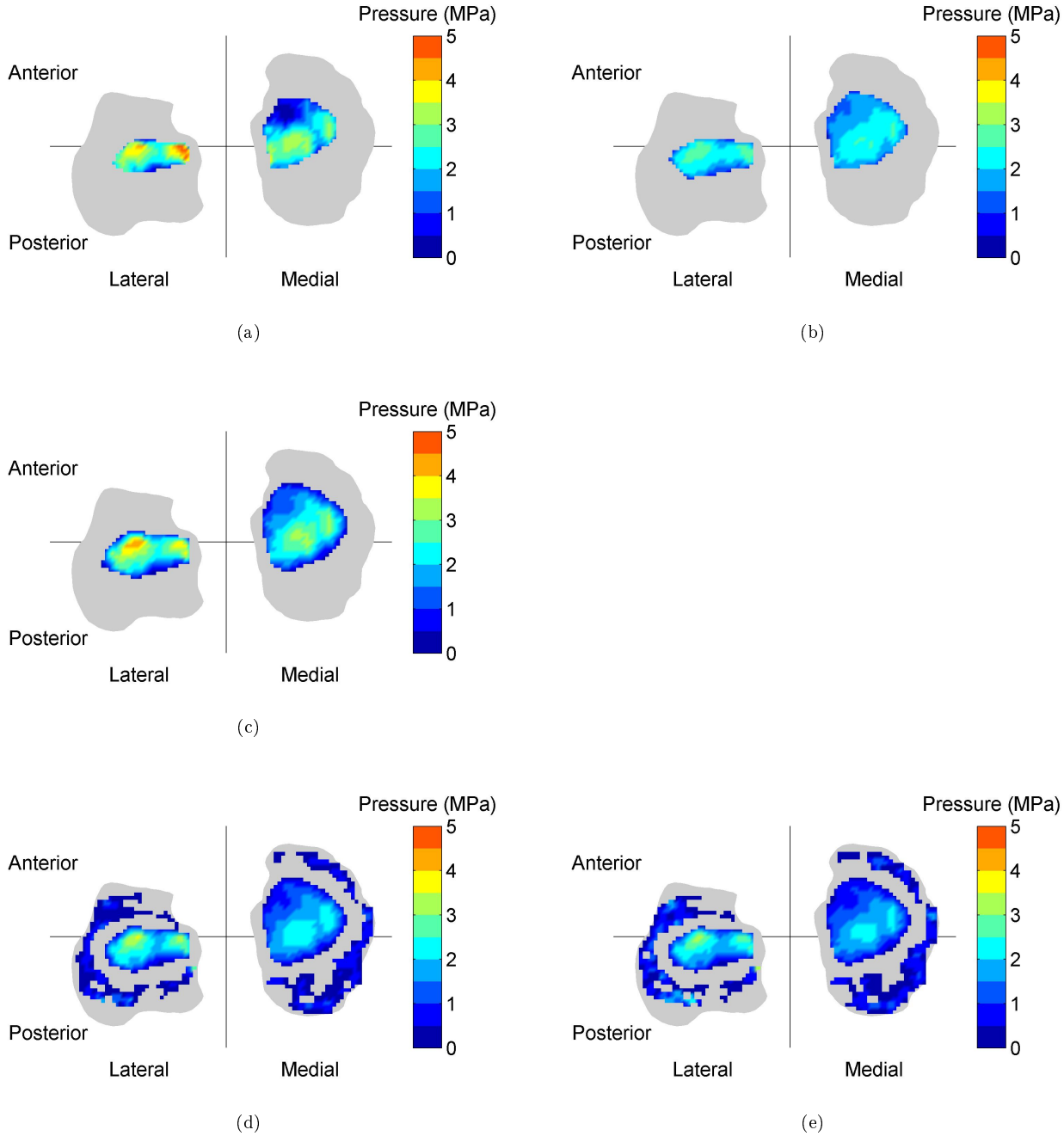

Figure 6.2: Interpolated results for 1500N applied load. (a) Impact120 without Menisci. (b) Impact50 without Menisci. (c) Cubic (Deneweth) without Menisci. (d) Cubic with Moran menisci. (e) Cubic with Erdemir menisci.

6.1.2.2 Noninterpolated pressure maps

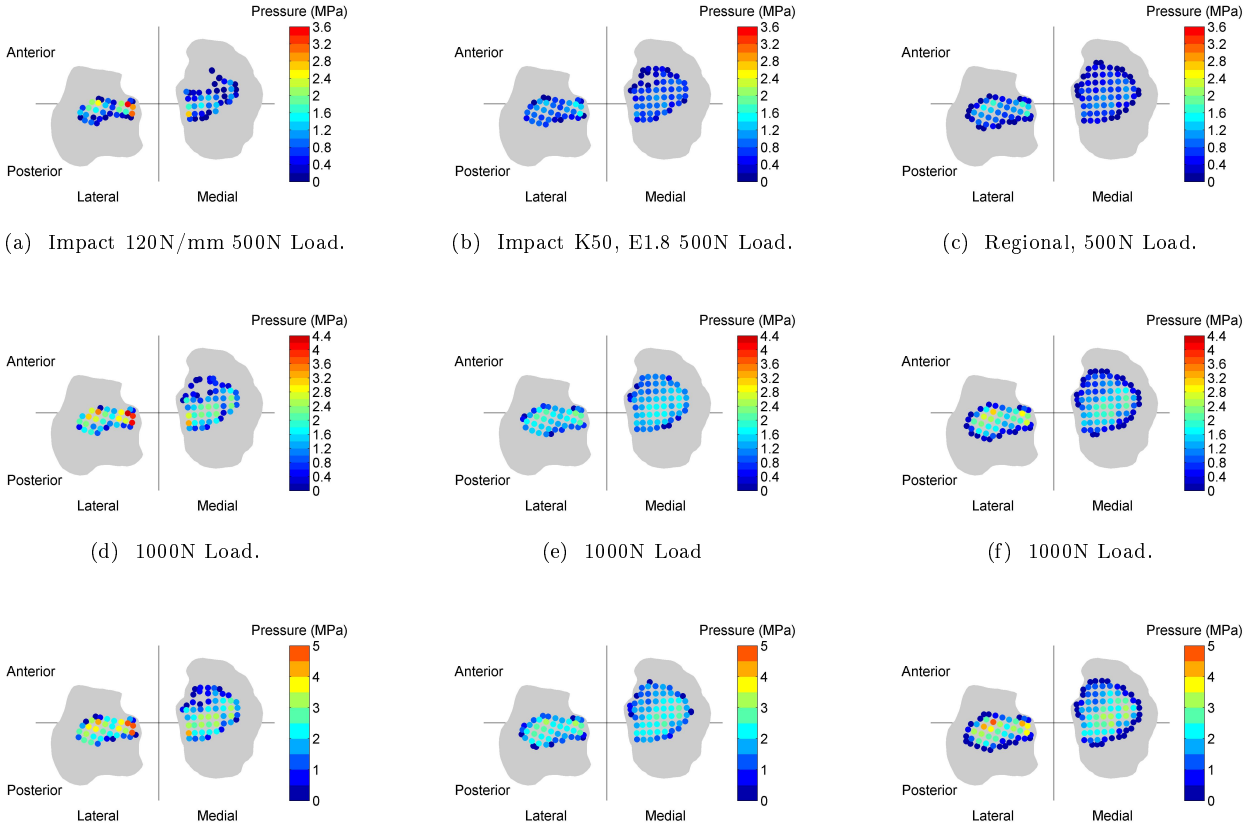

(a) Impact 120N/mm 500N Load.

(b) Impact K50, E1.8 500N Load.

(c) Regional, 500N Load.

(d) 1000N Load.

(e) 1000N Load

(f) 1000N Load.

(g) 1500N Load

(h) 1500N Load.

(i) 1500N Load

Figure 6.3: Non-interpolated pressure maps for stand simulations without mensici.

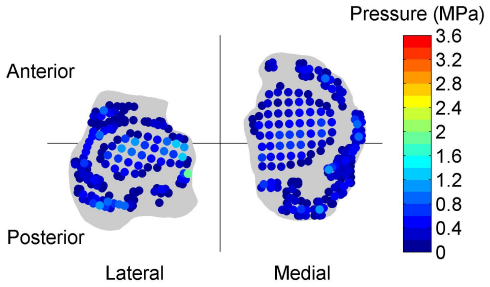

(a) Moran 500N

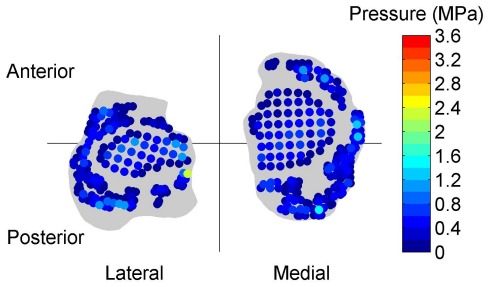

(b) Erdemir 500N

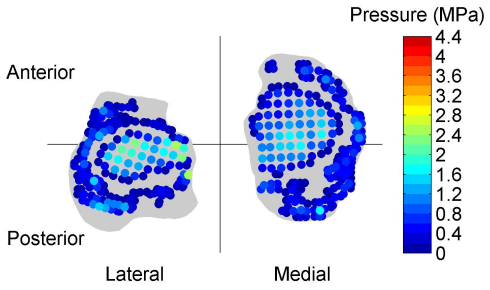

(c) Moran 1000N

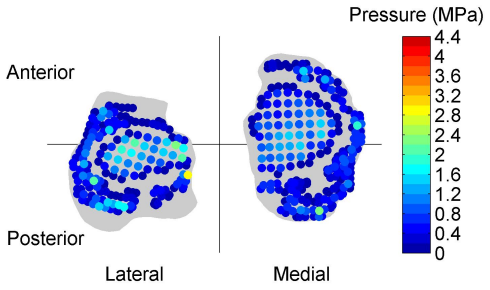

(d) Erdemir 1000N

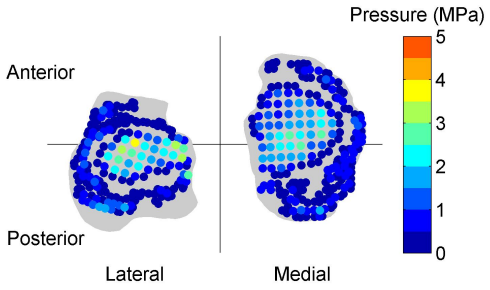

(e) Moran 1500N

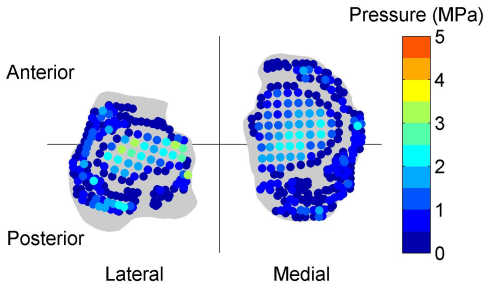

(f) Erdemir 1500N

Figure 6.4: Non-interpolated pressure maps for stand simulations with mensici. (a) Moran 500N. (b) Erdemir 500N. (c) Moran 1000N. (d) Erdemir 1000N. (e) Moran 1500N. (f) Erdemir 1500N.

6.2 Appendix B: Supplemental gait simulation data

6.2.1 Special considerations when interpreting results from Gilbert et al.

It is clear from pictures[10] in Bedi et al. (2012), from the same group as Gilbert et al. (2014), that placement of the sensing devices does not allow full coverage of the regions immediately at, anterior, and posterior to tibial eminence or at the periphery of the menisci. Without knowledge of the force read by the sensor versus applied force, which is not explicitly or implicity provided, it is difficult to quantify the expected difference in values such as contact area and cartilage-to-meniscus loading-sharing ratios compared to a result set with complete contact data.

However, Gilbert et al. (2014) uses the same experimental setup as Bedi et al. (2010), and given this is the same research group we can expect consistency. Given the reported mean contact area and pressure from Bedi et al. (2010), the force transmitted through the medial sensor at 45% of the gait cycle (75% stance) was 889N. Subtracting this from the applied 2130N gives 1241N. Gilbert et al. (2014) report the medial-lateral stress ratio at 45% of the gait cycle as 1.26 and the contact area ratio can be calculated as 515/468. Dividing the stress ratio by the contact area ratio gives the force ratio: 1.15. Thus, as mentioned before, assuming the Gilbert/Bedi group is methodologically consistent, one should expect a load of 773N. 889N added to 773N makes 1661N and this is 469N short of the reported 2130N. It is unknown how much of this remaining force is transmitted by cartilage-cartilage or cartilage-meniscus contact in the regions not covered by the sensor or how much may be attributed to error within the sensor calibration and data collection. It is notable that at 14% of the gait cycle the reported lateral mean peak contact stress is 7.26 ± 2.51 MPa. Given that saturation is a serious concern (see Figure 6.5) and the datasheet of the sensor used by Gilbert et al. (2014) reports a maximum pressure value of 7MPa (Tekscan), the results above this are of unknown quality.

[10] In particular, see figure 3. See also figure 3 in Bedi et al. (2010).

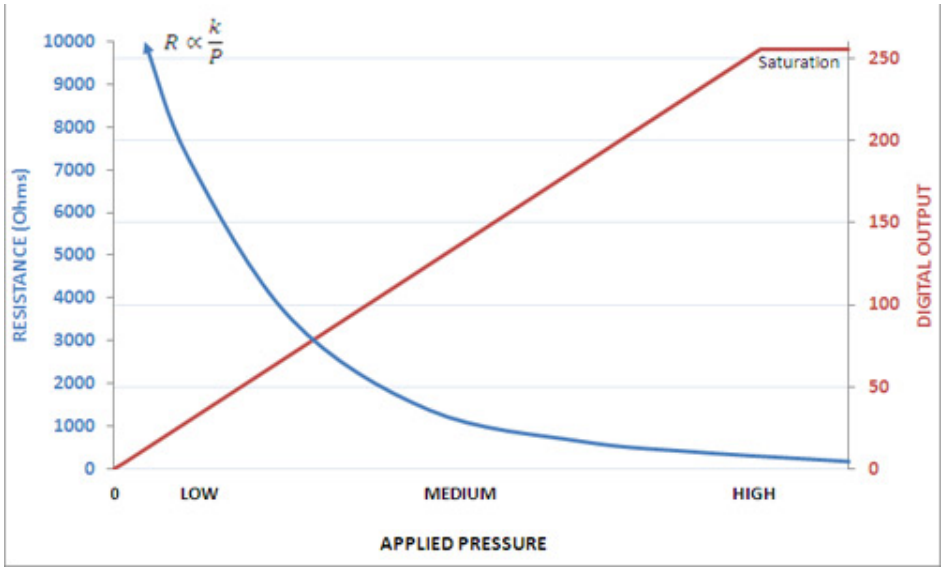

Figure 6.5: Saturation example figure from Tekscan (2015).

6.2.2 M1 utilizing Gilbert kinematic Set

Table 6.4: Numeric gait simulation results for M1 using Gilbert kinematics.

	Medial	Lateral
	Mean ± SD	Mean ± SD
Average Pressure (MPa)	1.24 ± 0.42	1.85 ± 1.03
Plateau Force/Total Force (%)	46 ± 4	54 ± 4
Meniscus Force/Plateau Force (%)	19 ± 12	47 ± 10
Plateau Area/Potential Area (%)	43 ± 10	40 ± 10
Meniscus Area/Potential Area (%)	12 ± 5	18 ± 3
Peak pressure (MPa)	5.41 ± 2.35	8.74 ± 4.64

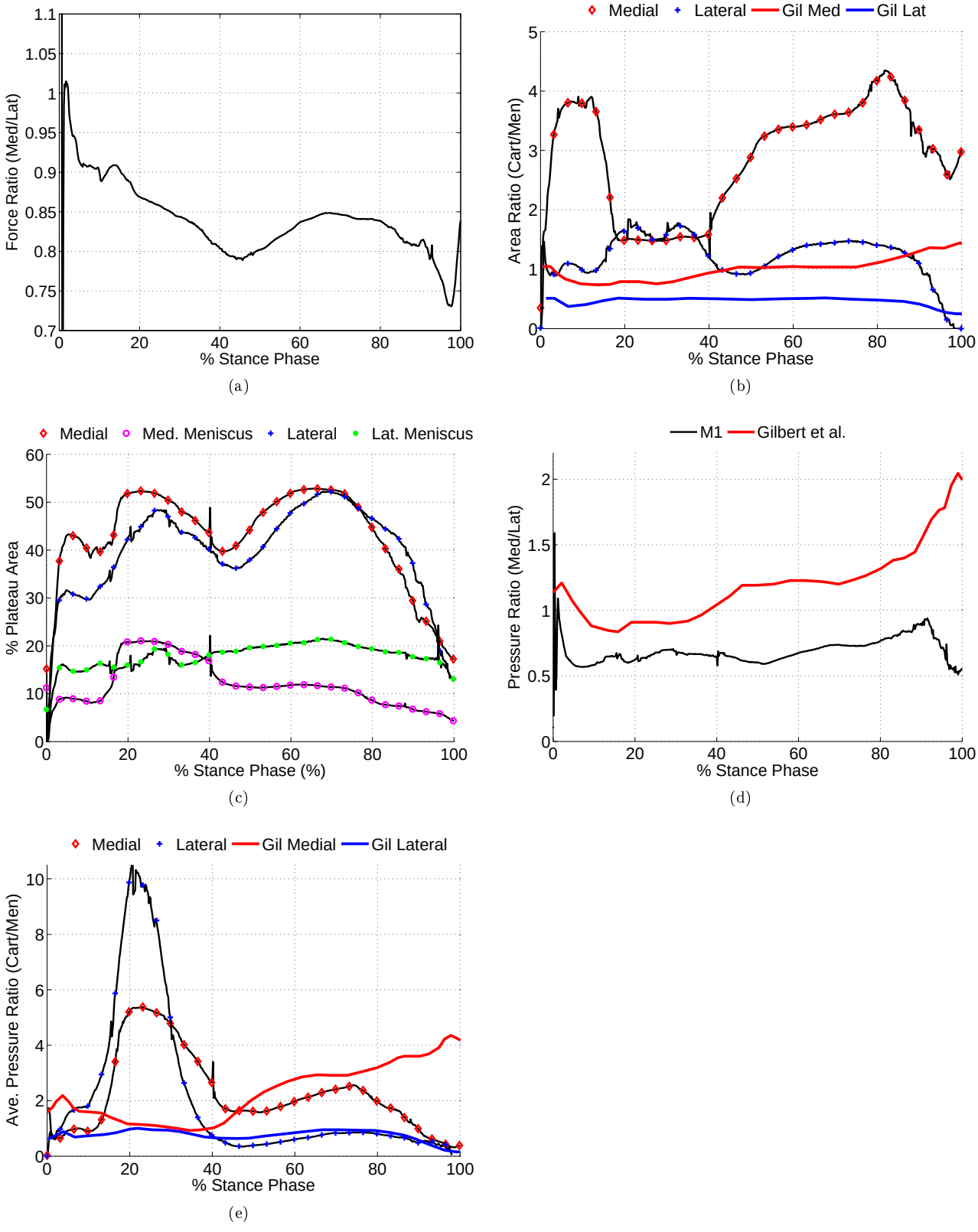

Figure 6.6: Supplemental gait results from M1 using Gilbert kinematics showing (a) Med-lat force ratio (b) Cart-men contact area ratios (c) % plateau area (d) Med-lat ave. pressure ratio (e) Cart-men ave. pressure ratio.

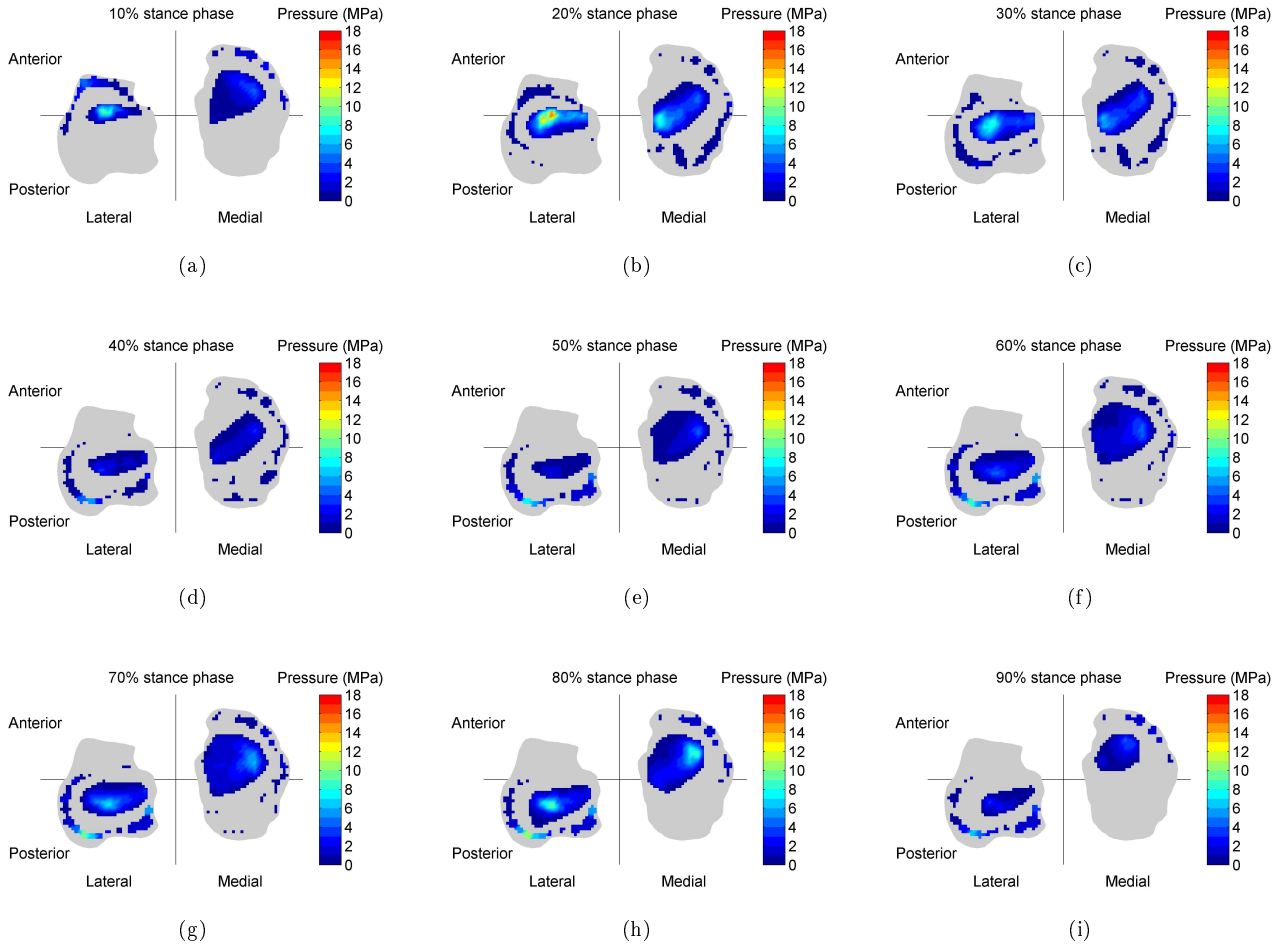

Figure 6.7: Pressure maps for M1 results using Gilbert kinematics at 10% intervals of stance phase.

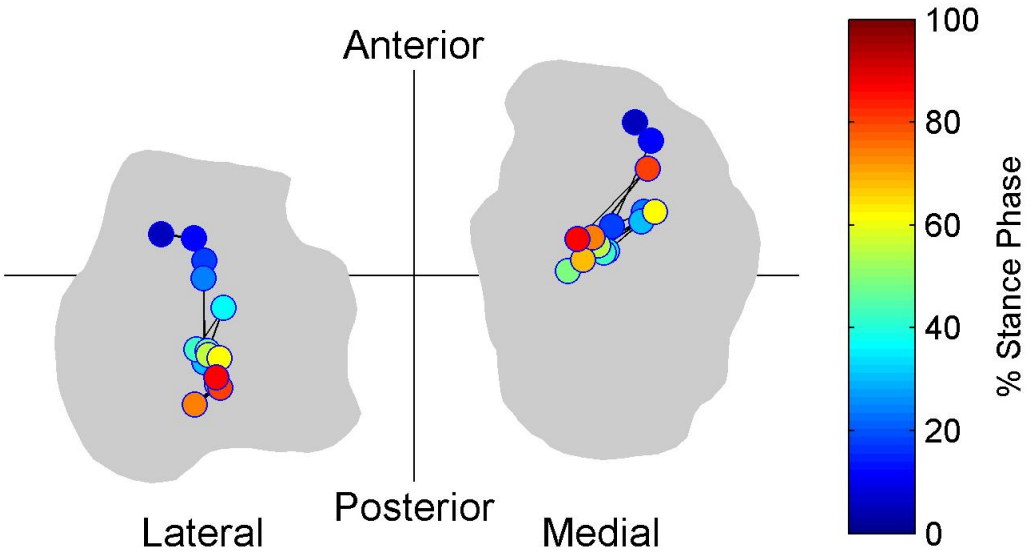

Figure 6.8: Location of the weighted center of pressure throughout stance phase.

6.3 Appendix C: Supplemental material property sensitivity study data

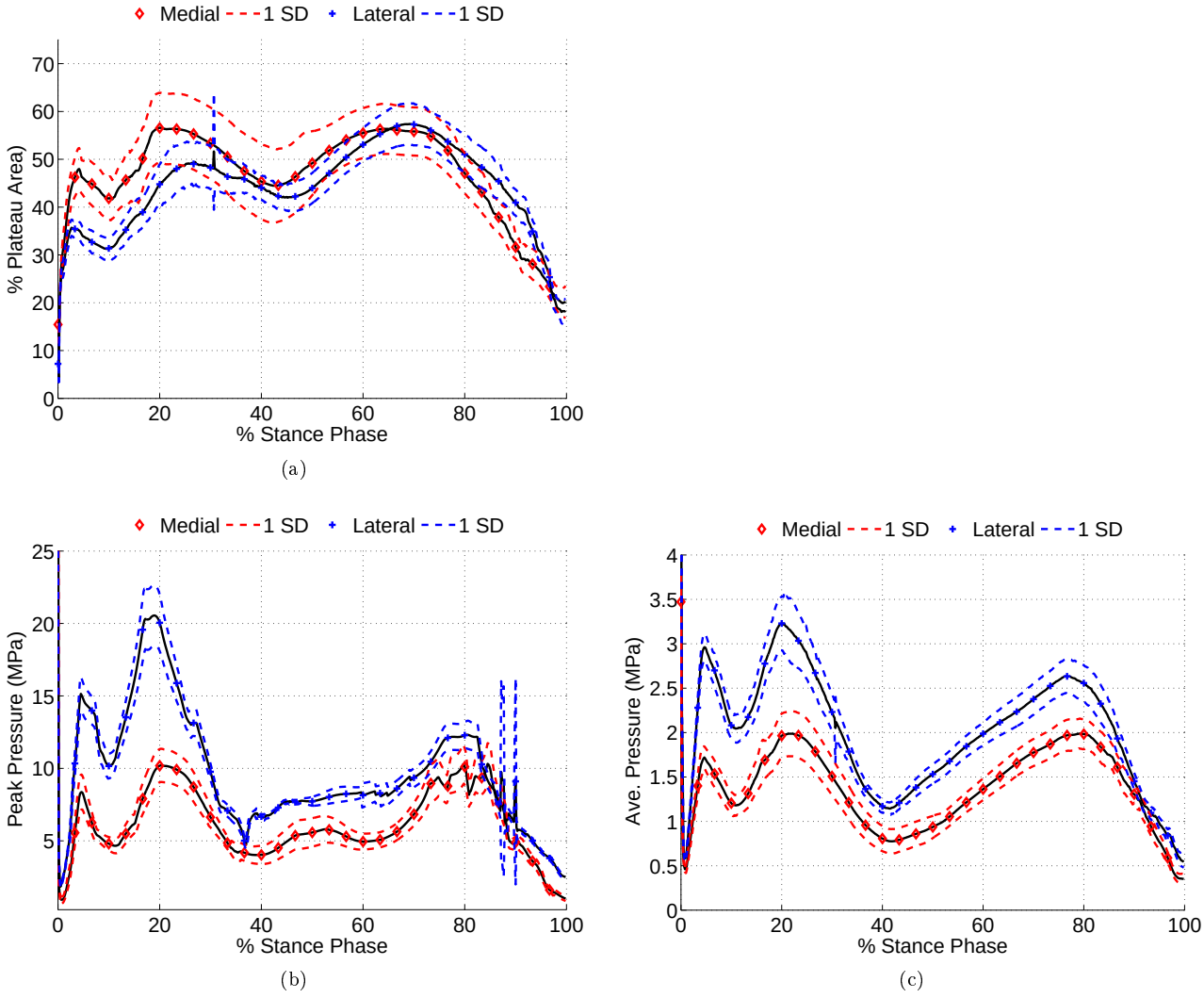

Figure 6.9: Mean and standard deviation of simulations run in the sensitivity analysis for (a) Contact area (b) Peak pressure (c) Average pressure.

Table 6.5: Numerical gait simulation results for different cartilage property sets.

		KRec	K1	K3
Average Pressure (MPa)	Med	1.39 ± 0.45	1.22 ± 0.41	1.53 ± 0.48
	Lat	2.03 ± 0.69	1.95 ± 0.67	2.23 ± 0.78
Average Peak Pressure (MPa)	Med	6.32 ± 2.98	5.32 ± 2.59	6.86 ± 3.13
	Lat	9.74 ± 4.22	9.39 ± 3.94	10.56 ± 4.84
Maximum Peak Pressure (MPa)	Med	10.55	9.00	11.65
	Lat	20.95	19.42	23.96
% of Potential Contact Area	Med	45 ± 9	53 ± 11	41 ± 9
	Lat	43 ± 9	45 ± 9	39 ± 8

		K5	K6	K7
Average Pressure (MPa)	Med	1.54 ± 0.49	1.27 ± 0.42	1.29 ± 0.43
	Lat	2.05 ± 0.71	1.82 ± 0.59	1.97 ± 0.66
Average Peak Pressure (MPa)	Med	7.14 ± 3.38	5.82 ± 2.78	5.83 ± 2.89
	Lat	9.65 ± 4.33	9.22 ± 3.63	9.58 ± 3.95
Maximum Peak Pressure (MPa)	Med	12.15	9.73	9.72
	Lat	20.91	18.50	20.05
% of Potential Contact Area	Med	41 ± 8	50 ± 10	49 ± 10
	Lat	43 ± 9	49 ± 10	44 ± 9

6.4 Appendix D: M1 Kinematic study utilizing Benoit kinematic Set

The "Gilbert" and "Benoit" kinematic sets are the tibial anterior-posterior translation and internal-external reported in Gilbert et al. (2014) and Benoit et al. (2006), respectively. However, axial loading was defined from Hsiung et al. (2013) (see Figure 6.10) instead of Gilbert et al. (2014), increasing peak axial loading by about 300N. For Beniot results directly comparable to the Gilbert simulation of Section 4, see Appendix 6.5. "Gilbert_2" utilizes the kinematic set from Gilbert et al. (2014) but uses initial position and orientaiton conditions from Benoit et al. (2006). Similarly, "Benoit_2" utilizes the kinematic set from Benoit et al. (2006) but uses initial position and orientation conditions from Gilbert et al. (2014). Benoit and Gilbert_2 simulations have the tibial in a more anterior position than Gilbert and Benoit_2 simulations. This tends to offload the posterior menisci thus lowering contact area and increasing contact pressures.

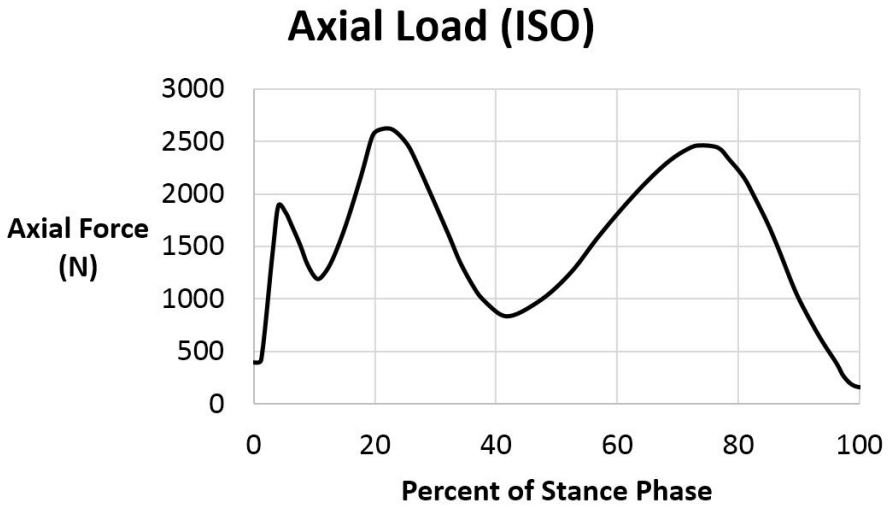

Figure 6.10: Axial loading as defined in Hsiung et al. (2013).

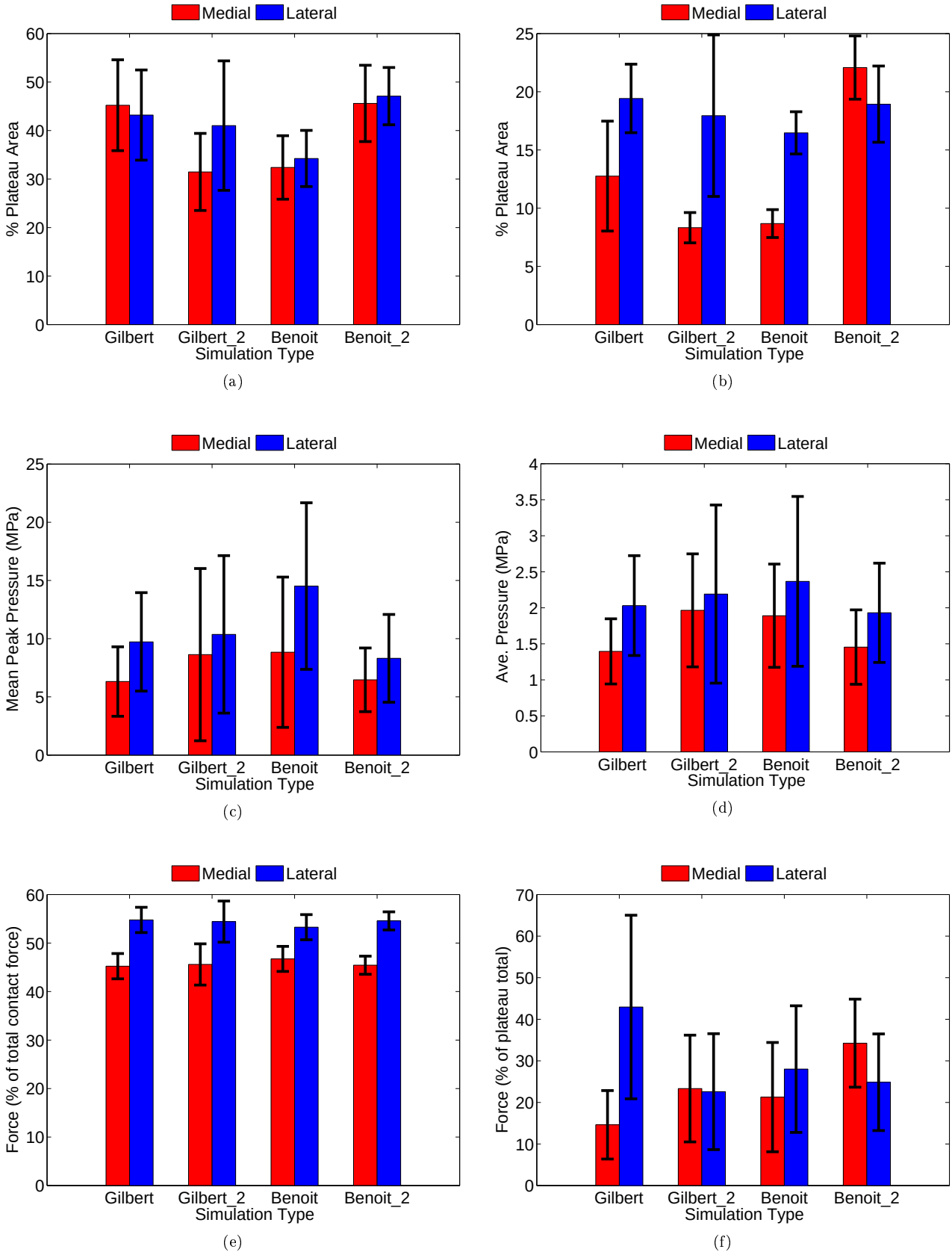

Figure 6.11: Comparison of M1 gait results for different kinematic and initial position sets for (a) % Plateau area (b) % Plateau area from menisci (c) Mean peak pressure (d) Average pressure (e) Plateau force (f) Plateau force from menisci.

Table 6.6: Comparison of numeric gait simulation results using Gilbert vs. Benoit kinematics.

Kinematic set	Gilbert		Benoit		% Difference	
	Medial	Lateral	Medial	Lateral	Medial	Lateral
	Mean ± SD	Mean ± SD	Mean ± SD	Mean ± SD	(Benoit-Gilbert) /Gilbert*100	
Average Pressure (MPa)	1.39 ± 0.45	2.03 ± 0.69	1.89 ± 0.72	2.37 ± 1.18	+36	+17
Plateau Force /Total Force (%)	45 ± 3	55 ± 3	47 ± 3	53 ± 3	+4	-4
Meniscus Force /Plateau Force (%)	15 ± 8	43 ± 22	21 ± 13	28 ± 15	+40	-35
Plateau Area /Potential Area (%)	45 ± 9	43 ± 9	32 ± 7	34 ± 6	-29	-21
Meniscus Area /Potential Area (%)	13 ± 5	19 ± 3	9 ± 1	16 ± 2	-31	-16
Peak Pressure (MPa)	6.32 ± 2.98	9.73 ± 4.23	8.84 ± 6.46	14.52 ± 7.15	+40	+49

Table 6.7: Numeric gait simulation results for Gilbert and Benoit kinematics with altered initial conditions.

Kinematic set	Gilbert_2		Benoit_2	
	Medial	Lateral	Medial	Lateral
	Mean ± SD	Mean ± SD	Mean ± SD	Mean ± SD
Average Pressure (MPa)	1.96 ± 0.78	2.19 ± 1.24	1.45 ± 0.52	1.93 ± 0.69
Plateau Force/Total Force (%)	46 ± 4	54 ± 4	45 ± 2	55 ± 2
Meniscus Force/Plateau Force (%)	23 ± 13	23 ±14	34 ± 11	25 ± 12
Plateau Area/Potential Area (%)	31 ± 8	41 ± 13	46 ± 8	47 ± 6
Meniscus Area/Potential Area (%)	8 ± 1	18 ± 7	22 ± 3	19 ± 3
Peak pressure (MPa)	8.63 ± 7.40	10.37 ± 6.76	6.46 ± 2.74	8.31 ± 3.77

6.5 Appendix E: Results from M1 simulation using Benoit kinematic set

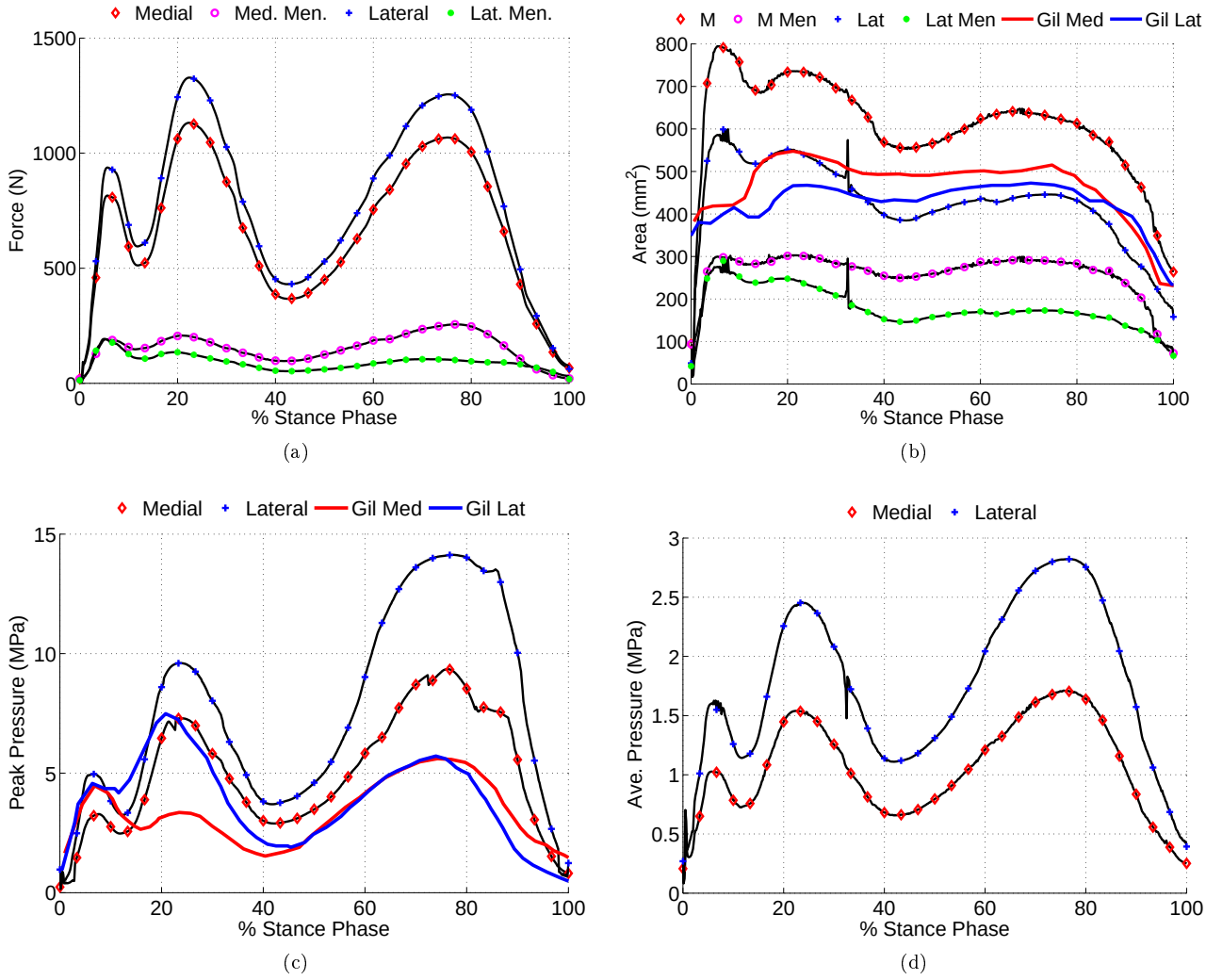

Figure 6.12: Results of M1 with Benoit kinematics for (a) Force (b) Contact Area (c) Peak pressure (d) Average pressure.

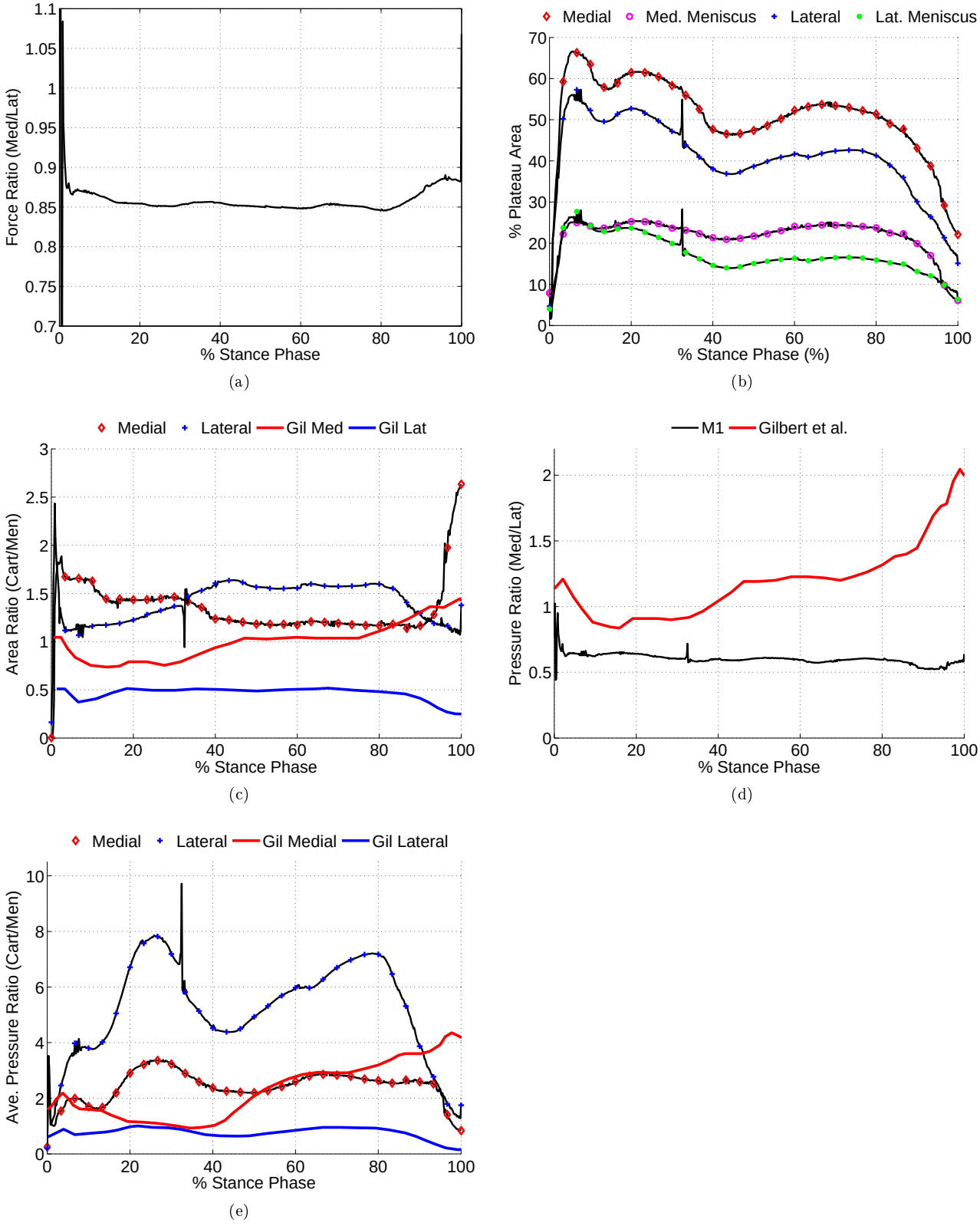

Figure 6.13: Supplemental gait results from M1 using Gilbert kinematics showing (a) Med-lat force ratio (b) Cart-men contact area ratios (c) % plateau area (d) Med-lat ave. pressure ratio (e) Cart-men ave. pressure ratio.

Table 6.8: Numeric gait simulation results for M1 using Benoit kinematics.

	Medial	Lateral
	Mean ± SD	Mean ± SD
Average Pressure (MPa)	1.06 ± 0.41	1.77 ± 0.67
Plateau Force/Total Force (%)	46 ± 1	54 ± 31
Meniscus Force/Plateau Force (%)	25 ± 7	14 ± 8
Plateau Area/Potential Area (%)	51 ± 10	41 ± 10
Meniscus Area/Potential Area (%)	22 ± 4	17 ± 4
Peak pressure (MPa)	5.05 ± 2.44	7.63 ± 4.06

6.6 Appendix F: Preliminary results from M1 simulation using Gilbert kinematics and subject-specific visual cartilage thickness estimates

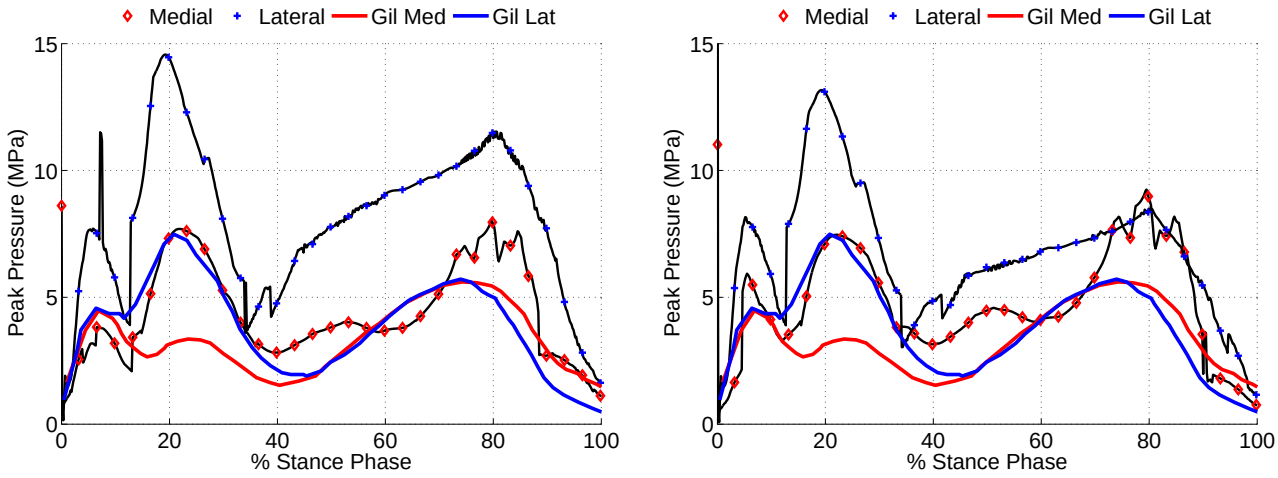

Figure 6.14: Peak pressure for the M1 model using cartilage material properties (a) K3 and (b) K5 from Deneweth (2013).

References

The nih almanac 2010 through 2011. Jan 2012. URL `http://www.nih.gov/about/almanac/archive`.

Fy 2012 performance and financial highlights. 2013. URL `http://www.nsf.gov/pubs/2013/nsf13003/nsf13003.pdf`.

Ermias S Abebe, GM Utturkar, DC Taylor, CE Spritzer, JP Kim, CT Moorman III, WE Garrett, and LE DeFrate. The effects of femoral graft placement on in vivo knee kinematics after anterior cruciate ligament reconstruction. *Journal of biomechanics*, 44(5):924–929, 2011.

M Adouni and A Shirazi-Adl. Evaluation of knee joint muscle forces and tissue stresses-strains during gait in severe oa versus normal subjects. *Journal of Orthopaedic Research*, 32(1):69–78, 2014.

Nicholas Ali and Gholamreza Rouhi. Barriers to predicting the mechanisms and risk factors of non-contact anterior cruciate ligament injury. *The Open Biomedical Engineering Journal*, (4):178–189, 2010.

Hippolite O Amadi, Chinmay M Gupte, Denny TT Lie, Ian D McDermott, Andrew A Amis, and Anthony MJ Bull. A biomechanical study of the meniscofemoral ligaments and their contribution to contact pressure reduction in the knee. *Knee Surgery, Sports Traumatology, Arthroscopy*, 16(11):1004–1008, 2008.

Shane A. Anderson and Richard F. Loeser. Why is osteoarthritis an age-related disease? *Best Practice and Research Clinical Rheumatology*, 24(1):15–26, 2010.

TP Andriacchi, PL Briant, SL Bevill, and S Koo. Rotational changes at the knee after acl injury cause cartilage thinning. *Clinical orthopaedics and related research*, 442:39, 2006.

Mark E Baratz, Freddie H Fu, and Richard Mengato. Meniscal tears: The effect of meniscectomy and of repair on intraarticular contact areas and stress in the human knee a preliminary report. *The American Journal of Sports Medicine*, 14(4):270–275, 1986.

Asheesh Bedi, Natalie H Kelly, Michael Baad, Alice JS Fox, Robert H Brophy, Russell F Warren, and Suzanne A Maher. Dynamic contact mechanics of the medial meniscus as a function of radial tear, repair, and partial meniscectomy. *The Journal of Bone & Joint Surgery*, 92(6):1398–1408, 2010.

Asheesh Bedi, Natalie Kelly, Michael Baad, Alice JS Fox, Yan Ma, Russell F Warren, and Suzanne A Maher. Dynamic contact mechanics of radial tears of the lateral meniscus: implications for treatment. *Arthroscopy: The Journal of Arthroscopic & Related Surgery*, 28(3):372–381, 2012.

Yanhong Bei and Benjamin J Fregly. Multibody dynamic simulation of knee contact mechanics. *Medical engineering and physics*, 26(9):777–789, 2004.

Daniel L Benoit, Dan K Ramsey, Mario Lamontagne, Lanyi Xu, Per Wretenberg, and Per Renström. Effect of skin movement artifact on knee kinematics during gait and cutting motions measured in vivo. *Gait & posture*, 24(2):152–164, 2006.

FS Bezerra, JN Alves, MAS Silva, ETL Trajano, TA Ferreira, HA Vasconcellos, and SS Valença. Quantitative and descriptive analysis of the meniscotibial ligament in human corpses. *Braz. J. Morphol. Sci*, 24(4):211–213, 2007.

JT Bingham, R Papannagari, SK Van de Velde, C Gross, TJ Gill, DT Felson, HE Rubash, and G Li. In vivo cartilage contact deformation in the healthy human tibiofemoral joint. *Rheumatology*, 47(11):1622–1627, 2008.

Cameron P Brown, Ross W Crawford, and Adekunle Oloyede. Indentation stiffness does not discriminate between normal and degraded articular cartilage. *Clinical Biomechanics*, 22(7):843–848, 2007.

Gregory Alexander Brown. *Load-Bearing Role of the Human Knee Meniscus*. PhD thesis, Massachusetts Institute of Technology, May 1990. URL http://hdl.handle.net/1721.1/29204.

Michael I Chen, Thomas P Branch, and William C Hutton. Is it important to secure the horns during lateral meniscal transplantation? a cadaveric study. *Arthroscopy: The Journal of Arthroscopic and Related Surgery*, 12(2):174–181, 1996.

Jessica M Deneweth. *Mapping the Biomechanical Properties of Human Knee Cartilage*. PhD thesis, 2013.

Charles F Dillon, Elizabeth K Rasch, Qiuping Gu, and Rosemarie Hirsch. Prevalence of knee osteoarthritis in the united states: arthritis data from the third national health and nutrition examination survey 1991-94. *The Journal of rheumatology*, 33 (11):2271–2279, 2006.

Martin Englund, Ali Guermazi, Daniel Gale, David J Hunter, Piran Aliabadi, Margaret Clancy, and David T Felson. Incidental meniscal findings on knee mri in middle-aged and elderly persons. *New England Journal of Medicine*, 359(11):1108–1115, 2008.

A Erdemir and S Sibole. Open knee: A three-dimensional finite element representation of the knee joint, user's guide, version 1.0. 0. *December*, 17:2010, 2010.

TJ Fairbank. Knee joint changes after meniscectomy. *Journal of Bone and Joint Surgery, British Volume*, 30(4):664–670, 1948.

David T Felson, Allan Naimark, Jennifer Anderson, Lewis Kazis, William Castelli, and Robert F Meenan. The prevalence of knee osteoarthritis in the elderly. the framingham osteoarthritis study. *Arthritis and Rheumatism*, 30(8):914–918, 1987.

Braden C Fleming, Per A Renstrom, Goran Ohlen, Robert J Johnson, Glenn D Peura, Bruce D Beynnon, and Gary J Badger. The gastrocnemius muscle is an antagonist of the anterior cruciate ligament. *Journal of Orthopaedic Research*, 19(6):1178 – 1184, 2001. ISSN 0736-0266. URL http://dx.doi.org/10.1016/S0736-0266(01)00057-2.

Craig A Fraser. Total knee replacement: The mechanical properties of the human knee meniscus. May 2011. URL https://sites.google.com/site/thehumankneemeniscus/contact-us.

Benjamin J. Fregly, W. Gregory Sawyer, Melinda K. Harman, and Scott A. Banks. Computational wear prediction of a total knee replacement from in vivo kinematics. *Journal of Biomechanics*, 38(2):305 – 314, 2005. URL http://dx.doi.org/10.1016/j.jbiomech.2004.02.013.

Toru Fukubayashi and Hlsashi Kurosawa. The contact area and pressure distribution pattern of the knee: a study of normal and osteoarthrotic knee joints. *Acta Orthopaedica*, 51(1-6):871–879, 1980.

DR Gale, CE Chaisson, SMS Totterman, RK Schwartz, ME Gale, and D Felson. Meniscal subluxation: association with osteoarthritis and joint space narrowing. *Osteoarthritis and Cartilage*, 7(6):526–532, 1999.

Simon M Gianotti, Stephen W Marshall, Patria A Hume, and Lorna Bunt. Incidence of anterior cruciate ligament injury and other knee ligament injuries: a national population-based study. *Journal of Science and Medicine in Sport*, 12(6):622–627, 2009.

Susannah Gilbert, Tony Chen, Ian D Hutchinson, Dan Choi, Clifford Voigt, Russell F Warren, and Suzanne A Maher. Dynamic contact mechanics on the tibial plateau of the human knee during activities of daily living. *Journal of biomechanics*, 47(9): 2006–2012, 2014.

AC Godest, M Beaugonin, E Haug, M Taylor, and PJ Gregson. Simulation of a knee joint replacement during a gait cycle using explicit finite element analysis. *Journal of biomechanics*, 35(2):267–275, 2002.

Henry Gray. *Anatomy of the Human Body*. Lea and Febiger, 20th edition, 1918. Published online at Bartleby.com, 2000.

Trent M Guess. Forward dynamics simulation using a natural knee with menisci in the multibody framework. *Multibody System Dynamics*, 28(1-2):37–53, 2012.

Trent M Guess, Ganesh Thiagarajan, Mohammad Kia, and Meenakshi Mishra. A subject specific multibody model of the knee with menisci. *Medical engineering and physics*, 32(5):505–515, 2010.

Trent M Guess, Hongzeng Liu, Sampath Bhashyam, and Ganesh Thiagarajan. A multibody knee model with discrete cartilage prediction of tibio-femoral contact mechanics. *Computer methods in biomechanics and biomedical engineering*, 16(3):256–270, 2013.

CM Gupte, A Smith, ID McDermott, AMJ Bull, RD Thomas, and AA Amis. Meniscofemoral ligaments revisited anatomical study, age corellation and clinical implications. *Journal of Bone & Joint Surgery, British Volume*, 84(6):846–851, 2002.

Karen N Hauch, Diego F Villegas, and Tammy L Haut Donahue. Geometry, time-dependent and failure properties of human meniscal attachments. *Journal of biomechanics*, 43(3):463–468, 2010.

Tammy L Haut Donahue, ML Hull, Mark M Rashid, and Christopher R Jacobs. How the stiffness of meniscal attachments and meniscal material properties affect tibio-femoral contact pressure computed using a validated finite element model of the human knee joint. *Journal of biomechanics*, 36(1):19–34, 2003.

JC Hsiung, SJ Hsu, JJ Liau, and Toru Maruyama. In-vitro wear measurement of artificial knee prostheses. *Life Science Journal*, 10(2), 2013.

Arthur Huang, ML Hull, and Stephen M Howell. The level of compressive load affects conclusions from statistical analyses to determine whether a lateral meniscal autograft restores tibial contact pressure to normal: a study in human cadaveric knees. *Journal of orthopaedic research*, 21(3):459–464, 2003.

Joanne M Jordan, Charles G Helmick, Jordan B Renner, Gheorghe Luta, Anca D Dragomir, Janice Woodard, Fang Fang, Todd A Schwartz, Lauren M Abbate, Leigh F Callahan, et al. Prevalence of knee symptoms and radiographic and symptomatic knee osteoarthritis in african americans and caucasians: the johnston county osteoarthritis project. *The Journal of rheumatology*, 34(1):172–180, 2007.

G.E. Kempson, M.A.R. Freeman, and S.A.V. Swanson. The determination of a creep modulus for articular cartilage from indentation tests on the human femoral head. *Journal of Biomechanics*, 4(4):239 – 250, 1971. ISSN 0021-9290. URL `http://dx.doi.org/10.1016/0021-9290(71)90030-3`.

Mohammad Kia. *A musculoskeletal model of a subject specific knee joint with menisci during the stance phase of a walk cycle*. PhD thesis, University of Missouri-Kansas City, 2011.

P Kumar, M Oka, J Toguchida, M Kobayashi, E Uchida, T Nakamura, and K Tanaka. Role of uppermost superficial surface layer of articular cartilage in the lubrication mechanism of joints. *Journal of Anatomy*, 199(3):241–250, 2001.

Hisashi Kurosawa, Toru Fukubayashi, and Hiroyuki Nakajima. Load-bearing mode of the knee joint: Physical behavior of the knee joint with or without menisci. *Clinical Orthopaedics and Related Research*, 149:283–290, June 1980.

Steven Kurtz, Fionna Mowat, Kevin Ong, Nathan Chan, Edmund Lau, and Michael Halpern. Prevalence of primary and revision total hip and knee arthroplasty in the united states from 1990 through 2002. *The Journal of Bone and Joint Surgery*, 87(7): 1487–1497, 2005.

Robert F LaPrade, Thomas J Gilbert, Timothy S Bollom, Fred Wentorf, and Gregory Chaljub. The magnetic resonance imaging appearance of individual structures of the posterolateral knee a prospective study of normal knees and knees with surgically verified grade iii injuries. *The American journal of sports medicine*, 28(2):191–199, 2000.

Stephen J Lee, Kirk J Aadalen, Prasanna Malaviya, Eric P Lorenz, Jennifer K Hayden, Jack Farr, Richard W Kang, and Brian J Cole. Tibiofemoral contact mechanics after serial medial meniscectomies in the human cadaveric knee. *The American journal of sports medicine*, 34(8):1334–1344, 2006.

Hongzeng Liu, Trent Guess, and Mohammed Kia. Discrete representation of cartilage in a multibody knee model. *American Society of Biomechanics Anual Conference*, 2009. URL `http://www.asbweb.org/conferences/2009/pdf/1061.pdf`.

John M Marzo and Jennifer Gurske-DePerio. Effects of medial meniscus posterior horn avulsion and repair on tibiofemoral contact area and peak contact pressure with clinical implications. *The American journal of sports medicine*, 37(1):124–129, 2009.

L McCann, E Ingham, Z Jin, and J Fisher. Influence of the meniscus on friction and degradation of cartilage in the natural knee joint. *Osteoarthritis and Cartilage*, 17(8):995–1000, 2009.

R.S. Moran. The mechanical properties and behavioural characteristics of human knee joint meniscus. Master's thesis, The University of Edinburgh, 2001.

Gavin Carson Paiva. Development of multibody soft tissue models and their tuning to experimental data: with a focus in the canine meniscus, 2011.

George A Paletta, Tim Manning, Edward Snell, Richard Parker, and John Bergfeld. The effect of allograft meniscal replacement on intraarticular contact area and pressures in the human knee a biomechanical study. *The American journal of sports medicine*, 25(5):692–698, 1997.

Amos Race and Andrew A. Amis. Loading of the two bundles of the posterior cruciate ligament: An analysis of bundle function in a-p drawer. *Journal of Biomechanics*, 29(7):873 – 879, 1996. ISSN 0021-9290. URL `http://dx.doi.org/10.1016/0021-9290(95)00161-1`.

Harald Roos, Mårten Laurén, Torsten Adalberth, Ewa M Roos, Kjell Jonsson, and L Stefan Lohmander. Knee osteoarthritis after meniscectomy: prevalence of radiographic changes after twenty-one years, compared with matched controls. *Arthritis and Rheumatism*, 41(4):687–693, 1998.

SA Shahane, C Ibbotson, R Strachan, and D Bickerstaff. The popliteofibular ligament: an anatomical study of the posterolateral corner of the knee. *Journal of Bone and Joint Surgery, British Volume*, 81(4):636–642, 1999.

DET Shepherd and BB Seedhom. Thickness of human articular cartilage in joints of the lower limb. *Annals of the rheumatic diseases*, 58(1):27–34, 1999.

NG Shrive, JJ O'Connor, and JW Goodfellow. Load-bearing in the knee joint. *Clinical orthopaedics and related research*, (131):279, 1978.

Tekscan. Mdl-medical-sensor-4010n-datasheet. URL `https://www.tekscan.com/products-solutions/medical-sensors/4010n?tab=specifications`. accessed March 5, 2015.

Tekscan. Tekscan technology: Tekscan sensor properties and performance, 2015. URL `https://www.tekscan.com/tekscan-technology`. accessed March 5, 2015.

M. Tissakht and A.M. Ahmed. Tensile stress-strain characteristics of the human meniscal material. *Journal of Biomechanics*, 28(4):411 – 422, 1995. ISSN 0021-9290. URL `http://dx.doi.org/10.1016/0021-9290(94)00081-E`.

JL Van Saase, LK Van Romunde, ARNOLD Cats, JP Vandenbroucke, and HA Valkenburg. Epidemiology of osteoarthritis: Zoetermeer survey. comparison of radiological osteoarthritis in a dutch population with that in 10 other populations. *Annals of the rheumatic diseases*, 48(4):271–280, 1989.

Peter S. Walker and Margaret Erkman. The role of the menisci in force transmission across the knee. *Clinical Orthopaedics and Related Research*, 109:184–192, June 1975.

CR Winby, Pauline Gerus, TB Kirk, and David Gavin Lloyd. Correlation between emg-based co-activation measures and medial and lateral compartment loads of the knee during gait. *Clinical Biomechanics*, 28(9):1014–1019, 2013.

G.T. Yamaguchi. *Dynamic Modeling of Musculoskeletal Motion: A Vectorized Approach for Biomechanical Analysis in Three Dimensions*. Springer, 2001. ISBN 978-0-7923-7430-5.

Jiang Yao, Jason Snibbe, Michael Maloney, and Amy L Lerner. Stresses and strains in the medial meniscus of an acl deficient knee under anterior loading: a finite element analysis with image-based experimental validation. *Journal of biomechanical engineering*, 128(1):135–141, 2006.

Warren Clarence Young and Richard Gordon Budynas. *Roark's formulas for stress and strain*, volume 7. McGraw-Hill New York, 2002.

Thore Zantop, Nadine Diermann, Tobias Schumacher, Steffen Schanz, Freddie H Fu, and Wolf Petersen. Anatomical and nonanatomical double-bundle anterior cruciate ligament reconstruction importance of femoral tunnel location on knee kinematics. *The American journal of sports medicine*, 36(4):678–685, 2008.

Ming Zhang, Arthur F.T Mak, and V.C Roberts. Finite element modelling of a residual lower-limb in a prosthetic socket: a survey of the development in the first decade. *Medical Engineering and Physics*, 20(5):360 – 373, 1998. ISSN 1350-4533. URL `http://dx.doi.org/10.1016/S1350-4533(98)00027-7`.

Curriculum Vita

Stephen Wilson is the second son of Kenneth and LeLynn Wilson and was born and raised in Portland, Oregon. He was homeschooled but enjoyed supplemental classes from New Covenant Christian Academy and Clackamas Community College. He graduated from high school in 2009 and entered the honors program of LeTourneau University (LETU). While at LETU, Stephen worked under Dr. Roger Gonzalez in junior and senior design on the ACL project. After graduating *summa cum laude* from the honors program with a B.S. in engineering with a biomedical concentration, Stephen accepted a research assistant position at The University of Texas at El Paso and began pursuing a M.S. in mechanical engineering in the summer of 2013.

Contact information

Email address: StephenPaulosWilson@gmail.com